UC Riverside

UC Riverside Electronic Theses and Dissertations

Title

Mass Spectrometry-Based Studies of DNA Lesions and Epigenetic Biomarkers

Permalink

https://escholarship.org/uc/item/9f2136fp

Author

Yu, Yang

Publication Date

2017

Peer reviewed|Thesis/dissertation

eScholarship.org Powered by the California Digital Library
University of California

UNIVERSITY OF CALIFORNIA
RIVERSIDE

Mass Spectrometry-Based Studies of DNA Lesions and Epigenetic Biomarkers

A Dissertation submitted in partial satisfaction
of the requirements for the degree of

Doctor of Philosophy

in

Environmental Toxicology

by

Yang Yu

September 2017

Dissertation Committee:
Dr. Yinsheng Wang, Chairperson
Dr. Constance I. Nugent
Dr. Jay Jianying Gan

Copyright by
Yang Yu
2017

The Dissertation of Yang Yu is approved:

_____

_____

_____

Committee Chairperson

University of California, Riverside

COPYRIGHT ACKNOWLEDGEMENTS

The text and figures in Chapter 1, in part or in full, are a reprint of the material as it appears in ***Chemical Research in Toxicology*** 2016, 29(12), p. 2008-2039. The coauthor (Ms. Yuxiang Cui, Dr. Laura J. Niedernhofer and Dr. Yinsheng Wang) listed in that publication wrote and revised the manuscript which forms the basis of this chapter.

The text and figures in Chapter 2, in part or in full, are a reprint of the material as it appears in ***Molecular & Cellular Proteomics*** 2016, 15(3), p. 810-817 and the supporting information therein. The coauthors (Dr. Candace R. Guerrero, Dr. Shuo Liu, Dr. Nicholas J. Amato, and Dr. Yogeshwar Sharma) contributed new reagents or analytic tools. The coauthor (Dr. Yinsheng Wang) listed in this publication directed and supervised the research which forms the basis of this chapter.

The text and figures in Chapter 3, in part or in full, are a reprint of the material as it appears in ***Analytical chemistry*** 2016, 88(16), p. 8036-8042 and the supporting information therein. The coauthors (Dr. Jianshuang Wang and Dr. Pengcheng Wang) contributed the synthesis of stable isotope-labeled standards. The coauthor (Dr. Yinsheng Wang) listed in this publication directed and supervised the research which forms the basis of this chapter.

ACKNOWLEDGEMENTS

My research in this dissertation would not be accomplished without the help from many people. First and foremost, I would like to express my sincere appreciation to my supervisor, Dr. Yinsheng Wang, for the continuous support and help of my Ph.D. study, for his patience, enthusiasm, immense knowledge and dedication to science. As an undergraduate majored in biological science, I started my doctoral study without too much experience in analytical chemistry. Dr. Wang taught me all the principles and techniques required for my research. Moreover, he provided me the precious opportunity to handle instruments i.e. HPLC and mass spectrometers by myself, which deepened my understanding of instrumentation and enabled me to become an independent researcher in analytical chemistry in the future. I appreciate all his contributions of time, suggestion and support on both my professional and personal growth.

Next, I would like to thank my committee members, Dr. Jay Jianying Gan and Dr. Constance I. Nugent, for their suggestions during my graduate career and discussion with my research. I truly appreciate their concerns, generous help and accessibility over the past five years. I am also grateful for the technical supports from facility staff members at UC Riverside. I would like to thank Dr. Dan Borchardt for his help with NMR measurements and data processing, and Dr. Richard Kondrat and Mr. Ron New for training me how to use the ESI-TOF mass spectrometer and Thermo TSQ Vantage mass spectrometer. In addition, I would like to thank my collaborators who provided me great opportunities for highly interdisciplinary study. They are Dr. Sanjeev Gupta at Albert

Einstein College of Medicine, Dr. Laura J. Niedernhofer at the Scripps Research Institute Florida, Dr. Xiqun Chen at Massachusetts General Hospital, Dr. David C. Volz at University of California, Riverside, Dr. Jikui Song at University of California, Riverside, Dr. Guoping Fan at University of California, Los Angeles, Dr. Gang (Greg) Wang at University of North Carolina at Chapel Hill and Dr. Andrew Xiao at Yale University.

My sincere thanks also give to the members of the Wang research group for their great contributions to my personal and professional development. I would like to thank Dr. Lijuan Fu, Dr. Shuo Liu, Dr. Yongsheng Xiao, Dr Lei Guo and Dr. Xiaogang Jiang for teaching me the details about the operation, maintenance and trouble-shooting of mass spectrometer and LC system, as well as corresponding data acquisition and analysis. I appreciate Dr. Lijuan Fu's comprehensive, generous and hand-by-hand training about all the details of LC-MS instrumentational knowledge, even when she was super busy on taking care of her baby and handling her own research projects. Especially I would like to thank Dr. Pengcheng Wang, being both my labmate and roommate for the past five years, for supporting me in research career and daily life. In addition, I appreciate Ms. Yuxiang Cui for contributing paragraphs and nice figures in my reviews and Ms. Gwendolyn Gonzalez for assisting the maintenance of nanoLC-MS system. My gratitude also extends to other former and current group members: Dr. Tao Bing, Dr. Xiaoxia Dai, Dr. Debin Ji, Dr. Lin Li, Dr. Nathan Price, Dr. John Prins, Dr. Ashley Swanson, Dr. Candace Guerrero, Dr. Nicholas Amato, Dr. Renee Williams, Dr. Jun Wu, Dr. Jiapeng Leng, Dr. Changjun You, Dr. Fan Zhang, Dr. Qian Cai, Dr. Nisana Andersen, Dr. Hua Du, Dr. Tianlu Wang, Dr. Rong Cai, Preston Williams, Nicole Williams, Eric Stephens, Zi Wang, Ji Jiang,

Jiabin Wu, Weili Miao, Xuejiao Dong, Ying Tan, Su Guo, Tianyu Qi and Jianan Sun.

Last but not the least, I would like to thank my parents and friends for supporting me spiritually throughout my Ph.D. study and my life in general. Here, I offer my best regards and blessings to all of those who supported me in any respect during the completion of my graduate study.

ABSTRACT OF THE DISSERTATION

Mass Spectrometry-Based Studies of DNA Lesions and Epigenetic Biomarkers

by

Yang Yu

Doctor of Philosophy, Graduate Program in Environmental Toxicology
University of California, Riverside, September 2017
Dr. Yinsheng Wang, Chairperson

LC-MS has been employed as a powerful tool for elucidating structures of compounds as well as providing accurate and unambiguous quantification of analytes. The focus of this dissertation is placed on the development of analytical methods for reliable quantification of chemically modified nucleosides in DNA, including oxidative stress-induced DNA lesions, carboxymethylated DNA adducts, and DNA epigenetic marks.

In chapter 2, I employed a nanoflow liquid chromatography-nanoelectrospray ionization-tandem mass spectrometry (NanoLC-NSI-MS^2) coupled with the isotope-dilution method for the simultaneous quantification of oxidatively induced DNA modifications. The quantification data suggested that aberrant copper accumulation may perturb genomic stability by elevating oxidatively induced DNA lesions, and by altering epigenetic pathways of gene regulation.

In chapter 3, I developed a highly sensitive nLC-nESI-MS^3 method for the simultaneous quantification of N^6-CMdA, O^6-CMdG and O^6-MedG. I was able to measure the levels of these three lesions with the use of low-microgram quantities of DNA from cultured human skin fibroblasts and human colorectal carcinoma cells treated with azaserine, a DNA carboxymethylating agent. The method reported here will be useful for the future investigations about the repair of the carboxymethylated DNA lesions and about the implications of these lesions in carcinogenesis.

In chapter 4, I employed LC-MS^3 and quantified the levels of 5-hmdC in different cancer cells treated with a glycolysis inhibitor or activators of AMP-activated protein kinase (AMPK) to gain insights into the relationship between aberrant metabolism and the levels of 5-hmdC in cancer cells. The data indicated that the altered metabolism in cancer cells could contribute, in part, to the diminished levels of 5-hmdC observed in cancer cells.

Table of Contents

Chapter 1 Introduction 1

Overview of DNA damage 1

Occurrence of oxidative stress-induced DNA lesions 1

Repair and biological consequences of oxidative-stress induced DNA lesions 12

Implications of oxidative-stress induced DNA lesions in human diseases 19

N-nitroso compounds (NOCs) 24

Formation of carboxymethylated DNA adducts 27

Biological consequences and repair mechanisms of carboxymethylated DNA adducts 32

Implications of carboxymethylated DNA lesions in human diseases 33

Detection of carboxymethylated DNA lesions 34

Scope of this dissertation 35

References 37

Chapter 2 Comprehensive assessment of oxidatively induced modifications of DNA in a rat model of human Wilson's Disease 60

Introduction 60

Materials and methods 63

Results 68

Discussion 79

References 82

Chapter 3 Quantification of azaserine-induced carboxymethylated and methylated DNA lesions in cells by nanoflow liquid chromatography-nanoelectrospray ionization tandem mass spectrometry coupled with the stable isotope-dilution method 87

Introduction 87

Experimental section 91

Results 97

Discussion 106

References 109

Chapter 4 LC-MS/MS for the investigation of the altered levels of 5-hmdC in cancer cells 113

Introduction 113

Experimental procedures 117

Results and discussion 120

Discussion 134
References 137
Chapter 5 Conclusions and Future Directions 142
Appendix A Supporting information for chapter 2 146
Appendix B Supporting information for chapter 3 153

List of Figures

Figure 1.1.Pathways for hydroxyl radical-mediated oxidation of dT. 5

Figure 1.2.Oxidation pathways of 5-mdC. a. ROS-induced oxidation of 5-mdC; b. TET-mediated oxidation of 5-mdC. 6

Figure 1.3.Proposed mechanism for the formation of 5'R- and 5'S-diastereomers of 8,5'-cyclo-2'-deoxyadenosine. 9

Figure 1.4.Structures of representative lipid peroxidation (LPO) products and LPO products-induced DNA adducts. 10

Figure 1.5.Formation process of typical endogenous NOCs. 26

Figure 1.6.Carboxymethylated DNA lesions and typical carboxymethylating agents 29

Figure 1.7.DNA carboxymethylation via diazoacetate (DA) 31

Figure 2.1.Representative NanoLC-NSI/MS^2 results for the quantifications of εdA (A), εdG (B), S-cdA (C) and S-cdG (D) in DNA of rat tissues. Shown are the selected-ion chromatograms (SICs) for monitoring the indicated MRM transitions for the analytes (top trace) and the isotope-labeled standards (bottom trace). 70

Figure 2.2.Quantification results for the levels of εdA and εdG (A), as well as S-cdA and S-cdG (B) in liver tissues of LEA (n = 6) and LEC (n = 5) rats as well as in brain tissues of LEA (n = 3) and LEC (n = 3) rats. The data represent the mean and standard deviation of the measurement results. The P values were calculated using unpaired two-tailed Student's t-test. #, $P > 0.05$; *, $P < 0.05$; **, $P < 0.01$; ***, $P < 0.001$. 73

Figure 2.3.Quantification results for the levels of 5-HmdC (A) and 5-mdC (B) in LEA rat liver tissues (n = 6), LEC rat liver tissues (n = 5), LEA rat brain tissues (n = 3) and LEC rat brain tissues (n = 3). The data represent the mean and standard deviation of the measurement results. The P values were calculated using unpaired two-tailed Student's t-test. #, $P > 0.05$; *, $P < 0.05$; **, $P < 0.01$; ***, $P < 0.001$. 75

Figure 2.4.(A) Representative LC-MS data for monitoring the Tet1-mediated oxidation of 5-mdC in a duplex DNA, d(AGCTC(5-mdC)GGTCA)/d(GTGACCGGAGCTG). Shown are the higher resolution "ultra-zoom-scan" MS results for monitoring the $[M - 3H]^{3-}$ ions of the initial 5-mdC-bearing DNA and its oxidation products. (B) Quantification results for the formation of 5-HmdC and 5-FodC in Tet-mediated oxidation of 5-mdC in the presence of a reaction buffer containing 75 μM Fe^{2+} and various concentrations of Cu^{2+} (at Cu^{2+}/Fe^{2+} molar ratios of 0, 0.25, 0.50, 1.0, 2.0 and 5.0). A control reaction was also conducted in the presence of 75 μM Cu^{2+} alone (1× Cu). 78

Figure 3.1.Representative selected-ion chromatograms (SICs) for monitoring the m/z 326→210→152 (A) and 328→212→152 (B) transitions for the $[M+H]^+$ ions of the unlabeled O^6-CMdG and $[D_2]$-O^6-CMdG, respectively, in the nucleoside mixture of genomic DNA extracted from the XPA-deficient human skin fibroblast cells treated with azaserine. Shown in the insets are the MS^3 spectra for the unlabeled and labeled O^6-CMdG. 100

Figure 3.2.Representative SICs for monitoring the m/z 310→194→148 (A) and m/z 313→197→150 transitions (B) for the $[M+H]^+$ ions of the unlabeled N^6-CMdA and $[^{13}C_2,^{15}N]$-N^6-CMdA, respectively, in the nucleoside mixture of genomic DNA extracted from the XPA-deficient human skin fibroblast cells treated with azaserine. Shown in the insets are the positive-ion MS^3 spectra for the unlabeled and labeled N^6-CMdA. 102

Figure 3.3.Representative SICs for monitoring the m/z 282→166→149 (A) and m/z 285→169→152 (B) transitions for the $[M+H]^+$ ions of unlabeled O^6-MedG and $[D_3]$-O^6-MedG, respectively, in the nucleoside mixture of genomic DNA extracted from the XPA-deficient human skin fibroblast cells treated with azaserine. Shown in the insets are the positive-ion MS^3 spectra for the unlabeled and labeled O^6-MedG. 103

Figure 3.4.LC−MS^3 quantification results for O^6-CMdG (A), O^6-MedG (B) and N^6-CMdA (C) in DNA samples isolated from XPA-deficient human skin fibroblast cells and human colorectal carcinoma HCT-116 cells treated with different concentrations of azaserine. The data represent the means and standard deviations of results obtained from three independent experiments. *, $p < 0.05$; **, $p < 0.01$; ***, $p < 0.001$. The p values were calculated by using an unpaired two-tailed t-test. 106

Figure 4.1.Representative selected-ion chromatograms (SICs) for monitoring the m/z 258 → 142 → 124 (top) and 261 → 144 → 126 (bottom) transitions for the $[M + H]^+$ ions of the unlabeled 5-hmdC and [1,3-$^{15}N_2$-2'-D]-5-hmdC, respectively, in the nucleoside mixture of genomic DNA extracted from cells. Shown in the insets are the MS^3 spectra for the unlabeled and labeled 5-hmdC. 122

Figure 4.2.Representative selected-ion chromatograms (SICs) for monitoring the m/z 242 → 126 (top) and 247 → 126 (bottom) transitions for the $[M + H]^+$ ions of the unlabeled 5-mdC and [1',2',3',4',5'-$^{13}C_5$]-5mdC, respectively, in the nucleoside mixture of genomic DNA extracted from cells. Shown in the insets are the MS^2 spectra for the unlabeled and labeled 5-mdC. 124

Figure 4.3.Representative selected-ion chromatograms (SICs) for monitoring the m/z 268 → 152 → 135 (top) and 273 → 157 → 139 (bottom) transitions for the $[M + H]^+$ ions of the unlabeled dG and [$^{15}N_5$]-dG, respectively, in the nucleoside mixture of genomic DNA extracted from cells. Shown in the insets are the MS^3 spectra for the unlabeled and labeled dG. 125

Figure 4.4.Proposed fragmentation pathways for unlabeled and labeled 5-hmdC (A), 5-mdC (B) and dG (C) in MS^n. 126

Figure 4.5.5-hmdC levels in cells treated with 8 mM 2-DG. 128

Figure 4.6.5-mdC levels in cells treated with 8 mM 2-DG. 129

Figure 4.7.5-hmdC levels in cells treated with 2 mM phenformin. 131

Figure 4.8.5-hmdC levels in cells treated with AMPK activators. 133

Figure A.1.The proposed fragmentation pathways for the $[M + H]^+$ ions of etheno DNA adducts (A) and cPus (B) lesions in MS/MS. 148

Figure A.2.Representative LC-MS^3 results for the quantifications of 5-HmdC (A) and 5-mdC (B) in rat tissues. Shown are the SICs for monitoring the indicated transitions for the analytes (top trace) and the labeled standards (bottom trace), and the inset shows the corresponding MS^3 spectra for the analytes and internal standards. The proposed fragmentation pathways for the $[M + H]^+$ ions of unlabeled and stable isotope-labeled nucleosides observed in MS^2 and MS^3 are shown on the right..... 149

Figure A.3.LC-MS^2 for monitoring the $[M – 3H]^{3-}$ ions of d(AGCTCXGGTCA) found in Tet1-catalyzed reaction mixture of the 11-mer duplex DNA, where 'X' is a 5-mdC, 5-HmdC or 5-FodC. Collisional activation of deprotonated ions of ODNs led to the loss of nucleobases (A, C, or G) and subsequent cleavages of the 3′ C-O bond of the same nucleoside to generate $[a_n – Base]$ and its complementary w_n ions. 151

Figure A.4.Calibration curves for the quantification of εdA, εdG, S-cdA, S-cdG and 5-mdC by LC-MS with the stable isotope dilution method. Plotted are the ratios of areas of peaks found in the SICs for monitoring the transitions as shown in Figure 1 and S2B versus the molar ratios of the unlabeled nucleoside over that of the corresponding stable isotope-labeled standard..... 152

Figure B.1.A representative HPLC trace for the enrichment of O^6-CMdG, O^6-MedG, and N^6-CMdA from the nucleoside mixture arising from digestion of genomic DNA isolated from human skin fibroblasts treated with azaserine. 'C', 'G', 'A', 'dC', 'dG', 'dT', 'dA' represent cytidine, guanosine, adenosine, 2'-deoxycytidine, 2'-deoxyguanosine, thymidine, and 2'-deoxyadenosine, respectively. 155

Figure B.2.Calibration curves for the quantitation of O^6-CMdG (A), O^6-MedG (B), and N^6-CMdA (C)..... 156

Figure B.3.Proposed major fragmentation pathways for the $[M + H]^+$ ions of unlabeled and labeled O^6-CMdG (A), O^6-MedG (B) and N^6-CMdA (C) observed in MS/MS and MS/MS/MS. The "N", "C" in red represent ^{15}N and ^{13}C, respectively, and the site of deuterium atom incorporation is indicated with a "D". 157

Figure B.4.Representative selected-ion chromatograms (SICs) for monitoring the m/z 326→210→152 (A) and 328→212→152 (B) transitions for the $[M+H]^+$ ions of the unlabeled O^6-CMdG and $[D_2]$-O^6-CMdG, respectively, in the nucleoside mixture of genomic DNA extracted from the XPA-deficient human skin fibroblast cells treated with azaserine. Shown in the insets are the MS^3 spectra for the unlabeled and labeled O^6-CMdG. 158

Figure B.5.Representative SICs for monitoring the m/z 282→166→149 (A) and m/z 285→169→152 (B) transitions for the $[M+H]^+$ ions of unlabeled O^6-MedG and $[D_3]$-O^6-MedG, respectively, in the nucleoside mixture of genomic DNA extracted from the XPA-deficient human skin fibroblast cells treated with azaserine. Shown in the insets are the positive-ion MS^3 spectra for the unlabeled and labeled O^6-MedG. 159

Figure B.6.Representative SICs for monitoring the m/z 310→194→148 (A) and m/z 313→197→150 transitions (B) for the $[M+H]^+$ ions of the unlabeled N^6-CMdA and $[^{13}C_2,^{15}N]$-N^6-CMdA, respectively, in the nucleoside mixture of genomic DNA extracted from the XPA-deficient human skin fibroblast cells treated with azaserine. Shown in the insets are the positive-ion MS^3 spectra for the unlabeled and labeled N^6-CMdA. 160

Figure B.7.Representative selected-ion chromatograms (SICs) for monitoring the m/z 326→210 (A) and 328→212→152 (B) transitions for the $[M+H]^+$ ions of the unlabeled O^6-CMdG, respectively, in standard solution. Shown in the insets are the MS^2 (top) and MS^3 (bottom) spectra for the unlabeled O^6-CMdG. 161

Figure B.8.Representative selected-ion chromatograms (SICs) as qualifier for monitoring the m/z 326→210 (A) and 328→212→152 (B) transitions for the $[M+H]^+$ ions of the unlabeled O^6-CMdG, respectively, in the nucleoside mixture of genomic DNA extracted from the HCT-116 human colorectal carcinoma cells treated with azaserine. Shown in the insets are the MS^2 (top) and MS^3 (bottom) spectra for the unlabeled O^6-CMdG. 162

Figure B.9.Representative SICs as qualifier for monitoring the m/z 282→166 (A) and m/z 285→169→152 (B) transitions for the $[M+H]^+$ ions of unlabeled O^6-MedG, respectively, in standard solution. Shown in the insets are the positive-ion MS^2 (top) and MS^3 (bottom) spectra for the unlabeled O^6-MedG. 163

Figure B.10.Representative SICs as qualifier for monitoring the m/z 282→166 (A) and m/z 285→169→152 (B) transitions for the $[M+H]^+$ ions of unlabeled O^6-MedG, respectively, in the nucleoside mixture of genomic DNA extracted from the HCT-116

human colorectal carcinoma cells treated with azaserine. Shown in the insets are the positive-ion MS^2 (top) and MS^3 (bottom) spectra for the unlabeled O^6-MedG. 164

Figure B.11.Representative SICs as qualifier for monitoring the m/z 310→194 (A) and m/z 313→197→150 transitions (B) for the $[M+H]^+$ ions of the unlabeled N^6-CMdA, respectively, in standard solution. Shown in the insets are the positive-ion MS^2 (top) and MS^3 (bottom) spectra for the unlabeled N^6-CMdA. 165

Figure B.12.Representative SICs as qualifier for monitoring the m/z 310→194 (A) and m/z 313→197→150 transitions (B) for the $[M+H]^+$ ions of the unlabeled N^6-CMdA, respectively, in the nucleoside mixture of genomic DNA extracted from the HCT-116human colorectal carcinoma cells treated with azaserine. Shown in the insets are the positive-ion MS^2 (top) and MS^3 (bottom) spectra for the unlabeled N^6-CMdA. 166

List of Tables

Table 3.1.Intra-day and inter-day precision and accuracy for the measurements of N^6-CMdA, O^6-CMdG and O^6-MedG, reported as Relative Standard Deviation (RSD) and Percent Recovery, respectively. 98

Table A.1.A list of MRM transitions employed for the quantifications of the five oxidative stress-induced DNA lesions and their corresponding stable isotope-labeled standards. 146

Table A.2.A summary of the levels of oxidatively induced DNA modifications as well as 5-mdC in the liver and brain tissues of rats. The data represent mean ± standard deviation of LC-MS/MS results for the analysis of liver tissues from 5 LEC or 6 LEA rats, and brain tissues of 3 LEA and 3 LEC rats. 147

Table B.1.The limits of quantitation (LOQ) for O^6-CMdG, N^6-CMdA, and O^6-MedG. The data represent the means and standard deviations of the results from three measurements of the unlabeled lesion standards in three separate days. 153

Table B.2.A summary of the levels of O^6-CMdG, O^6-MedG and N^6-CMdA in GM04429 and HCT-116 cells treated with different concentrations of azaserine (in lesions per 10^7 nucleosides). The data represent the means and standard deviations of results from three independent experiments. 154

List of Schemes

Scheme 3.1.Formation of diazoacetate and its induction of O^6-CMdG, O^6-MedG, and N^6-CMdA. 89

Scheme 4.1.TET-mediated oxidation of 5-mdC. 114

Scheme 4.2.structures of 2-DG, metformin, phenformin and AICAR. 116

Chapter 1 Introduction

Overview of DNA damage

In human cells, the integrity of genetic information is constantly challenged by endogenous and exogenous chemical agents that can induce DNA damage. Because of the existence of multiple nucleophilic sites in nucleobases, including the *N*7, O^6, C8, and N^2 of guanine; the *N*1, *N*3, and *N*7 of adenine; the O^2 and O^4 of thymine; and the O^2 and N^4 of cytosine, DNA is susceptible to attack by reactive electrophiles (1-3). In addition, reactive free radicals, i.e. hydroxyl radical (•OH) arising from oxidative stress, can also induce the formation of DNA adducts (4,5).

To counteract the deleterious effects of DNA lesions, cells are evolved with multiple repair mechanisms, such as base-excision repair (BER), nucleotide-excision repair (NER), mismatch repair (MMR), homologous recombination (HR), and non-homologous end joining (NHEJ), to efficiently remove DNA lesions from the genome. The unrepaired DNA adducts may accumulate in cells and lead to adverse biological consequences by perturbing the accuracy and efficiency of DNA replication and transcription (6,7).

Occurrence of oxidative stress-induced DNA lesions

Reactive oxygen species (ROS) constitute an important class of DNA damaging agents, and they are continuously generated in cells as a consequence of endogenous metabolism and/or exposure to environmental toxicants (8). ROS encompass a variety of chemical species, e.g. superoxide anion radical ($O_2^{-\bullet}$), hydrogen peroxide (H_2O_2),

hydroxyl radical ($^{\bullet}OH$), and singlet oxygen ($^1O_2$). In this vein, mitochondrion is considered a major source of ROS production in cells, where electrons leaking from the electron transport chain during mitochondrial respiration can combine with molecular oxygen to generate $O_2^{-\bullet}$, which can be subsequently converted to H_2O_2 by superoxide dismutase (SOD) (9). H_2O_2, which diffuses freely in the cellular environment, may react with the reduced-state transition metal ions to give $^{\bullet}OH$ via the Fenton-type reactions (10):

$$Cu^+/Fe^{2+} + H_2O_2 \rightarrow Cu^{2+}/Fe^{3+} + {}^{\bullet}OH + OH^-$$

Oxidation of biomolecules depends on the location of ROS production and the redox potential of the biomolecules. Some of the aforementioned ROS, such as $O_2^{-\bullet}$ and $^{\bullet}OH$, are extremely unstable, whereas others, like H_2O_2, are relatively long-lived (8,11,12). Infection and inflammation activate inflammatory cells, which induce and activate various oxidant-generating enzymes (13). Activated inflammatory cells produce $O_2^{\bullet-}$ through nicotinamide adenine dinucleotide phosphate (NADPH) oxidase complexes or xanthine oxidase, and these cells release high concentrations of oxidant-generating enzymes such as myeloperoxidase and eosinophil peroxidase through degranulation (13-17). These enzymes produce high concentrations of reactive oxygen, nitrogen and halogen species such as superoxide anion, nitric oxide, peroxynitrite, hydrogen peroxide, hypochlorous acid and hypobromous acid at sites of inflammation (13,18). Although intended to neutralize invading pathogens, these reactive chemical species can result in collateral DNA damage of host cells. Aside from damaging DNA directly, ROS may also lead to DNA damage indirectly, through reaction with lipids, proteins and other cellular

components to produce electrophilic species that can react with DNA (19,20). In particular, peroxidation of polyunsaturated fatty acids (PUFA) can give rise to a multitude of reactive aldehydes that can conjugate with DNA to yield DNA adducts (19,20).

$^{\bullet}$OH is highly reactive toward DNA. It can abstract a hydrogen atom from the 5-methyl group of thymine and 5-methylcytosine to produce the 5-methyl radical of the two pyrimidine bases (Figures 1.1 and 1.2) (21). In addition, the 5-methyl radical may also form from one-electron oxidation of the pyrimidine bases followed by deprotonation (22,23). The 5-methyl radical can be transformed to produce 5-hydroxymethyl-2′-deoxyuridine (5-hmdU) and 5-formyl-2′-deoxyuridine (5-fdU) (24-26), 5-hydroxymethyl-2′-deoxycytidine (5-hmdC) and 5-formyl-2′-deoxycytidine (5-fdC) (22). Along this line, it was found recently that the oxidation of 5-mdC could also be catalyzed by Fe(II)- and 2-oxoglutarate (2-OG)-dependent ten-eleven translocation (TET) family dioxygenases (27-29). The resulting 5-hmdC, 5-fdC and 5-carboxyl-2′-deoxycytidine (5-cadC) can be considered as epigenetic marks (Figure 1.2) (29-34). In addition, the removal of 5-fdC and 5-cadC by the base excision repair (BER) machinery is thought to play an important role in active cytosine demethylation in mammalian systems (31,35). Aside from being an oxidation product of thymidine, 5-hmdU may also arise from the deamination of 5-hydroxymethyl-2′-deoxycytidine (5-hmdC) (36,37). In addition, Pfaffeneder *et al.* (38) reported that TET enzymes could catalyze directly the formation of 5-hmdU from thymidine in DNA of mouse embryonic stem cells (mESCs), and they also found that the deamination of 5-hmdC did not contribute significantly to the 5-hmdU

level in mESCs (Figure 1.2) (38). 5-fdU can be formed from thymidine by exposure to ionizing irradiation, one-electron photooxidation and Fenton-type reactions and its yield was similar or somewhat lower than that of 8-oxo-dG (26,39-42).

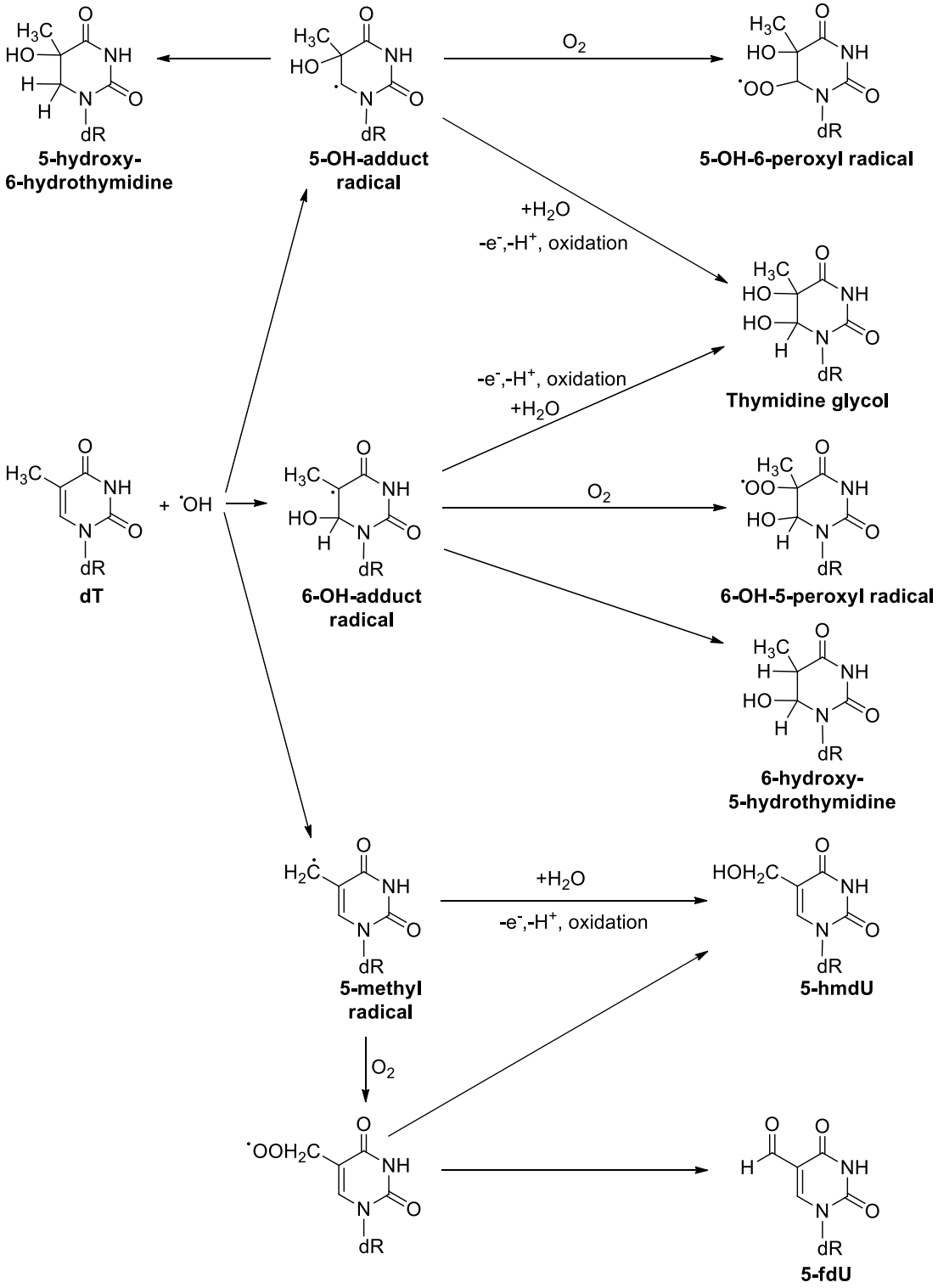


Figure 1.1.Pathways for hydroxyl radical-mediated oxidation of dT.

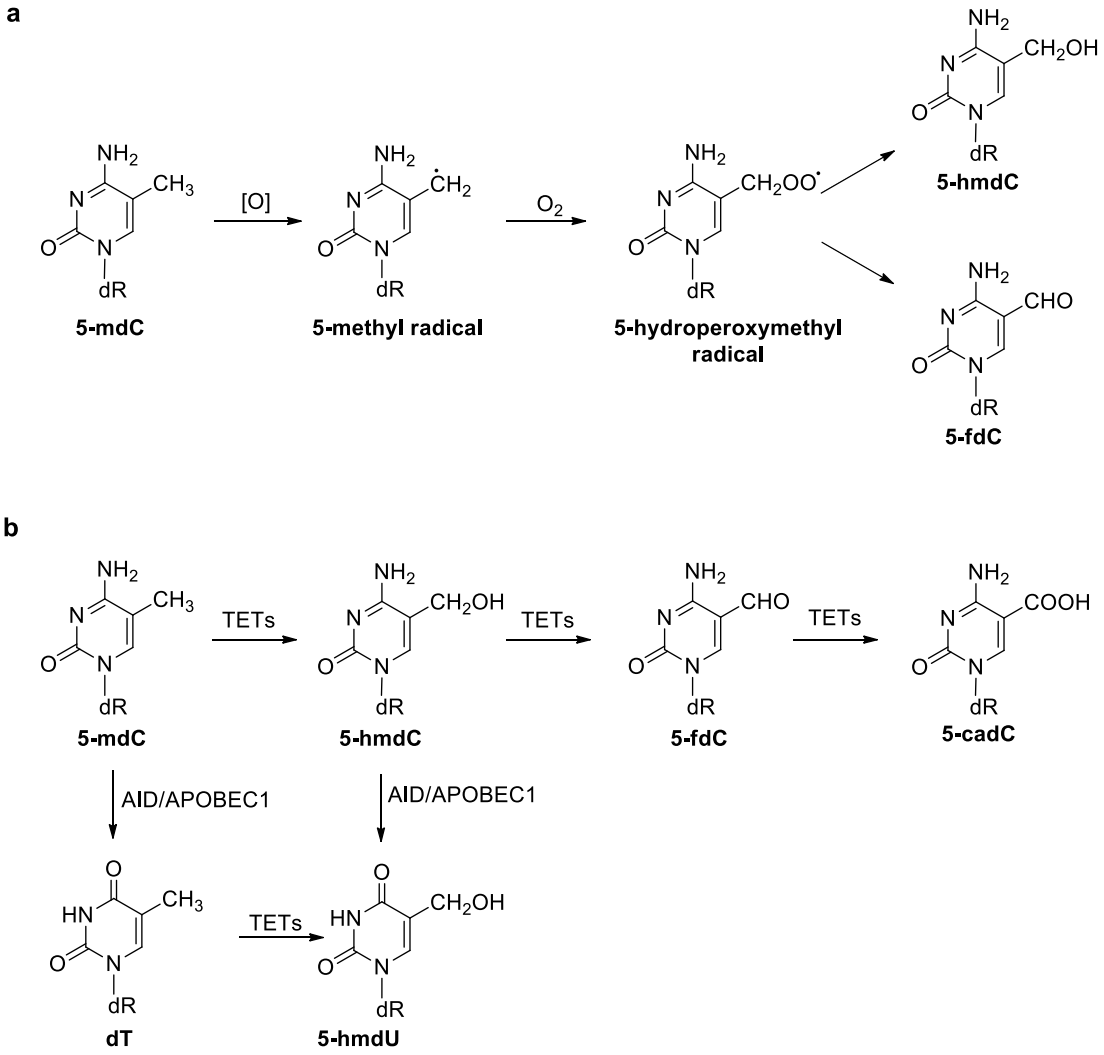


Figure 1.2.Oxidation pathways of 5-mdC. a. ROS-induced oxidation of 5-mdC; b. TET-mediated oxidation of 5-mdC.

Apart from the above-mentioned single-nucleobase lesions, ROS may also induce the formation of bulky DNA lesions. In this context, exposure to ROS from a variety of experimental system was found to induce CC→TT and mCG→TT tandem base substitutions, suggesting that ROS may induce the formation of intrastrand cross-link lesions (43-46). In addition, Randerath *et al*. (47,48), by using thin-layer chromatography

(TLC) analysis of ^{32}P-postlabeled DNA digestion products, demonstrated the existence of I (indigenous)-compounds, the bulky DNA modifications which increase markedly with aging in tissues of healthy laboratory animals and are derived from endogenous reactive intermediates of nutrient and oxygen metabolism. Especially, the type II I-compounds include several bulky DNA lesions, which are enhanced by treatment with a pro-oxidant carcinogen ferric nitrilotriacetate (Fe-NTA) in kidney DNA of rodents and are identical to these lesions generated in DNA or oligodeoxyribonucleotides (ODNs) treated with Fenton reagents *in vitro* (47). Later, a modified ^{32}P-postlabeling assay demonstrated that four type II I-compounds in mammalian tissue DNA are dinucleotides containing the bulky 5'*S* diastereomer of 8,5'-cyclo-2'-deoxyadenosine (cdA) as the 3' nucleoside (49). The dinucleotides arise from the incomplete hydrolysis of the phosphodiester bond on the 5' side of the modified nucleoside with the enzymes used in the ^{32}P-postlabeling assay (49).

The formation of purine cyclonucleosides (cPus) was proposed to arise from a single hydroxyl radical attack via a two-step mechanism (Figure 1.3) (50,51). In this respect, hydroxyl radical abstracts a hydrogen atom from the C5' of 2-deoxyribose, yielding a carbon-centered radical, which attacks the C8 of adenine or guanine to form a new C-C bond. The resulting conjugate can lose an electron and a proton to give cdA and cdG. Molecular oxygen can inhibit this reaction by directly reacting with the C5' radical, thereby preventing intramolecular cyclization (52,53). The above cyclization reaction yields two diastereomers at similar frequencies in calf thymus DNA exposed to ionizing radiation under anaerobic conditions (54). However, the 5'*R* diastereomers of cdA and

cdG were induced in calf thymus DNA by Fenton-type reagents at markedly higher levels than the 5'*S* counterparts, with cdG being produced at a higher yield than cdA (55). Moreover, the cPus could be detected at appreciable levels in cells and animal tissues (56-63).

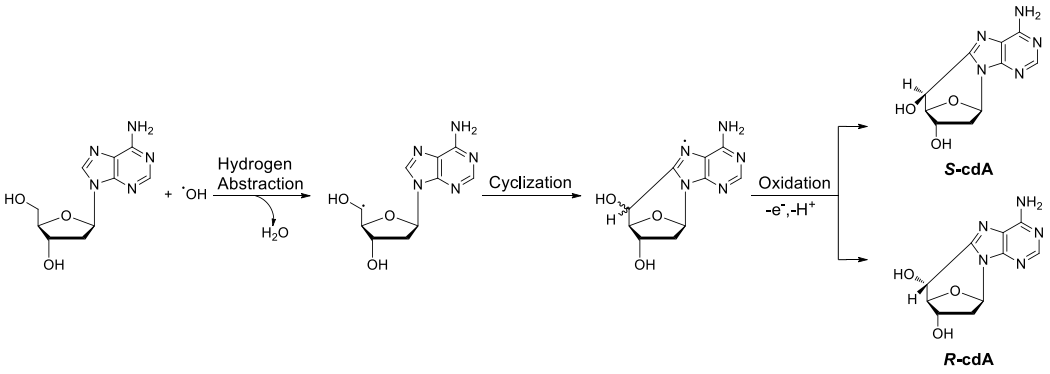


Figure 1.3.Proposed mechanism for the formation of 5'*R*- and 5'*S*-diastereomers of 8,5'-cyclo-2'-deoxyadenosine.

ROS can also attack biomolecules other than DNA. Specifically, hydroxyl radical initiates the peroxidative degradation of lipids by abstracting a hydrogen atom from polyunsaturated fatty acids (PUFA) (20,64-71). The resulting lipid radical (L$^{\bullet}$) is first converted to a lipid peroxyl radical (LOO$^{\bullet}$) in the presence of O_2, leading to the formation of a lipid hydroperoxide (LOOH) via hydrogen atom abstraction, and finally to an alkoxyl radical (LO$^{\bullet}$) by the transition metal ion-catalyzed Fenton-type reaction. Further fragmentations of peroxyl and alkoxyl radicals give rise to reactive aldehydes, including malondialdehyde (MDA), acrolein, crotonaldehyde, 2-hexenal, 4-hydroxy-2-hexenal (HHE), 4-hydroxy-2-nonenal (HNE), 4-oxo-2-nonenal (ONE), 4-hydroperoxy-(2*E*)-nonenal (HPNE), 9,12-dioxo-(10*E*)-dodecenoic acid (DODE), 5,8-dioxo-(10*E*)-octenoic acid (DOOE), 2,4-decadienal (DDE) and 4,5-epoxy-(2*E*)-decenal (EDE), etc. (Figure 1.4) (19,20,71).

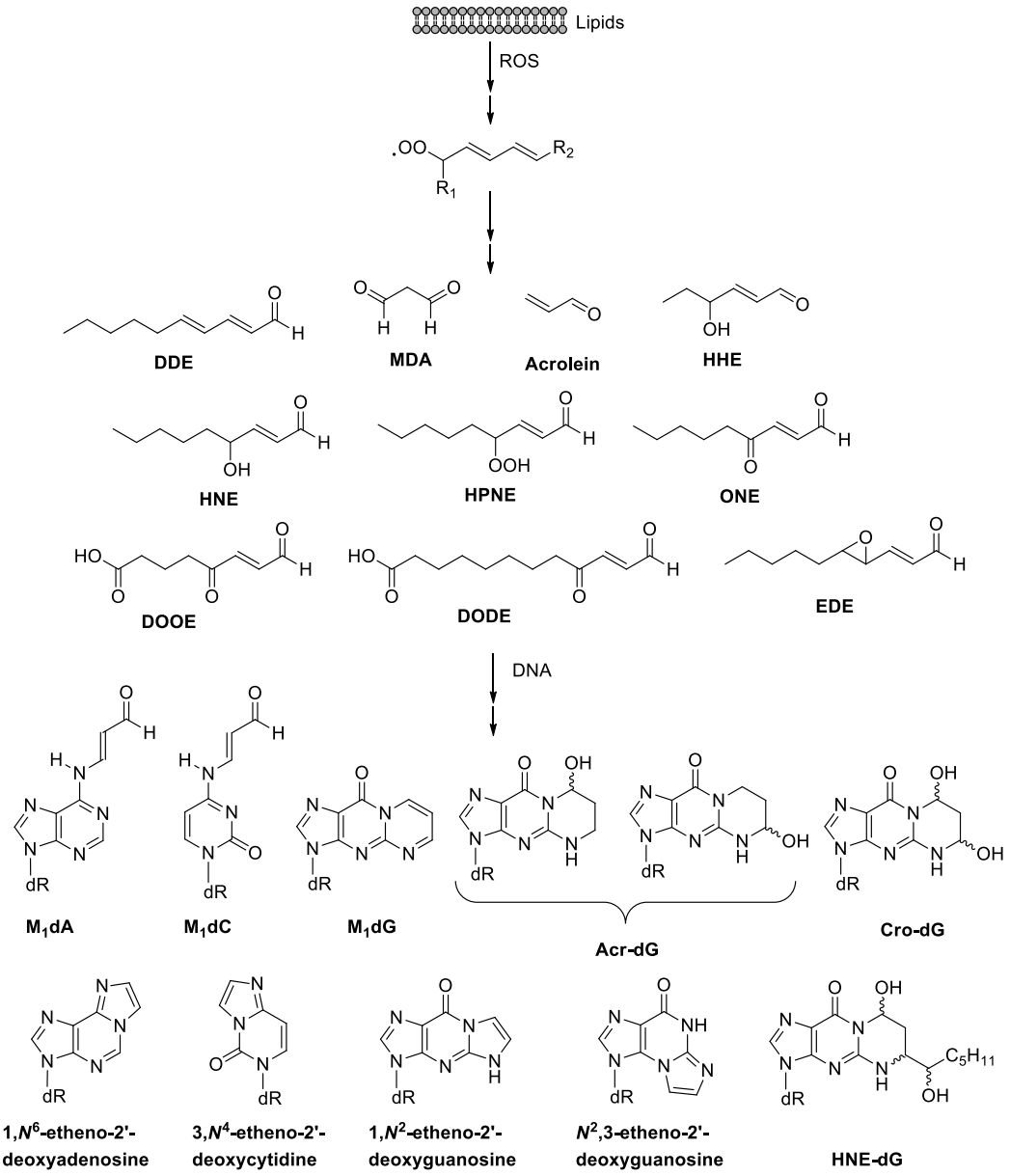


Figure 1.4.Structures of representative lipid peroxidation (LPO) products and LPO products-induced DNA adducts.

The aldehydes formed from lipid peroxidation can react with DNA to generate a variety of DNA adducts (Figure 1.4) (19,20,71). In this vein, malondialdehyde reacts with guanine, adenine and cytosine in DNA to form exocyclic pyrimido-[1,2-α]purine-

10(3*H*)-one-2'-deoxyribose (M_1dG), linear N^6-(3-oxopropenyl)-2'-deoxyadenosine (M_1dA) and N^4-(3-oxopropenyl)-2'-deoxycytidine (M_1dC), respectively (Figure 7) (20). The α,β-unsaturated LPO products, such as acrolein, crotonaldehyde and HNE, can lead to the formation of different diastereomers of exocyclic six-membered ring propano adducts in DNA with or without substituted alkyl side chains. The α,β-unsaturated aldehydes can undergo Michael addition with the N^2-amino group of dG to give N^2-(3-oxopropyl)-dG adducts, followed by cyclization of *N*1 with the aldehyde moiety to generate the corresponding exocyclic 1,N^2-propano-dG products (Acr-dG, Cro-dG, and HNE-dG, etc.) (72). This cyclization is reversible, and the ensuing release of the aldehyde functionality can induce the generation of DNA interstrand cross-links and DNA-protein cross-links (19,73,74). Along this line, it is worth noting that the unsubstituted Cro-dG can also arise from consecutive reactions of guanine with two molecules of acetaldehyde (75).

Another type of LPO-induced DNA adducts, etheno adducts, possess unsaturated five-membered exocyclic rings attached to nucleobases. Previous studies proposed a putative mechanism for the formation of etheno adducts from HNE-derived epoxide intermediate, where the α,β-unsaturated HNE can be converted to reactive intermediate 2,3-epoxy-4-hydroxynonanal by auto-oxidation or by oxidation with H_2O_2 (66,67,76,77). The resulting reactive epoxy aldehyde can further react with DNA to yield the etheno adducts with or without substituted alkyl side chains, such as 1,N^6-etheno-2'-deoxyadenosine (εdA), 3,N^4-etheno-2'-deoxycytidine (εdC), 1,N^2-etheno-2'-deoxyguanosine (1,N^2-εdG) and N^2,3-etheno-2'-deoxyguanosine (N^2,3-εdG), etc

(66,67,76,77). N^2,3-εdG can also be induced in DNA from exposure to carcinogen vinyl chloride via a similar epoxide initiation mechanism (78). Additionally, Lee *et al*. (79,80) demonstrated possible HNE-independent pathways for the formation of 1,N^2-εdG initiated from either another LPO product EDE or HNE precursor HPNE, suggesting the existence of probable controversies concerning the mechanism for the formation of etheno DNA adducts *in vivo*. The above-mentioned DNA adducts emanating from products of LPO could be detected at appreciable levels *in vivo* (60,75,81-97).

Repair and biological consequences of oxidative-stress induced DNA lesions

To minimize mutation induction and to maintain genome integrity, cells are equipped with multiple DNA repair systems to enable efficient removal of DNA lesions from the genome. Unrepaired DNA lesions may elicit cytotoxic and mutagenic effects by perturbing the accuracy and efficiency of DNA replication and transcription. Chemical synthesis of ODNs harboring site-specifically inserted and structurally defined DNA lesions, along with *in-vitro* biochemical assay and shuttle vector-based cellular experiments, has provided important insights into how the oxidative stress-induced DNA lesions are repaired and how they compromise the flow of genetic information by inhibiting DNA replication and transcription and inducing mutations in these processes (98,99).

5-hmdU formed from dT oxidation pairs with dA, while 5-hmdU produced by oxidation and deamination of 5-mdC pairs with dG. Earlier studies of 5-hmdU focused on its role as an oxidatively induced DNA lesion from dT and revealed that the modified nucleoside is weakly mutagenic (100), does not block DNA polymerases (101), pairs

with dA in Watson-Crick geometry (102), and it even replaces thymidine in bacteriophage DNA (103). The excision activity of 5-hmU in 5-hmU:A pair was much lower than that in 5-hmU:G pair by human cell extracts (104). 5-hmU:G can be excised by TDG, SMUG1, MBD4 (105-108) and with some weak activity by NEIL1 (107). SMUG1 was also found to remove 5-hmU:A, albeit with lower activity (105). These attributes of 5-hmdU are in agreement with the recent hypothesis that this modified nucleoside may assume an epigenetic role (38,109). The occurrence, repair, and biological consequences of 5-hmdU were previously reviewed (110,111).

5-fdU does not strongly block DNA polymerases (112). Although high-fidelity DNA polymerases can incorporate any of the 4-dNTPs opposite the lesion *in vitro*, 5-fdU is weakly mutagenic (0.01 – 0.04% mutation frequencies in double-stranded vectors) and it induces T→G and T→A transversions in simian COS-7 cells (113). 5-fdU is predominantly repaired by the BER pathway. AlkA in *E. coli* (114-116) and SMUG1 in mammalian cells (117-119) are the major enzymes for the removal of 5-fdU from DNA. Nth, Fpg and Nei in *E. coli*, SpNth1 in *Schizosaccharomyces pombe* (a homolog of *E. coli* endonuclease III), human Nth1 and Mbd4, and mouse Nth1 and Tdg can also excise 5-fdU from DNA (117,120-123). Similar as 5-hmU, 5-fdU in DNA exists as 5-fU:A (formed from A:T base pair) or 5-fU:G (formed from 5mC:G base pair). The former form can be removed by *E. coli* AlkA protein (114,115) and the latter may be repaired by AlkA protein and MutHLS mismatch repair system (e.g. *E. coli* mismatch uracil DNA glycosylase, Mug) (116,120), suggesting the involvement of MMR pathway in the repair of 5-fdU. Meanwhile, repair initiated by SMUG1 can excise 5-fdU opposite any of the

four nucleobases, with the highest activity towards 5-fU:C and 5-fU:T (119). Subsequent repair process will lead to T→G and T→A transversions, which is in agreement with the T→G and T→A transversions induced by this lesion in mammalian cells. In addition, KsgA was recently reported to remove 5-fU:C mispair in *E. coli*, and mutation in ksgA resulted in increased spontaneous mutations in *mutM mutY* and *nth nei* background (124). The repair of 5-fdU was also found to be modulated by a nearby apurinic/apyrimidinic (AP) site. When an AP site is located directly opposite 5-fdU, it is repaired through long-patch BER pathway; by contrast, when the AP site is shifted it is primarily repaired by the short-patch BER pathway (125).

Previous studies have provided significant insights about how the oxidized 5-mdC derivatives influence the efficiency and accuracy of DNA replication and transcription. An *in vitro* mutagenesis assay illustrated that, among the oxidized 5-mdC derivatives, only 5-fdC is marginally mutagenic, leading to 1-2% C→T transition (126). 5-hmdC, 5-fdC and 5-cadC are slightly mutagenic in *E. coli* cells, where C→T transition mutation occurs at frequencies of 0.17-1.12% (127). In this vein, 5-fdC was found to block DNA replication and lead to mutation in simian COS-7 cells, with bypass efficiencies and mutation frequencies being 39-90% and 0.03-0.28%, respectively (128). Moreover, Ji *et al*. (129) demonstrated that, in HEK293T human embryonic kidney epithelial cells, 5-fdC and 5-cadC constituted modest blocks to DNA replication (with a 30% reduction in bypass efficiencies) without inducing detectable mutations in human cells, whereas replicative bypass of 5-hmdC is highly accurate and efficient.

An *in vitro* assay demonstrated that the yeast and mammalian RNA polymerase II (Pol II)-mediated polymerization rates and specificity constants for GTP incorporation against 5-fC and 5-caC were reduced significantly compared with those for unmodified C template, whereas no changes were observed for 5-mC and 5-hmC templates (130). Additionally, the substrate specificity was reduced by ~30 fold for 5-fC-containing template in comparison with C template (130). Later, You *et al*. (129) revealed that 5-fC and 5-caC displayed marginal mutagenic (~0.7-1.7%) and modest inhibitory (31-50%) effects on transcription mediated by T7RNAP, or human RNA polymerase II (hRNAPII) *in vitro* and in HEK293T cells. In addition, 5-hmC did not compromise appreciably the efficiency or accuracy of transcription *in vitro* or in HEK293T cells (129). The lack of pronounced deleterious effects of 5-hmC, 5-fC and 5-caC on replication or transcription is in keeping with the potential roles of these oxidized 5-mC derivatives in epigenetic regulation.

Different from the passive DNA cytosine demethylation where 5-mdC is diluted during replication (131,132), it has been proposed that the Tet-mediated oxidation of 5-mdC to 5-fdC and 5-cadC may play an important role in active cytosine demethylation in mammals, a process that results in the loss of 5-mdC independent of DNA replication. Along this line, the excision of 5-fdC and 5-cadC from DNA by thymine DNA glycosylase (TDG) and the following action through the BER pathway may result in the restoration with unmodified cytosine (30,133). It was found that genetic depletion or catalytic inactivation of TDG leads to embryonic lethality in mice (106,134), indicating the significant roles of TDG in maintaining epigenetic stability during embryonic

development. An alternative active cytosine demethylation pathway was also proposed: The AID (activation-induced cytidine deaminase)/APOBEC (apolipoprotein B mRNA editing enzyme, catalytic polypeptide-like) proteins can deaminate 5-hmdC to give 5-hmdU, which is then removed by TDG or SMUG1 (single-stranded-selective monofunctional uracil DNA glycosylase 1) and finally restored to unmodified cytosine through BER (36,106). Nevertheless, this mechanism is still controversial because the purified AID/APOBEC proteins exhibit no detectable activity toward 5-hmC deamination *in vitro* (135).

Multiple lines of evidence support that cdA and cdG are repaired by the NER pathway. First, cleavage products of cdA-containing duplex DNA emanating from NER activity in human cell nuclear extract was observed, and depletion of XPA protein led to a pronounced decrease in such cleavage (136). By contrast, no correction of the lesion by direct damage reversal or base excision repair was detected (136). Second, genetic depletion of ERCC1 gave rise to elevated accumulation of cdA and cdG in mouse tissues (57,63). Third, transcriptional bypass assay revealed that cdA and cdG are substrates for transcription-coupled NER pathway in mammalian cells (137).

cdA and cdG were found to be strong blockades to DNA replication, and replicative bypass of these lesions are highly mutagenic. With the use of DNA containing a site-specifically inserted cdA as template, both the 5′*R*- and 5′*S*-diastereomers of cdA were observed to block primer extension by replicative polymerases, including human DNA polymerase δ and T7 DNA polymerase (136,138). *S*-cdA and *S*-cdG were strongly blocking to DNA replication in *E. coli* and human cells and induced substantial

frequencies of mutations at the lesion sites, where cdA induces A→T mutation, and cdG induces mainly G→A and G→T mutations (139-141). Additionally, Pol η, Pol ι, and Pol ζ, but not Pol κ, assume crucial roles in promoting replication across *S*-cdA and *S*-cdG in human cells (141), and Pol V plays a major role in bypassing these lesions in *E. coli* (139,140).

It was found that both *S*-cdA and *S*-cdG strongly inhibited transcription and induced transcriptional mutagenesis *in vitro* and in mammalian cells (137,142). Different from the observations made from replication studies, *S*-cdA and *S*-cdG primarily induce a 5'-A mutation during transcription in human cells, where the lesions direct human RNA polymerase II to misincorporate an adenosine nucleotide opposite the template base situated on the 5' side of the lesions. Furthermore, when placed on the template strand of an actively transcribed gene, both *S*-cdA and *S*-cdG were primarily repaired by transcription-coupled NER pathway in mammalian cells (137).

Previous *in vitro* primer extension assay showed that both human Pol α and Pol β were primarily blocked by LPO-induced etheno DNA adduct εdA with minimal extension (143). Pol η was capable of catalyzing a substantial amount of bypass across the lesion, where the polymerase incorporated all four nucleotides opposite εdA with different preferences. Human Pol ι, a paralog of Pol η, was blocked by εdA with a very small amount of synthesis past εdA, which results in insertion of C and, to a much lesser extent, T, opposite εdA (143). The mutagenic potential of εdA was also investigated using a single-stranded shuttle vector system in *E. coli* and in COS7 simian kidney cells. A non-mutagenic dTMP incorporation opposite εdA was found as the nearly exclusive

event in *E. coli*; the lesion is, however, highly mutagenic in COS7 cells, which leads to a very high frequency of A→G transition (63%), followed by A→T (6%) and A→C (1%) transversions (144). Different from what was observed in COS7 cells, εdA induced all three possible base substitutions at similar frequencies (1.5-3% each) in HeLa human cervical cancer cells (145). Levine *et al*. (146) also reported that, when placed on the leading strand, εdA induces A→T (7%), A→C (5%) and A→G (2%) mutations in HeLa human cervical cancer cells, and A→G (5%) and A→C (2%) mutations in HCT-116 human colorectal carcinoma cells. Similar as what was observed for εdA, the mutagenic properties of εdC were found to be strikingly different in *E. coli* and COS7 cells (2% in uninduced *E. coli* cells, 32% in SOS-induced *E. coli* cells, and 81% in COS7 cells) (147). 1,N^2-εdG is moderately mutagenic and directs the incorporation of the correct nucleotide (dCMP) in >80% of the replication events in *E. coli* (148). N^2,3-εdG specifically induces a very low frequency (0.5%) of G→A transition during DNA replication in *E. coli* (149). The above-mentioned etheno adducts can be repaired by multiple DNA repair pathways, including BER and AlkB/ALKBH family dioxygenases-mediated direct damage reversal, which were previously reviewed (150,151).

The mutagenicity of malondialdehyde (MDA)-induced DNA adducts was measured in the *lacZα* forward mutation assay in *E. coli* (152). The most common type of mutations induced by MDA were base-pair substitutions (76%), though frameshift mutations were detected in 16% of the induced mutants and they were comprised of mainly single-nucleotide additions in runs of reiterated bases (152). Modified genomes containing a C opposite M_1G resulted in roughly equal frequencies of G→A and G→T

mutations with few G→C mutations. The (-)-strand was replicated only 20% of the time when M_1dG was present. M_1dG was also found to be a substrate for the NER pathway in *E. coli* (153). In addition, MDA-induced mutations, such as large insertions and deletions, were found after lesion-carrying shuttle vectors undergo replication in human cells (154). Furthermore, replication studies also demonstrated that M_1dG can induce -1 and -2 frameshift mutations when positioned in a reiterated $(CpG)_4$ sequence, but not when positioned in a non-reiterated sequence in *E. coli* or COS-7 cells (155). Recently, Singh *et al*. (156) revealed that AlkB could repair Acr-dG and M_1dG *in vitro*, suggesting an important role for the AlkB family of dioxygenases in protecting against the deleterious biological consequences of acrolein- and MDA-induced DNA adducts *in vivo*. For more detailed discussion about the mutagenic consequences, replication bypass and repair of DNA lesions induced by lipid peroxidation byproducts, the readers should consult a recent review by Minko *et al* (19).

Implications of oxidative-stress induced DNA lesions in human diseases

The oxidative stress-induced DNA lesions may have significant impact on human health, including the natural processes of aging, neurodegeneration and carcinogenesis. Recently, the development of LC-MS coupled with isotope-dilution method for the unambiguous identification and accurate quantification of multiple DNA lesions, have provided profound insights into the involvement of DNA lesions in different pathological conditions (157-159).

5-hmdU can be produced from oxidative stress as well as epigenetic machinery (i.e. Tet-mediated oxidation of thymidine). 5-hmdU has been detected in murine and

human tissues (160), although the physiological implications are less well explored. A number of studies have been conducted in measuring 5-fdU. Earlier quantification of 5-fdU in DNA was performed using GC-MS analysis of the modified nucleobase released from DNA with the use of formic acid or 70% (w/w) hydrogen fluoride in pyridine (39,40). Stable isotope dilution coupled with LC-MS/MS was later developed for the quantification of 5-fdU, but with relatively poor detection limit (161). Derivatization with Girard reagent T significantly improved the detection limit and has been applied for the detection of 5-fdU in DNA of HeLa-S3 cells (162) and *Trypanosoma brucei* (163). 5-fdU has also been detected in various tissues of LEA and LEC rats with LC-MS/MS/MS in the negative-ion mode (56). Higher levels of 5-fdU were observed in the liver of 3-month old LEC rats (56), which model Wilson disease, a disease characterized by hepatitis and hepatocellular carcinoma (164). Wilson's disease arises from mutations in *ATP7B*, which encodes a transporter protein required for hepatic excretion of copper ions (164). This results in accumulation of copper ion and increased ROS production (165,166). This finding provides a vivid illustration of the role of oxidative DNA damage in transition metal-induced diseases such as Wilson's disease.

Global 5-hmC levels are lower in a variety of human cancers including breast, liver, lung, pancreatic and prostate cancers than in normal tissues (132). One mechanism to explain this is that cancer-related gain-of-function mutations in *IDH1* and *IDH2* genes cause an increase in production of the oncometabolite (*R*)-2-hydroxyglutarate ((*R*)-2-HG) instead of production of the normal product 2-oxogluterate (2-OG). In contrast, cancer-related mutations in two Krebs cycle genes, fumarate hydratase (*FH*) and succinate

dehydrogenase (*SDH*), lead to accumulation of their substrates, fumarate and succinate, respectively. (*R*)-2-HG, succinate and fumarate, which are structurally similar to 2-OG, act as competitive inhibitors of 2-OG-dependent TET activity, leading to diminished levels of 5-hmC in some tumors (167-175). Additionally, Jin *et al*. (176) reported pronounced depletion of 5-hmdC in multiple human cancers in an *IDH* mutation-independent manner, indicating the existence of alternative mechanism(s) involved in the loss of 5-hmdC. Together, the data suggest that 5-hmdC levels may serve as a useful molecular biomarker for cancer detection and diagnosis (176).

It has been shown that 5-hmC, 5-fC and 5-caC may serve as epigenetic marks in addition to being intermediates for active cytosine demethylation in mammals (33,34,60,177,178). In this vein, 5-hmC, 5-fC and 5-caC are recognized by some specific cellular proteins critical for chromatin remodeling and transcriptional regulation (179-185). Thus, the homeostasis of these oxidized 5-mdC derivatives is crucial for maintaining normal cellular function, whereas the loss or aberrant accumulation of these epigenetic marks may lead to deleterious biological consequences and diseases. For instance, LC-MS/MS results revealed a significantly lower level of 5-hmdC in liver of diseased LEC rats compared to control LEA rats, though no difference was found in the levels of 5-mdC (60). *In vitro* biochemical assays showed that Cu^{2+} ions could directly inhibit the activity of TET enzymes, suggesting that in LEC rats perturbation of 5-hmdC-mediated epigenetic signaling contributes to the etiology of Wilson's disease (60).

The implication of bulky DNA lesions was also investigated. Markedly elevated levels of 5′*R*- and 5′*S*-diastereomers of cdA and cdG were found in the liver of LEC rat

model of Wilson's disease (56). Moreover, the levels of these lesions increased with age in the liver and brain of LEC rats, illustrating a correlation with disease progression (56). cPus also accumulate in the genomic DNA of wild-type mice with age, providing further evidence of accumulation of endogenous lesions over the lifespan of mammals and a potential contribution of these lesions to aging (57). Mitra *et al*. (61) detected greater levels of cPus lesions in the skin of a murine model of human melanoma. The increase in cPus levels is ultraviolet radiation-independent but pheomelanin pigment dependent, suggesting that pigment-driven oxidative stress and the resultant oxidative DNA damage contribute to melanoma in humans even in the absence of UV exposure (61).

In an earlier review, Brooks (52) proposed that chemically stable bulky DNA lesions, such as cPus, may play a crucial role in neurodegeneration in XP patients (186) Since brain is not directly exposed to sunlight, the accumulation of ROS-induced bulky DNA lesions in brains of XP patients may contribute to neuron loss in these patients. In support of this, in *Ercc1*$^{-/\Delta}$ mice, with defective nucleotide excision repair of cPus and progressive neurodegeneration (187), the lesions accumulate more rapidly in brain than in normal mice. However, as neurodegeneration progresses, the number of cPus decreases significantly in brain, suggesting a direct causal role of oxidative DNA damage in the loss of neurons in the brain (57). A recent technique improvement by employing nano-flow liquid chromatography-nanoelectrospray ionization coupled with tandem mass spectrometry provided much better sensitivity in measuring cPus as well as LPO-induced εdA and εdG lesions in liver and brain tissues of LEA and LEC rats (60). Simultaneous quantification of these two different types of lesions demonstrated a preferential

accumulation of direct ROS-induced cPus *in vivo* (60). This result indicates that cPus may contribute to the etiology of oxidative stress-induced diseases to a greater extent than the etheno adducts arising from byproducts of lipid peroxidation (60).

Earlier reviews discussed the application of LPO-induced DNA lesions as potential biomarkers for cancer risk assessment in humans with cancer-prone diseases such as chronic pancreatitis, ulcerative colitis, or Crohn's disease, as well as in patients with alcohol abuse-related chronic hepatitis, fatty liver, fibrosis, or cirrhosis (81,188). Results from an isotope dilution-capillary LC-MS/MS method, revealed a significant increase in levels of Acr-dG in Alzheimer's disease (AD) patients compared to controls in DNA isolated from the hippocampus/parahippocampal gyrus (189). This, along with the existence of potential acrolein-derived DNA-peptide cross-links (72), provides evidence to support the correlation between acrolein-induced DNA damage and AD pathogenesis. The LPO-induced bulky exocyclic 1,N^2-propano-dG adducts may play a significant role in driving congenital abnormalities, myelodysplasia, acute myeloid leukemia (AML) and certain solid tumors in patients suffering from Fanconi anemia (FA) (190-192). FA is an autosomal recessive disease caused by deficiency in the repair of DNA interstrand cross-links. As discussed previously, the DNA interstrand cross-links generated from the ring-open form of 1,N^2-propano-dG are likely substrates of FA repair pathway and, if left unrepaired, these crosslinks impede replication and transcription, causing chromosomal breaks and translocations that can drive disease in FA patients (193).

_N_-nitroso compounds (NOCs)

Human genome is continuously assaulted by a variety of endogenous and exogenous toxicants which can give rise to DNA damage and compromise genomic integrity (194). DNA carboxymethylation can be induced upon the exposure of DNA to either *N*-nitroso compounds (NOCs) or other carboxymethylating agents (195-200). Specifically, the NOCs consist of a nitroso group (-N=O) bound to a nitrogen atom. Humans are constantly exposed to series of exogenous NOCs which are often found in foods, tobacco, and pharmaceutical products. For instance, it is firstly confirmed the environmental occurrence of the trace of NOCs, *N*-nitrosodimethylamine (NDMA), in nitrite-preserved herring used in sheep fodder (201). Later a variety of NOCs, i.e. NDMA, *N*-nitrosodiethylamine, *N*-nitrosopyrrolidine, *N*-nitrosopiperidine, were wildly found in beer, bacon, sausage, cured meats and pickles (202). Tobacco-specific nitrosamines (TSNAs) are the nitrosation products of nicotine and related alkaloids, which are only observed in tobacco. Several tobacco-specific nitrosamines, i.e. *N*'-nitrosonornicotine (NNN), 4-(methylnitrosamino)-1-(3-pyridyl)-1-butanone (NNK), 4-(methylnitrosamino)-1-(3-pyridyl)-1-butanol (NNAL), *N*'-nitrosoanatabine (NAT), *N*'-nitrosoanabasine (NAB), 4-(methylnitrosamino)-4-(3-pyridyl)-1-butanol (*iso*-NNAL), and 4-(methylnitrosamino)-4-(3-pyridyl) butanoic acid (*iso*-NNAC) have been identified in tobacco products (203-206). The nitrosation of nicotine and its demethylation product nornicotine can lead to the formation of NNK and NNN, respectively. Further reduction of NNK can generate NNAL. NAB and NAT are derived from nitrosation of anabasine and anatabine, respectively (203,204,206). Chemotherapeutic alkylnitrosoureas, i.e. 1,3-

bis(2-chloroethyl)-1-nitrosourea (BCNU); 1-(2-chloroethyl)-3-cyclohexyl-1-nitrosourea (CCNU); 1-(2-chloroethyl)-3-methylcyclohexyl-1-nitrosourea (meCCNU); 1-(4-arnino-2-methyl-5-pyrimidinyl)-methyl-3-(2-chloroethyl)-3-nitrosourea (ACNU) and the monofunctional nitrosourea derivative streptozotocin, have been applied as chemotherapeutic anti-cancer medicines for a series of tumors including small cell lung cancer, lymphomas, mycosis fungicides, multiple myeloma, glioma and malignant melanoma (207,208).

Despite the prevalence of these exogenous sources, a significant amount of NOCs are generated from endogenous agents. It has been estimated that 45-75% of the total human exposure to NOCs occurs *in vivo* (209,210). Endogenous NOCs are generated from the nitrosation of amines and amides in stomach and intestine. The major reactions involved in this process are listed in the equations below (Figure 1.5).

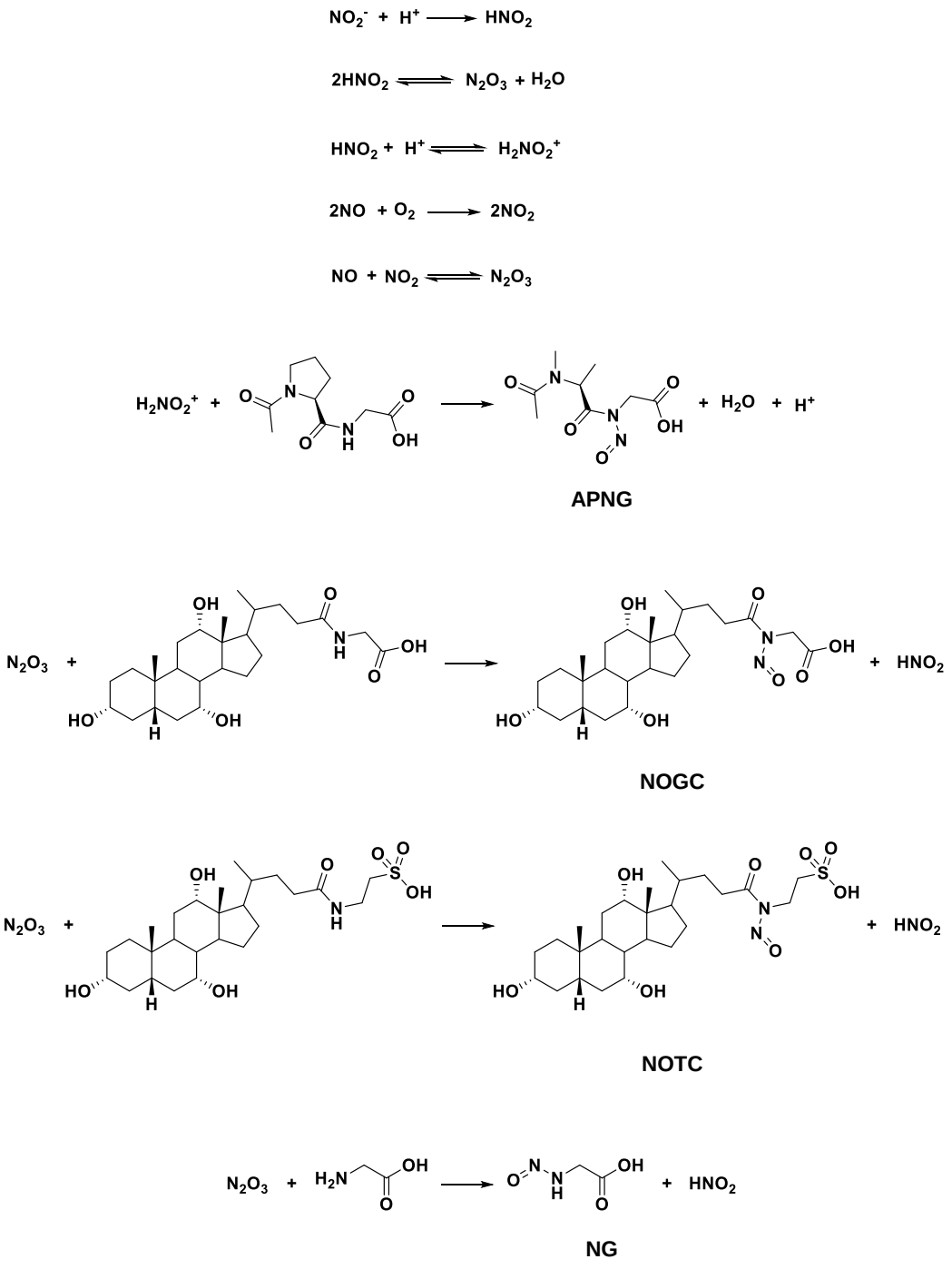


Figure 1.5.Formation process of typical endogenous NOCs.

On one hand, the acidification of nitrite (NO_2^-) in the low pH environment of stomach yields nitrous acid, which can be further acidified to generate $H_2NO_2^+$. The resulting $H_2NO_2^+$ can react with amide to produce *N*-nitrosamide, i.e. *N*-(*N*^{6}-acetyl-L-prolyl)-*N*-nitrosoglycine (APNG) (Figure 1.5) (211-213). One the other hand, endogenous nitric oxide (NO), arising from chronic inflammation (i.e. inflammatory bowel disease (IBD) and *Helicobacter pylori*-induced gastritis), microbiota and red meat derived heme-NO, can be readily oxidized into nitrogen dioxide (NO_2) (Figure 1.5) (214-216). The reaction between HNO_2 and NO or two molecules of HNO_2 can further lead to the formation of N_2O_3, which can nitrosate amines, leading to the formation of *N*-nitrosamine, including *N*-nitroso bile acid conjugates (e.g. *N*-nitrosoglycocholic acid (NOGC) and *N*-nitrosotaurocholic acid (NOTC)) as well as *N*-nitrosoglycine (NG) (Figure 1.5) (211-213).

Formation of carboxymethylated DNA adducts

N-Nitroso bile acid conjugates, such as NOGC and NOTC, have previously been reported to exert mutagenic activity. Incubation of calf thymus DNA with NOGC *in vitro* generated *N*7-carboxymethylguanine (*N*7-CMG), *N*3-carboxymethyladenine (*N*3-CMA), and *O*^{6}-carboxymethylguanine (*O*^{6}-CMG) lesions (Figure 1.6) (195,199). Other reactive agents, such as APNG, NG, potassium diazoacetate (KDA) and the pancreatic carcinogen azaserine (AS) can also carboxymethylate DNA *in vitro* and *in vivo* (Figure 1.6). For instance, Harrison *et al*. (217) demonstrated the generation of *O*^{6}-CMdG in calf thymus DNA treated with azaserine, APNG, and KDA, with the levels at 7.3, 393.9, and 496 μmol of *O*^{6}-CMdG per mol of dG, respectively. KDA were also found to induce the

formation of *N*3-CMdT, O^4-CMdT, N^6-CMdA and N^4-CMdC in calf thymus DNA (210,218). In this line, *N*7-CMG were found in Lewis rat pancreatic acinar cells treated with [^{14}C]-azaserine (219). Similar, by using a novel LC-MS quantification method, Yu et al. demonstrated azaserine dose-dependent induction of O^6-CMdG in both GM04429 human skin fibroblasts and HCT-116 human colon carcinoma cells (220). In addition, Wang *et al*. (200) reported a non-NOCs agent glyoxal-induced formation of N^2-CMdG in calf thymus DNA as well as glyoxal and glucose HEK293T human kidney epithelial cells.

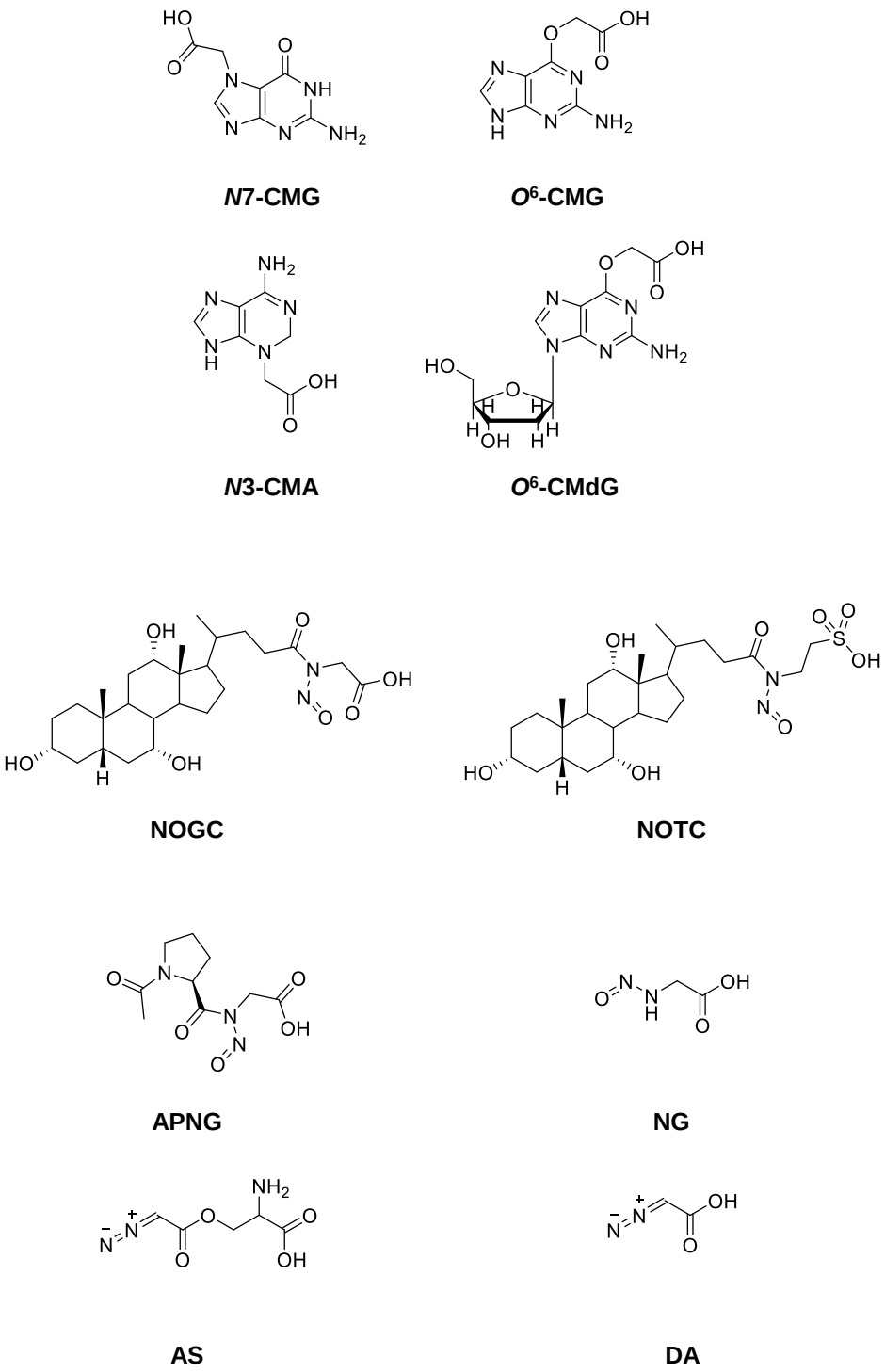


Figure 1.6.Carboxymethylated DNA lesions and typical carboxymethylating agents

It is proposed that DNA carboxymethylation induced by NOCs, KDA and AS requires the involvement of a highly reactive intermediate, diazoacetate (DA), which can further give rise to carboxymethyldiazonium and methyldiazonium ions, leading to the formation of carboxymethylated and methylated DNA, respectively (Figure 1.7) (210,221-223).

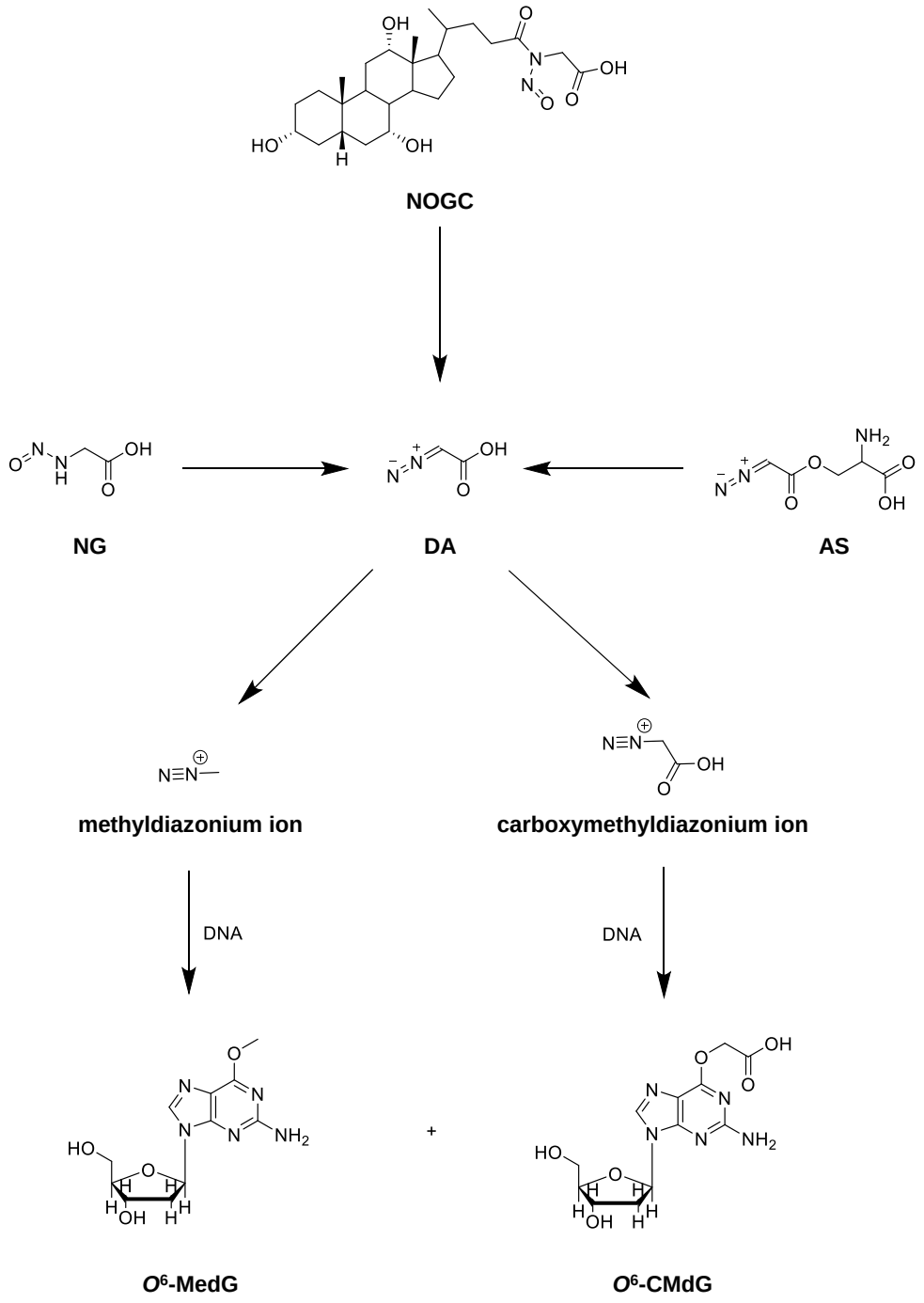


Figure 1.7.DNA carboxymethylation via diazoacetate (DA)

Biological consequences and repair mechanisms of carboxymethylated DNA adducts

The biological consequences and repair mechanisms of carboxymethylated DNA lesions have already been carried out during the past decades. Previous results of *in vivo* replication of KDA-treated shuttle vector harboring a human *p53* sequence in yeast cells demonstrated that KDA induced almost equal percentages of G → A transitions (35% in total mutations) as well as G → T (10-16% in total mutations) and A → T (12-20% in total mutations) transversions in human *p53* gene (221). In this line, site-specific mutagenesis by four carboxymethylated DNA lesions, N^6-CMdA, N^4-CMdC, *N*3-CMdT and O^4-CMdT was studied in *E. coli* cells by using next generation sequencing (140). Both N^6-CMdA and N^4-CMdC were not mutagenic and not able to block replication of DNA in wild-type AB1157 *E. coli* cells, with the bypass efficiencies being ~ 83% and 98%, respectively (140). In contrast, both *N*3-CMdT and O^4-CMdT were blocking in wild-type AB1157 *E. coli* cells, with the bypass efficiencies being 55% and ~49%, respectively. Both *N*3-CMdT and O^4-CMdT were highly mutagenic in wild-type *E. coli* cells, producing T → A transition and T → C transversion with mutation frequencies being 66% and 86%, respectively (140). Recently, by using a lesion-containing double-stranded shuttle vector replication assay in HEK 293T cells, Wu *et al*. (224) investigated comprehensively the effects of five carboxymethylated DNA lesions, O^6-CMdG, N^6-CMdA, N^4-CMdC, *N*3-CMdT and O^4-CMdT on the efficiency and fidelity of DNA replication in human cells. Similarly, neither N^6-CMdA nor N^4-CMdC was found to perturb DNA replication or induce mutations in HEK 293T cells, whereas *N*3-CMdT, O^4-CMdT and O^6-CMdG moderately perturbed DNA replication, inducing mutations of T →

A (81%), T → C (68%) and G → A (6.4%), respectively (224). In addition, *N*3-CMdT and O^4-CMdT were also found to compromise the fidelity and efficiency of DNA transcription in mouse embryonic fibroblast (MEF) cells (225). Previous studies showed that the lymphoblastoid cell lines derived from xeroderma pigmentosum complementation group A (XPA) patients were significantly more sensitive to DNA carboxymethylating agent azaserine than corresponding wild-type cells, indicating the involvement of NER pathway in repair of carboxymethylated DNA lesions (223). Moreover, O^6-CMdG were demonstrated to the substrate of a suicidal protein O^6-methylguanine-DNA-methyltransferase (MGMT) *in vitro*, which was previously reported to repair O^6-MedG *in vivo* (226).

Implications of carboxymethylated DNA lesions in human diseases

NOCs have been demonstrated to play important roles in carcinogenesis of certain cancers, including gastric and colorectal cancer (CRC) (201,211). A widely accepted model of the etiology of gastric cancer indicated that intragastric nitrosation may serve as a source of DNA damage during the early stages of cancer development (227). This hypothesis was supported by previous studies showed that red meat-rich diet can increase the risk of colorectal cancer. Lewin *et al*. (222) observed a red meat consumption induced marked increase of endogenous NOCs formation and the correlated significantly higher levels of O^6-CMG in colonic exfoliated cells. Recently, Hemeryck *et al.* (228) systematically studied the red meat consumption induced possible genotoxic effects compared to white meat, and the interfering role of dietary fat in Sprague-Dawley rats, with the liver, duodenum and colon DNA adductomes analyzed. Quantitative results

revealed that 22 DNA adduct types arising from alkylation, nitrosation and/or oxidation processes, were significantly increased upon the consumption of beef and/or fat-supplemented beef or chicken compared to chicken-only diet. This result was consistent with the current hypothesis that NOCs and LPOs can arise from red meat and high fat intake, and tend to give rise to DNA adducts (228). Moreover, Gottschalg *et al.* (221) explored the mutation pattern induced by NOCs *in vivo* and illustrated that the replication of KDA-treated, human *p53* gene-containing plasmid in yeast cells yielded a remarkable similar mutation pattern of *p53* gene as those found in human stomach and colorectal cancers, which was different from the one arising from DNA methylating agent MNU-treatment (221). In light of the previously reported 16:1 molar ratio between KDA-induced O^6-CMdG and O^6-MedG in calf thymus DNA, and the predominant G → A transition mutation induced by O^6-MedG, it was proposed that DNA carboxymethylation, but not methylation, may contribute to the mutation pattern of human *p53* gene found in gastrointestinal cancers (199,221).

Detection of carboxymethylated DNA lesions

Due to the significance of DNA carboxymethylation in etiology of human gastrointestinal cancer, unambiguous identification and accurate assessment of carboxymethylated DNA adducts may provide further insights into the involvement of human exposure to NOCs and other DNA carboxymethylating agents in the carcinogenesis of gastric and colorectal cancers. Owing to the limited levels of chemically induced DNA lesions in cellular and tissue samples (2,3), analytical methods used for quantifying carboxymethylated DNA adducts should be ultrasensitive and

specific to achieve the measurement of the low abundance DNA lesions in the presence of excess amount of unmodified nucleosides. Early studies of DNA carboxymethylation have developed a series of techniques, such as radioactive based ^{32}P-postlabeling method (229), immunoslot blot assay (198) and combined immunoaffinity/HPLC methods (199,217,221) to detect O^6-CMdG and O^6-MedG *in vitro* and *in vivo*. Recently LC-MS has made enormous gains in its ability to detect DNA adducts, providing both accurate and sensitive quantification as well as structure information for the DNA lesions, without the usage of expensive antibodies and radioactive ^{32}P. Especially, the tandem mass spectrometry combined with stable isotope dilution method has already been considered as a golden standard for DNA adduct analysis due to its high specificity, sensitivity, and accuracy (3).

Scope of this dissertation

LC-MS has been employed as a powerful tool for elucidating the structures as well as providing accurate and unambiguous quantification of analytes. The focus of this dissertation is placed on development of analytical methods for reliable quantification of chemically modified DNA, i.e. oxidative stress induced DNA lesions, the DNA epigenetic biomarkers and carboxymethylated DNA adducts. In this vein, the *S*-diastereomers of 8,5'-cyclo-2'-deoxypurines (*S*-cdA and *S*-cdG), LPO product-induced εdA and εdG, 5-mdC and its oxidation product 5-hmdC, as well as carboxymethylated DNA lesions O^6-CMdG and N^6-CMdA were chosen as the subjects of study.

In chapter 2, I developed a nanoflow liquid chromatography-nanoelectrospray ionization-tandem mass spectrometry (nanoLC-NSI-MS^2) coupled with the isotope-dilution method for the simultaneous quantification of oxidatively induced DNA modifications, including direct ROS-induced cPus and two exocyclic adducts induced by byproducts of LPO, i.e. εdA and εdG, in liver and brain tissues of Long-Evans cinnamon (LEC) rats, the animal models of human Wilson's disease. The quantification data indicated the involvement of aberrant copper accumulation and resulting oxidative stress in etiology of human Wilson's disease.

In chapter 3, I employed a highly sensitive nLC-nESI-MS^3 method for the simultaneous quantification of N^6-CMdA, O^6-CMdG and O^6-MedG. I measured successfully the levels of these three lesions with the use of low-microgram quantities of DNA from cultured GM04429 human skin fibroblasts and HCT-116 human colorectal carcinoma cells treated with azaserine, a DNA carboxymethylating agent.

In chapter 4, I applied an LC-MS^3 quantification of 5-hmdC in different cancer cells treated with a glycolysis inhibitor 2-deoxy-D-glucose or AMP-activated protein kinase (AMPK) activators, i.e. metformin, phenformin or 5-aminoimidazole-4-carboxamide ribonucleotide (AICAR) to gain insights into the relationship between aberrant metabolism and the levels of 5-hmdC in cancer cells.

References

1. Liu, S. and Wang, Y. (2015) Mass spectrometry for the assessment of the occurrence and biological consequences of DNA adducts. *Chemical Society Reviews*, **44**, 7829-7854.

2. Tretyakova, N., Goggin, M., Sangaraju, D. and Janis, G. (2012) Quantitation of DNA Adducts by Stable Isotope Dilution Mass Spectrometry. *Chemical Research in Toxicology*, **25**, 2007-2035.

3. Tretyakova, N., Villalta, P.W. and Kotapati, S. (2013) Mass Spectrometry of Structurally Modified DNA. *Chemical Reviews*, **113**, 2395-2436.

4. Yu, Y., Cui, Y., Niedernhofer, L.J. and Wang, Y. (2016) Occurrence, Biological Consequences, and Human Health Relevance of Oxidative Stress-Induced DNA Damage. *Chem. Res. Toxicol.*, **29**, 2008-2039.

5. Cadet, J. and Davies, K.J.A. (2017) Oxidative DNA damage & repair: An introduction. *Free Radical Biol. Med.*, **107**, 2-12.

6. Bauer, N.C., Corbett, A.H. and Doetsch, P.W. (2015) The current state of eukaryotic DNA base damage and repair. *Nucleic Acids Res.*, **43**, 10083-10101.

7. Chatterjee, N. and Walker, G.C. (2017) Mechanisms of DNA damage, repair, and mutagenesis. *Environ. Mol. Mutag.*, **58**, 235-263.

8. Finkel, T. and Holbrook, N.J. (2000) Oxidants, oxidative stress and the biology of ageing. *Nature*, **408**, 239-247.

9. Balaban, R.S., Nemoto, S. and Finkel, T. (2005) Mitochondria, oxidants, and aging. *Cell*, **120**, 483-495.

10. Stohs, S.J. and Bagchi, D. (1995) Oxidative mechanisms in the toxicity of metal ions. *Free Radic. Biol. Med.*, **18**, 321-336.

11. De Bont, R. and van Larebeke, N. (2004) Endogenous DNA damage in humans: a review of quantitative data. *Mutagenesis*, **19**, 169-185.

12. Evans, M.D., Dizdaroglu, M. and Cooke, M.S. (2004) Oxidative DNA damage and disease: induction, repair and significance. *Mutation Research/Reviews in Mutation Research*, **567**, 1-61.

13. Ohshima, H., Tatemichi, M. and Sawa, T. (2003) Chemical basis of inflammation-induced carcinogenesis. *Arch. Biochem. Biophys.*, **417**, 3-11.

14. Winterbourn, C.C. and Kettle, A.J. (2013) Redox reactions and microbial killing in the neutrophil phagosome. *Antioxidants & Redox Signaling*, **18**, 642-660.

15. Rayner, B.S., Love, D.T. and Hawkins, C.L. (2014) Comparative reactivity of myeloperoxidase-derived oxidants with mammalian cells. *Free Radical Biol. Med.*, **71**, 240-255.

16. Panday, A., Sahoo, M.K., Osorio, D. and Batra, S. (2015) NADPH oxidases: an overview from structure to innate immunity-associated pathologies. *Cell. Mol. Immunol.*, **12**, 5-23.

17. Valko, M., Izakovic, M., Mazur, M., Rhodes, C.J. and Telser, J. (2004) Role of oxygen radicals in DNA damage and cancer incidence. *Mol. Cell. Biochem.*, **266**, 37-56.

18. Lonkar, P. and Dedon, P.C. (2011) Reactive species and DNA damage in chronic inflammation: reconciling chemical mechanisms and biological fates. *Int. J. Cancer*, **128**, 1999-2009.

19. Minko, I.G., Kozekov, I.D., Harris, T.M., Rizzo, C.J., Lloyd, R.S. and Stone, M.P. (2009) Chemistry and biology of DNA containing 1,N^2-deoxyguanosine adducts of the α,β-unsaturated aldehydes acrolein, crotonaldehyde, and 4-hydroxynonenal. *Chem. Res. Toxicol.*, **22**, 759-778.

20. Marnett, L.J. (1999) Lipid peroxidation—DNA damage by malondialdehyde. *Mutation Research/Fundamental and Molecular Mechanisms of Mutagenesis*, **424**, 83-95.

21. von Sonntag, C. (1987) *The Chemical Basis of Radiation Biology*. Taylor & Francis, London.

22. Bienvenu, C., Wagner, J.R. and Cadet, J. (1996) Photosensitized oxidation of 5-methyl-2'-deoxycytidine by 2-methyl-1,4-naphthoquinone: Characterization of 5-(hydroperoxymethyl)-2'-deoxycytidine and stable methyl group oxidation products. *J. Am. Chem. Soc.*, **118**, 11406-11411.

23. Wagner, J.R. and Cadet, J. (2010) Oxidation reactions of cytosine DNA components by hydroxyl radical and one-electron oxidants in aerated aqueous solutions. *Acc. Chem. Res.*, **43**, 564-571.

24. Dizdaroglu, M. and Jaruga, P. (2012) Mechanisms of free radical-induced damage to DNA. *Free Radical Res.*, **46**, 382-419.

25. Teoule, R. (1987) Radiation-induced DNA damage and its repair. *Int. J. Radiat Biol.*, **51**, 573-589.

26. Kasai, H., Iida, A., Yamaizumi, Z., Nishimura, S. and Tanooka, H. (1990) 5-Formyldeoxyuridine: a new type of DNA damage induced by ionizing-radiation and its mutagenicity to Salmonella strain TA102. *Mutat. Res.*, **243**, 249-253.

27. Tahiliani, M., Koh, K.P., Shen, Y.H., Pastor, W.A., Bandukwala, H., Brudno, Y., Agarwal, S., Iyer, L.M., Liu, D.R., Aravind, L. *et al.* (2009) Conversion of 5-methylcytosine to 5-hydroxymethylcytosine in mammalian DNA by MLL partner TET1. *Science*, **324**, 930-935.

28. Ito, S., Shen, L., Dai, Q., Wu, S.C., Collins, L.B., Swenberg, J.A., He, C. and Zhang, Y. (2011) Tet proteins can convert 5-methylcytosine to 5-formylcytosine and 5-carboxylcytosine. *Science*, **333**, 1300-1303.

29. He, Y.F., Li, B.Z., Li, Z., Liu, P., Wang, Y., Tang, Q.Y., Ding, J.P., Jia, Y.Y., Chen, Z.C., Li, L. *et al.* (2011) Tet-mediated formation of 5-carboxylcytosine and its excision by TDG in mammalian DNA. *Science*, **333**, 1303-1307.

30. Pastor, W.A., Pape, U.J., Huang, Y., Henderson, H.R., Lister, R., Ko, M., McLoughlin, E.M., Brudno, Y., Mahapatra, S., Kapranov, P. *et al.* (2011) Genome-wide mapping of 5-hydroxymethylcytosine in embryonic stem cells. *Nature*, **473**, 394-397.

31. Wu, H., D'Alessio, A.C., Ito, S., Wang, Z.B., Cui, K.R., Zhao, K.J., Sun, Y.E. and Zhang, Y. (2011) Genome-wide analysis of 5-hydroxymethylcytosine distribution reveals its dual function in transcriptional regulation in mouse embryonic stem cells. *Genes Dev.*, **25**, 679-684.

32. Raiber, E.A., Beraldi, D., Ficz, G., Burgess, H.E., Branco, M.R., Murat, P., Oxley, D., Booth, M.J., Reik, W. and Balasubramanian, S. (2012) Genome-wide distribution of 5-formylcytosine in embryonic stem cells is associated with transcription and depends on thymine DNA glycosylase. *Genome Biol.*, **13**.

33. Shen, L., Wu, H., Diep, D., Yamaguchi, S., D'Alessio, A.C., Fung, H.L., Zhang, K. and Zhang, Y. (2013) Genome-wide analysis reveals TET- and TDG-dependent 5-methylcytosine oxidation dynamics. *Cell*, **153**, 692-706.

34. Song, C.X., Szulwach, K.E., Dai, Q., Fu, Y., Mao, S.Q., Lin, L., Street, C., Li, Y.J., Poidevin, M., Wu, H. *et al.* (2013) Genome-wide profiling of 5-formylcytosine reveals its roles in epigenetic priming. *Cell*, **153**, 678-691.

35. Lu, X.Y., Zhao, B.S. and He, C. (2015) TET family proteins: oxidation activity, interacting molecules, and functions in diseases. *Chem. Rev.*, **115**, 2225-2239.

36. Guo, J.U., Su, Y.J., Zhong, C., Ming, G.L. and Song, H.J. (2011) Hydroxylation of 5-methylcytosine by TET1 promotes active DNA demethylation in the adult brain. *Cell*, **145**, 423-434.

37. Branco, M.R., Ficz, G. and Reik, W. (2012) Uncovering the role of 5-hydroxymethylcytosine in the epigenome. *Nat. Rev. Genet.*, **13**, 7-13.

38. Pfaffeneder, T., Spada, F., Wagner, M., Brandmayr, C., Laube, S.K., Eisen, D., Truss, M., Steinbacher, J., Hackner, B., Kotljarova, O. *et al.* (2014) Tet oxidizes thymine to 5-hydroxymethyluracil in mouse embryonic stem cell DNA. *Nat. Chem. Biol.*, **10**, 574-581.

39. Bjelland, S., Eide, L., Time, R.W., Stote, R., Eftedal, I., Volden, G. and Seeberg, E. (1995) Oxidation of thymine to 5-formyluracil in DNA: mechanisms of formation, structural implications, and base excision by human cell free extracts. *Biochemistry*, **34**, 14758-14764.

40. Douki, T., Delatour, T., Paganon, F. and Cadet, J. (1996) Measurement of oxidative damage at pyrimidine bases in gamma-irradiated DNA. *Chem. Res. Toxicol.*, **9**, 1145-1151.

41. MurataKamiya, N., Kamiya, H., Muraoka, M., Kaji, H. and Kasai, H. (1997) Comparison of oxidation products from DNA components by γ-irradiation and Fenton-type reactions. *J. Radiat. Res.*, **38**, 121-131.

42. Hong, H., Cao, H., Wang, Y. and Wang, Y. (2006) Identification and quantification of a guanine−thymine intrastrand cross-link lesion induced by Cu(II)/H_2O_2/ascorbate. *Chem. Res. Toxicol.*, **19**, 614-621.

43. Feig, D.I., Reid, T.M. and Loeb, L.A. (1994) Reactive oxygen species in tumorigenesis. *Cancer Res.*, **54**, 1890s-1894s.

44. Lee, D.H., O'Connor, T.R. and Pfeifer, G.P. (2002) Oxidative DNA damage induced by copper and hydrogen peroxide promotes CG→TT tandem mutations at methylated CpG dinucleotides in nucleotide excision repair-deficient cells. *Nucleic Acids Res.*, **30**, 3566-3573.

45. Reid, T.M. and Loeb, L.A. (1993) Tandem double CC→TT mutations are produced by reactive oxygen species. *Proceedings of the National Academy of Sciences*, **90**, 3904-3907.

46. Newcomb, T.G., Allen, K.J., Tkeshelashvili, L. and Loeb, L.A. (1999) Detection of tandem CC→TT mutations induced by oxygen radicals using mutation-specific PCR. *Mutation Research/Fundamental and Molecular Mechanisms of Mutagenesis*, **427**, 21-30.

47. Randerath, K., Randerath, E., Zhou, G.-D. and Li, D. (1999) Bulky endogenous DNA modifications (I-compounds)—possible structural origins and functional implications. *Mutation Research/Fundamental and Molecular Mechanisms of Mutagenesis*, **424**, 183-194.

48. Randerath, K., Reddy, M.V. and Disher, R.M. (1986) Age- and tissue-related DNA modifications in untreated rats: detection by ^{32}P-postlabeling assay and possible significance for spontaneous tumor induction and aging. *Carcinogenesis*, **7**, 1615-1617.

49. Randerath, K., Zhou, G.-D., Somers, R.L., Robbins, J.H. and Brooks, P.J. (2001) A ^{32}P-postlabeling assay for the oxidative DNA lesion 8,5'-cyclo-2'-deoxyadenosine in mammalian tissues: Evidence that four type II I-compounds are dinucleotides containing the lesion in the 3' nucleotide. *J. Biol. Chem.*, **276**, 36051-36057.

50. Jaruga, P. and Dizdaroglu, M. (2008) 8,5′-Cyclopurine-2′-deoxynucleosides in DNA: mechanisms of formation, measurement, repair and biological effects. *DNA Repair*, **7**, 1413-1425.

51. Chatgilialoglu, C., Ferreri, C. and Terzidis, M.A. (2011) Purine 5',8-cyclonucleoside lesions: chemistry and biology. *Chem. Soc. Rev.*, **40**, 1368-1382.

52. Brooks, P.J. (2007) The case for 8,5'-cyclopurine-2'-deoxynucleosides as endogenous DNA lesions that cause neurodegeneration in xeroderma pigmentosum. *Neuroscience*, **145**, 1407-1417.

53. Dizdaroglu, M. (1986) Free-radical-induced formation of an 8,5'-cyclo-2'-deoxyguanosine moiety in deoxyribonucleic acid. *Biochem. J*, **238**, 247-254.

54. Dirksen, M.-L., Blakely, W.F., Holwitt, E. and Dizdaroglu, M. (1988) Effect of DNA conformation on the hydroxyl radical-induced formation of 8,5'-cyclopurine 2'-deoxyribonucleoside residues in DNA. *Int. J. Radiat Biol.*, **54**, 195-204.

55. Guerrero, C.R., Wang, J. and Wang, Y. (2013) Induction of 8,5'-cyclo-2'-deoxyadenosine and 8,5'-cyclo-2'-deoxyguanosine in isolated DNA by Fenton-type reagents. *Chem. Res. Toxicol.*, **26**, 1361-1366.

56. Wang, J., Yuan, B., Guerrero, C., Bahde, R., Gupta, S. and Wang, Y. (2011) Quantification of oxidative DNA lesions in tissues of Long-Evans Cinnamon rats by capillary high-performance liquid chromatography−tandem mass spectrometry coupled with stable isotope-dilution method. *Anal. Chem.*, **83**, 2201-2209.

57. Wang, J., Clauson, C.L., Robbins, P.D., Niedernhofer, L.J. and Wang, Y. (2012) The oxidative DNA lesions 8,5'-cyclopurines accumulate with aging in a tissue-specific manner. *Aging Cell*, **11**, 714-716.

58. Kirkali, G., de Souza-Pinto, N.C., Jaruga, P., Bohr, V.A. and Dizdaroglu, M. (2009) Accumulation of (5'*S*)-8,5'-cyclo-2'-deoxyadenosine in organs of Cockayne syndrome complementation group B gene knockout mice. *DNA Repair*, **8**, 274-278.

59. Egler, R.A., Fernandes, E., Rothermund, K., Sereika, S., de Souza-Pinto, N., Jaruga, P., Dizdaroglu, M. and Prochownik, E.V. (2005) Regulation of reactive oxygen species, DNA damage, and *c-Myc* function by peroxiredoxin 1. *Oncogene*, **24**, 8038-8050.

60. Yu, Y., Guerrero, C.R., Liu, S., Amato, N.J., Sharma, Y., Gupta, S. and Wang, Y. (2016) Comprehensive assessment of oxidatively induced modifications of DNA in a rat model of human Wilson's disease. *Mol. Cell. Proteomics*, **15**, 810-817.

61. Mitra, D., Luo, X., Morgan, A., Wang, J., Hoang, M.P., Lo, J., Guerrero, C.R., Lennerz, J.K., Mihm, M.C., Wargo, J.A. *et al.* (2012) An ultraviolet-radiation-independent pathway to melanoma carcinogenesis in the red hair/fair skin background. *Nature*, **491**, 449-453.

62. Shaked, H., Hofseth, L.J., Chumanevich, A., Chumanevich, A.A., Wang, J., Wang, Y., Taniguchi, K., Guma, M., Shenouda, S., Clevers, H. *et al.* (2012) Chronic epithelial NF-κB activation accelerates APC loss and intestinal tumor initiation through iNOS up-regulation. *Proceedings of the National Academy of Sciences*, **109**, 14007-14012.

63. Tilstra, J.S., Robinson, A.R., Wang, J., Gregg, S.Q., Clauson, C.L., Reay, D.P., Nasto, L.A., St Croix, C.M., Usas, A., Vo, N. *et al.* (2012) NF-κB inhibition delays DNA damage–induced senescence. and aging in mice. *The Journal of Clinical Investigation*, **122**, 2601-2612.

64. Girotti, A.W. (1985) Mechanisms of lipid peroxidation. *J. Free Radic. Biol. Med.*, **1**, 87-95.

65. Halliwell, B. and Chirico, S. (1993) Lipid peroxidation: its mechanism, measurement, and significance. *The American Journal of Clinical Nutrition*, **57**, 715S-724S.

66. Burcham, P.C. (1998) Genotoxic lipid peroxidation products: their DNA damaging properties and role in formation of endogenous DNA adducts. *Mutagenesis*, **13**, 287-305.

67. Chung, F.-L., Chen, H.-J.C. and Nath, R.G. (1996) Lipid peroxidation as a potential endogenous source for the formation of exocyclic DNA adducts. *Carcinogenesis*, **17**, 2105-2111.

68. Nair, J., Barbin, A., Velic, I. and Bartsch, H. (1999) Etheno DNA-base adducts from endogenous reactive species. *Mutation Research/Fundamental and Molecular Mechanisms of Mutagenesis*, **424**, 59-69.

69. Winczura, A., Zdżalik, D. and Tudek, B. (2012) Damage of DNA and proteins by major lipid peroxidation products in genome stability. *Free Radical Res.*, **46**, 442-459.

70. Prado, F.M., Oliveira, M.C.B., Miyamoto, S., Martinez, G.R., Medeiros, M.H.G., Ronsein, G.E. and Di Mascio, P. (2009) Thymine hydroperoxide as a potential source of singlet molecular oxygen in DNA. *Free Radical Biol. Med.*, **47**, 401-409.

71. Blair, I.A. (2008) DNA adducts with lipid peroxidation products. *J. Biol. Chem.*, **283**, 15545-15549.

72. Minko, I.G., Kozekov, I.D., Kozekova, A., Harris, T.M., Rizzo, C.J. and Lloyd, R.S. (2008) Mutagenic potential of DNA–peptide crosslinks mediated by acrolein-derived DNA adducts. *Mutation Research/Fundamental and Molecular Mechanisms of Mutagenesis*, **637**, 161-172.

73. Stone, M.P., Cho, Y.-J., Huang, H., Kim, H.-Y., Kozekov, I.D., Kozekova, A., Wang, H., Minko, I.G., Lloyd, R.S., Harris, T.M. *et al.* (2008) Interstrand DNA cross-links induced by α,β-unsaturated aldehydes derived from lipid peroxidation and environmental sources. *Acc. Chem. Res.*, **41**, 793-804.

74. Kozekov, I.D., Nechev, L.V., Moseley, M.S., Harris, C.M., Rizzo, C.J., Stone, M.P. and Harris, T.M. (2003) DNA interchain cross-links formed by acrolein and crotonaldehyde. *J. Am. Chem. Soc.*, **125**, 50-61.

75. Garcia, C.C.M., Angeli, J.P.F., Freitas, F.P., Gomes, O.F., de Oliveira, T.F., Loureiro, A.P.M., Di Mascio, P. and Medeiros, M.H.G. (2011) [$^{13}C_2$]-acetaldehyde promotes unequivocal formation of 1,N^2-Propano-2'-deoxyguanosine in human cells. *J. Am. Chem. Soc.*, **133**, 9140-9143.

76. el Ghissassi, F., Barbin, A., Nair, J. and Bartsch, H. (1995) Formation of 1,N^6-ethenoadenine and 3,N^4-ethenocytosine by lipid peroxidation products and nucleic acid bases. *Chem. Res. Toxicol.*, **8**, 278-283.

77. Bartsch, H., Nair, J. and Owen Robert, W. (2002) Exocyclic DNA adducts as oxidative stress markers in colon carcinogenesis: potential role of lipid peroxidation, dietary fat and antioxidants. *Biol. Chem.*, **383**, 915-921.

78. Swenberg, J.A., Fedtke, N., Ciroussel, F., Barbin, A. and Bartsch, H. (1992) Etheno adducts formed in DNA of vinyl chloride-exposed rats are highly persistent in liver. *Carcinogenesis*, **13**, 727-729.

79. Lee, S.H., Arora, J.A., Oe, T. and Blair, I.A. (2005) 4-Hydroperoxy-2-nonenal-Induced Formation of 1,N2-Etheno-2‘-deoxyguanosine Adducts. *Chem. Res. Toxicol.*, **18**, 780-786.

80. Lee, S.H., Oe, T. and Blair, I.A. (2002) 4,5-Epoxy-2(E)-decenal-Induced Formation of 1,N6-Etheno-2‘-deoxyadenosine and 1,N2-Etheno-2‘-deoxyguanosine Adducts. *Chem. Res. Toxicol.*, **15**, 300-304.

81. Nair, U., Bartsch, H. and Nair, J. (2007) Lipid peroxidation-induced DNA damage in cancer-prone inflammatory diseases: A review of published adduct types and levels in humans. *Free Radical Biol. Med.*, **43**, 1109-1120.

82. Chen, H.-J. and Lin, W.-P. (2009) Simultaneous quantification of 1,N^2-propano-2'-deoxyguanosine adducts derived from acrolein and crotonaldehyde in human placenta and leukocytes by isotope dilution nanoflow LC nanospray ionization tandem mass spectrometry. *Anal. Chem.*, **81**, 9812-9818.

83. Chen, H.-J.C. (2011) Analysis of DNA adducts in human samples: Acrolein-derived exocyclic DNA adducts as an example. *Mol. Nutr. Food Res.*, **55**, 1391-1400.

84. Chen, H.-J.C., Chiang, L.-C., Tseng, M.-C., Zhang, L.L., Ni, J. and Chung, F.-L. (1999) Detection and quantification of 1,N^6-ethenoadenine in human placental DNA by mass spectrometry. *Chem. Res. Toxicol.*, **12**, 1119-1126.

85. Chen, H.-J.C. and Chiu, W.-L. (2005) Association between cigarette smoking and urinary excretion of 1,N^2-ethenoguanine measured by isotope dilution liquid chromatography-electrospray ionization/tandem mass spectrometry. *Chem. Res. Toxicol.*, **18**, 1593-1599.

86. Chen, H.-J.C., Lin, G.-J. and Lin, W.-P. (2010) Simultaneous quantification of three lipid peroxidation-derived etheno adducts in human DNA by stable isotope dilution nanoflow liquid chromatography nanospray ionization tandem mass spectrometry. *Anal. Chem.*, **82**, 4486-4493.

87. Chen, H.-J.C., Lin, T.-C., Hong, C.-L. and Chiang, L.-C. (2001) Analysis of 3,N^4-ethenocytosine in DNA and in human urine by isotope dilution gas chromatography/negative ion chemical ionization/mass spectrometry. *Chem. Res. Toxicol.*, **14**, 1612-1619.

88. Chen, H.-J.C. and Lin, W.-P. (2011) Quantitative analysis of multiple exocyclic DNA adducts in human salivary DNA by stable isotope dilution nanoflow liquid chromatography-nanospray ionization tandem mass spectrometry. *Anal. Chem.*, **83**, 8543-8551.

89. Chen, H.-J.C., Wu, C.-F., Hong, C.-L. and Chang, C.-M. (2004) Urinary excretion of 3,N^4-etheno-2'-deoxycytidine in humans as a biomarker of oxidative stress: association with cigarette smoking. *Chem. Res. Toxicol.*, **17**, 896-903.

90. Zhang, S., Villalta, P.W., Wang, M. and Hecht, S.S. (2006) Analysis of crotonaldehyde- and acetaldehyde-derived 1,N^2-propanodeoxyguanosine adducts in DNA from human tissues using liquid chromatography electrospray ionization tandem mass spectrometry. *Chem. Res. Toxicol.*, **19**, 1386-1392.

91. Garcia, C.C.M., Freitas, F.P., Di Mascio, P. and Medeiros, M.H.G. (2010) Ultrasensitive simultaneous quantification of 1,N^2-etheno-2'-deoxyguanosine and 1,N^2-propano-2'-deoxyguanosine in DNA by an online liquid chromatography−electrospray tandem mass spectrometry assay. *Chem. Res. Toxicol.*, **23**, 1245-1255.

92. Loureiro, A.P.M., Marques, S.A., Garcia, C.C.M., Di Mascio, P. and Medeiros, M.H.G. (2002) Development of an on-line liquid chromatography-electrospray tandem mass spectrometry assay to quantitatively determine 1,N^2-Etheno-2'-deoxyguanosine in DNA. *Chem. Res. Toxicol.*, **15**, 1302-1308.

93. Nair, J., Strand, S., Frank, N., Knauft, J., Wesch, H., Galle, P.R. and Bartsch, H. (2005) Apoptosis and age-dependant induction of nuclear and mitochondrial etheno-DNA adducts in Long-Evans Cinnamon (LEC) rats: enhanced DNA damage by dietary curcumin upon copper accumulation. *Carcinogenesis*, **26**, 1307-1315.

94. Ma, B., Villalta, P.W., Balbo, S. and Stepanov, I. (2014) Analysis of a malondialdehyde–deoxyguanosine adduct in human leukocyte DNA by liquid chromatography nanoelectrospray–high-resolution tandem mass spectrometry. *Chem. Res. Toxicol.*, **27**, 1829-1836.

95. Chaudhary, A.K., Nokubo, M., Marnett, L.J. and Blair, I.A. (1994) Analysis of the malondialdehyde-2'-deoxyguanosine adduct in rat liver DNA by gas chromatography/electron capture negative chemical ionization mass spectrometry. *Biol. Mass Spectrom.*, **23**, 457-464.

96. Zhang, Y., Chen, S.-Y., Hsu, T. and Santella, R.M. (2002) Immunohistochemical detection of malondialdehyde–DNA adducts in human oral mucosa cells. *Carcinogenesis*, **23**, 207-211.

97. Leuratti, C., Watson, M.A., Deag, E.J., Welch, A., Singh, R., Gottschalg, E., Marnett, L.J., Atkin, W., Day, N.E., Shuker, D.E.G. *et al.* (2002) Detection of malondialdehyde DNA adducts in human colorectal mucosa: relationship with diet and the presence of adenomas. *Cancer Epidemiology Biomarkers & Prevention*, **11**, 267-273.

98. Delaney, J.C. and Essigmann, J.M. (2008) Biological properties of single chemical-DNA adducts: a twenty year perspective. *Chem. Res. Toxicol.*, **21**, 232-252.

99. You, C. and Wang, Y. (2016) Mass spectrometry-based quantitative strategies for assessing the biological consequences and repair of DNA adducts. *Acc. Chem. Res.*, **49**, 205-213.

100. Levy, D.D. and Teebor, G.W. (1991) Site directed substitution of 5-hydroxymethyluracil for thymine in replicating phi-X-174am3 DNA via synthesis of 5-hydroxymethyl-2'-deoxyuridine-5'-triphosphate. *Nucleic Acids Res.*, **19**, 3337-3343.

101. Herrala, A.M. and Vilpo, J.A. (1989) Template-primer activity of 5-(hydroxymethyl)uracil-containing DNA for prokaryotic and eukaryotic DNA and RNA polymerases. *Biochemistry*, **28**, 8274-8277.

102. Mellac, S., Fazakerley, G.V. and Sowers, L.C. (1993) Structures of base pairs with 5-(hydroxymethyl)-2'-deoxyuridine in DNA determined by NMR spectroscopy. *Biochemistry*, **32**, 7779-7786.

103. Kallen, R.G., Marmur, J. and Simon, M. (1962) Occurrence of a new pyrimidine base replacing thymine in a bacteriophage DNA: 5-hydroxymethyl uracil. *J. Mol. Biol.*, **5**, 248-250.

104. Rusmintratip, V. and Sowers, L.C. (2000) An unexpectedly high excision capacity for mispaired 5-hydroxymethyluracil in human cell extracts. *Proc. Natl. Acad. Sci. U. S. A.*, **97**, 14183-14187.

105. Wibley, J.E.A., Waters, T.R., Haushalter, K., Verdine, G.L. and Pearl, L.H. (2003) Structure and specificity of the vertebrate anti-mutator uracil-DNA glycosylase SMUG1. *Mol. Cell*, **11**, 1647-1659.

106. Cortellino, S., Xu, J.F., Sannai, M., Moore, R., Caretti, E., Cigliano, A., Le Coz, M., Devarajan, K., Wessels, A., Soprano, D. *et al.* (2011) Thymine DNA glycosylase Is essential for active DNA demethylation by linked deamination-base excision repair. *Cell*, **146**, 67-79.

107. Morera, S., Grin, I., Vigouroux, A., Couve, S., Henriot, V., Saparbaev, M. and Ishchenko, A.A. (2012) Biochemical and structural characterization of the glycosylase domain of MBD4 bound to thymine and 5-hydroxymethyuracil-containing DNA. *Nucleic Acids Res.*, **40**, 9917-9926.

108. Hashimoto, H., Hong, S., Bhagwat, A.S., Zhang, X. and Cheng, X.D. (2012) Excision of 5-hydroxymethyluracil and 5-carboxylcytosine by the thymine DNA glycosylase domain: its structural basis and implications for active DNA demethylation. *Nucleic Acids Res.*, **40**, 10203-10214.

109. Zarakowska, E., Gackowski, D., Foksinski, M. and Olinski, R. (2014) Are 8-oxoguanine (8-oxoGua) and 5-hydroxymethyluracil (5-hmUra) oxidatively damaged DNA bases or transcription (epigenetic) marks? *Mutat. Res.-Genet. Toxicol. Environ. Mutag.*, **764**, 58-63.

110. Bjelland, S. and Seeberg, E. (2003) Mutagenicity, toxicity and repair of DNA base damage induced by oxidation. *Mutation Research/Fundamental and Molecular Mechanisms of Mutagenesis*, **531**, 37-80.

111. Olinski, R., Starczak, M. and Gackowski, D. (2016) Enigmatic 5-hydroxymethyluracil: Oxidatively modified base, epigenetic mark or both? *Mutat. Res. - Rev. Mut. Res.*, **767**, 59-66.

112. Klungland, A., Paulsen, R., Rolseth, V., Yamada, Y., Ueno, Y., Wiik, P., Matsuda, A., Seeberg, E. and Bjelland, S. (2001) 5-Formyluracil and its nucleoside derivatives confer toxicity and mutagenicity to mammalian cells by interfering with normal RNA and DNA metabolism. *Toxicol. Lett.*, **119**, 71-78.

113. Kamiya, H., Murata-Kamiya, N., Karino, N., Ueno, Y., Matsuda, A. and Kasai, H. (2002) Induction of T→G and T→A transversions by 5-formyluracil in mammalian cells. *Mutat. Res.-Genet. Toxicol. Environ. Mutag.*, **513**, 213-222.

114. Bjelland, S., Birkeland, N.K., Benneche, T., Volden, G. and Seeberg, E. (1994) DNA glycosylase activities for thymine residues oxidized in the methyl-troup are functions of the AlkA enzyme in *Escherichia coli*. *J. Biol. Chem.*, **269**, 30489-30495.

115. Masaoka, A., Terato, H., Kobayashi, M., Honsho, A., Ohyama, Y. and Ide, H. (1999) Enzymatic repair of 5-formyluracil I. Excision of 5-formyluracil site-specifically incorporated into oligonucleotide substrates by AlkA protein (*Escherichia coli* 3-methyladenine DNA glycosylase II). *J. Biol. Chem.*, **274**, 25136-25143.

116. Terato, H., Masaoka, A., Kobayashi, M., Fukushima, S., Ohyama, Y., Yoshida, M. and Ide, H. (1999) Enzymatic repair of 5-formyluracil II. Mismatch formation between 5-formyluracil and guanine during DNA replication and its recognition by two proteins involved in base excision repair (AlkA) and mismatch repair (MutS). *J. Biol. Chem.*, **274**, 25144-25150.

117. Matsubara, M., Masaoka, A., Tanaka, T., Miyano, T., Kato, N., Terato, H., Ohyama, Y., Iwai, S. and Ide, H. (2003) Mammalian 5-formyluracil-DNA glycosylase. 1. Identification and characterization of a novel activity that releases 5-formyluracil from DNA. *Biochemistry*, **42**, 4993-5002.

118. Masaoka, A., Matsubara, M., Hasegawa, R., Tanaka, T., Kurisu, S., Terato, H., Ohyama, Y., Karino, N., Matsuda, A. and Ide, H. (2003) Mammalian 5-formyluracil-DNA glycosylase. 2. role of SMUG1 uracil-DNA glycosylase in repair of 5-formyluracil and other oxidized and deaminated base lesions. *Biochemistry*, **42**, 5003-5012.

119. Knaevelsrud, I., Slupphaug, G., Leiros, I., Matsuda, A., Ruoff, P. and Bjelland, S. (2009) Opposite-base dependent excision of 5-formyluracil from DNA by hSMUG1. *Int. J. Radiat Biol.*, **85**, 413-420.

120. Liu, P.F., Burdzy, A. and Sowers, L.C. (2003) Repair of the mutagenic DNA oxidation product, 5-formyluracil. *DNA Repair*, **2**, 199-210.

121. Zhang, Q.M., Miyabe, I., Matsumoto, Y., Kino, K., Sugiyama, H. and Yonei, S. (2000) Identification of repair enzymes for 5-formyluracil in DNA - Nth, Nei, and MutM proteins of *Escherichia coli*. *J. Biol. Chem.*, **275**, 35471-35477.

122. Miyabe, I., Zhang, Q.M., Kino, K., Sugiyama, H., Takao, M., Yasui, A. and Yonei, S. (2002) Identification of 5-formyluracil DNA glycosylase activity of human hNTH1 protein. *Nucleic Acids Res.*, **30**, 3443-3448.

123. Yonekura, S., Nakamura, N., Doi, T., Sugiyama, H., Yamamoto, K., Yonei, S. and Zhang, Q. (2007) Recombinant *Schizosaccharomyces pombe* Nth1 protein exhibits DNA glycosylase activities for 8-oxo-7,8-dihydroguanine and thymine residues oxidized in the methyl group. *J. Radiat. Res.*, **48**, 417-424.

124. Zhang-Akiyama, Q.M., Morinaga, H., Kikuchi, M., Yonekura, S.I., Sugiyama, H., Yamamoto, K. and Yonei, S. (2009) KsgA, a 16S rRNA adenine methyltransferase, has a novel DNA glycosylase/AP lyase activity to prevent mutations in Escherichia coli. *Nucleic Acids Res.*, **37**, 2116-2125.

125. Belousova, E.A., Vasil'eva, I.A., Moor, N.A., Zatsepin, T.S., Oretskaya, T.S. and Lavrik, O.I. (2013) Clustered DNA lesions containing 5-formyluracil and AP Site: repair via the BER system. *PLoS One*, **8**, e68576.

126. Münzel, M., Lischke, U., Stathis, D., Pfaffeneder, T., Gnerlich, F.A., Deiml, C.A., Koch, S.C., Karaghiosoff, K. and Carell, T. (2011) Improved synthesis and mutagenicity of oligonucleotides containing 5-hydroxymethylcytosine, 5-formylcytosine and 5-carboxylcytosine. *Chemistry – A European Journal*, **17**, 13782-13788.

127. Xing, X.-W., Liu, Y.-L., Vargas, M., Wang, Y., Feng, Y.-Q., Zhou, X. and Yuan, B.-F. (2013) Mutagenic and cytotoxic properties of oxidation products of 5-methylcytosine revealed by next-generation sequencing. *PLoS One*, **8**, e72993.

128. Kamiya, H., Tsuchiya, H., Karino, N., Ueno, Y., Matsuda, A. and Harashima, H. (2002) Mutagenicity of 5-formylcytosine, an oxidation product of 5-methylcytosine, in DNA in mammalian cells. *J. Biochem.*, **132**, 551-555.

129. Ji, D., You, C., Wang, P. and Wang, Y. (2014) Effects of Tet-Induced oxidation products of 5-methylcytosine on DNA replication in mammalian cells. *Chem. Res. Toxicol.*, **27**, 1304-1309.

130. Kellinger, M.W., Song, C.-X., Chong, J., Lu, X.-Y., He, C. and Wang, D. (2012) 5-formylcytosine and 5-carboxylcytosine reduce the rate and substrate specificity of RNA polymerase II transcription. *Nat. Struct. Mol. Biol.*, **19**, 831-833.

131. Zheng, G., Fu, Y. and He, C. (2014) Nucleic acid oxidation in DNA damage repair and epigenetics. *Chem. Rev.*, **114**, 4602-4620.

132. Lu, X., Zhao, B.S. and He, C. (2015) TET family proteins: Oxidation activity, interacting molecules, and functions in diseases. *Chem. Rev.*, **115**, 2225-2239.

133. Maiti, A. and Drohat, A.C. (2011) Thymine DNA glycosylase can rapidly excise 5-formylcytosine and 5-carboxylcytosine: potential implications for active demethylation of CpG sites. *J. Biol. Chem.*, **286**, 35334-35338.

134. Cortazar, D., Kunz, C., Selfridge, J., Lettieri, T., Saito, Y., MacDougall, E., Wirz, A., Schuermann, D., Jacobs, A.L., Siegrist, F. *et al.* (2011) Embryonic lethal phenotype reveals a function of TDG in maintaining epigenetic stability. *Nature*, **470**, 419-423.

135. Nabel, C.S., Jia, H., Ye, Y., Shen, L., Goldschmidt, H.L., Stivers, J.T., Zhang, Y. and Kohli, R.M. (2012) AID/APOBEC deaminases disfavor modified cytosines implicated in DNA demethylation. *Nat. Chem. Biol.*, **8**, 751-758.

136. Kuraoka, I., Bender, C., Romieu, A., Cadet, J., Wood, R.D. and Lindahl, T. (2000) Removal of oxygen free-radical-induced 5',8-purine cyclodeoxynucleosides from DNA by the nucleotide excision-repair pathway in human cells. *Proceedings of the National Academy of Sciences*, **97**, 3832-3837.

137. You, C., Dai, X., Yuan, B., Wang, J., Wang, J., Brooks, P.J., Niedernhofer, L.J. and Wang, Y. (2012) A quantitative assay for assessing the effects of DNA lesions on transcription. *Nat. Chem. Biol.*, **8**, 817-822.

138. Kuraoka, I., Robins, P., Masutani, C., Hanaoka, F., Gasparutto, D., Cadet, J., Wood, R.D. and Lindahl, T. (2001) Oxygen free radical damage to DNA: translesion synthesis by human DNA polymerase η and resistance to exonuclease action at cyclopurine deoxynucleoside residues. *J. Biol. Chem.*, **276**, 49283-49288.

139. Jasti, V.P., Das, R.S., Hilton, B.A., Weerasooriya, S., Zou, Y. and Basu, A.K. (2011) (5'*S*)-8,5'-cyclo-2'-deoxyguanosine is a strong block to replication, a potent pol V-dependent mutagenic lesion, and is inefficiently repaired in *Escherichia coli*. *Biochemistry*, **50**, 3862-3865.

140. Yuan, B., Wang, J., Cao, H., Sun, R. and Wang, Y. (2011) High-throughput analysis of the mutagenic and cytotoxic properties of DNA lesions by next-generation sequencing. *Nucleic Acids Res.*, **39**, 5945-5954.

141. You, C., Swanson, A.L., Dai, X., Yuan, B., Wang, J. and Wang, Y. (2013) Translesion synthesis of 8,5'-cyclopurine-2'-deoxynucleosides by DNA polymerases η, ι, and ζ. *J. Biol. Chem.*, **288**, 28548-28556.

142. Marietta, C. and Brooks, P.J. (2007) Transcriptional bypass of bulky DNA lesions causes new mutant RNA transcripts in human cells. *Embo Reports*, **8**, 388-393.

143. Hang, B., Chenna, A., Guliaev, A.B. and Singer, B. (2003) Miscoding properties of 1,N^6-ethanoadenine, a DNA adduct derived from reaction with the antitumor agent 1,3-bis(2-chloroethyl)-1-nitrosourea. *Mutation Research/Fundamental and Molecular Mechanisms of Mutagenesis*, **531**, 191-203.

144. Pandya, G.A. and Moriya, M. (1996) 1,N6-Ethenodeoxyadenosine, a DNA adduct highly mutagenic in mammalian cells. *Biochemistry*, **35**, 11487-11492.

145. Tolentino, J.H., Burke, T.J., Mukhopadhyay, S., McGregor, W.G. and Basu, A.K. (2008) Inhibition of DNA replication fork progression and mutagenic potential of 1,N-6-ethenoadenine and 8-oxoguanine in human cell extracts. *Nucleic Acids Res.*, **36**, 1300-1308.

146. Levine, R.L., Yang, I.-Y., Hossain, M., Pandya, G.A., Grollman, A.P. and Moriya, M. (2000) Mutagenesis induced by a single 1,N^6-ethenodeoxyadenosine adduct in human cells. *Cancer Res.*, **60**, 4098-4104.

147. Moriya, M., Zhang, W., Johnson, F. and Grollman, A.P. (1994) Mutagenic potency of exocyclic DNA adducts: marked differences between *Escherichia coli* and simian kidney cells. *Proceedings of the National Academy of Sciences*, **91**, 11899-11903.

148. Langouët, S., Mican, A.N., Müller, M., Fink, S.P., Marnett, L.J., Muhle, S.A. and Guengerich, F.P. (1998) Misincorporation of nucleotides opposite five-membered exocyclic ring guanine derivatives by *Escherichia coli* polymerases *in vitro* and *in vivo*: 1,N^2-ethenoguanine, 5,6,7,9-tetrahydro-9-oxoimidazo[1,2-*a*]purine, and 5,6,7,9-tetrahydro-7-hydroxy-9-oxoimidazo[1,2-*a*]purine. *Biochemistry*, **37**, 5184-5193.

149. Cheng, K.C., Preston, B.D., Cahill, D.S., Dosanjh, M.K., Singer, B. and Loeb, L.A. (1991) The vinyl chloride DNA derivative N^2,3-ethenoguanine produces G→A transitions in *Escherichia coli*. *Proceedings of the National Academy of Sciences*, **88**, 9974-9978.

150. Gros, L., Ishchenko, A.A. and Saparbaev, M. (2003) Enzymology of repair of etheno-adducts. *Mutation Research/Fundamental and Molecular Mechanisms of Mutagenesis*, **531**, 219-229.

151. Zdżalik, D., Domańska, A., Prorok, P., Kosicki, K., van den Born, E., Falnes, P.Ø., Rizzo, C.J., Guengerich, F.P. and Tudek, B. (2015) Differential repair of etheno-DNA adducts by bacterial and human AlkB proteins. *DNA Repair*, **30**, 1-10.

152. Benamira, M., Johnson, K., Chaudhary, A., Bruner, K., Tibbetts, C. and Marnett, L.J. (1995) Induction of mutations by replication of malondialdehyde modified M13 DNA in *Escherichia coil*: determination of the extent of DNA modification, genetic requirements for mutagenesis, and types of mutations induced. *Carcinogenesis*, **16**, 93-99.

153. Fink, S.P., Reddy, G.R. and Marnett, L.J. (1997) Mutagenicity in *Escherichia coli* of the major DNA adduct derived from the endogenous mutagen malondialdehyde. *Proceedings of the National Academy of Sciences*, **94**, 8652-8657.

154. Niedernhofer, L.J., Daniels, J.S., Rouzer, C.A., Greene, R.E. and Marnett, L.J. (2003) Malondialdehyde, a product of lipid peroxidation, is mutagenic in human cells. *J. Biol. Chem.*, **278**, 31426-31433.

155. VanderVeen, L.A., Hashim, M.F., Shyr, Y. and Marnett, L.J. (2003) Induction of frameshift and base pair substitution mutations by the major DNA adduct of the endogenous carcinogen malondialdehyde. *Proceedings of the National Academy of Sciences*, **100**, 14247-14252.

156. Singh, V., Fedeles, B.I., Li, D., Delaney, J.C., Kozekov, I.D., Kozekova, A., Marnett, L.J., Rizzo, C.J. and Essigmann, J.M. (2014) Mechanism of repair of acrolein- and malondialdehyde-derived exocyclic guanine adducts by the α-ketoglutarate/Fe(II) dioxygenase AlkB. *Chem. Res. Toxicol.*, **27**, 1619-1631.

157. Liu, S. and Wang, Y. (2015) Mass spectrometry for the assessment of the occurrence and biological consequences of DNA adducts. *Chem. Soc. Rev.*, **44**, 7829-7854.

158. Tretyakova, N., Goggin, M., Sangaraju, D. and Janis, G. (2012) Quantitation of DNA adducts by stable isotope dilution mass spectrometry. *Chem. Res. Toxicol.*, **25**, 2007-2035.

159. Tretyakova, N., Villalta, P.W. and Kotapati, S. (2013) Mass spectrometry of structurally modified DNA. *Chem. Rev.*, **113**, 2395-2436.

160. Liu, S., Wang, J., Su, Y., Guerrero, C., Zeng, Y., Mitra, D., Brooks, P.J., Fisher, D.E., Song, H. and Wang, Y. (2013) Quantitative assessment of Tet-induced oxidation products of 5-methylcytosine in cellular and tissue DNA. *Nucleic Acids Res.*, **41**, 6421-6429.

161. Frelon, S., Douki, T., Ravanat, J.L., Pouget, J.P., Tornabene, C. and Cadet, J. (2000) High-performance liquid chromatography-tandem mass spectrometry measurement of radiation-induced base damage to isolated and cellular DNA. *Chem. Res. Toxicol.*, **13**, 1002-1010.

162. Hong, H.H. and Wang, Y.S. (2007) Derivatization with Girard reagent T combined with LC-MS/MS for the sensitive detection of 5-formyl-2'-deoxyuridine in cellular DNA. *Anal. Chem.*, **79**, 322-326.

163. Bullard, W., da Rosa-Spiegler, J.L., Liu, S., Wang, Y.S. and Sabatini, R. (2014) Identification of the glucosyltransferase that converts hydroxymethyluracil to base J in the trypanosomatid genome. *J. Biol. Chem.*, **289**, 20273-20282.

164. Wu, J., Forbes, J.R., Chen, H.S. and Cox, D.W. (1994) The LEC rat has a deletion in the copper transporting ATPase gene homologous to the Wilson disease gene. *Nat. Genet.*, **7**, 541-545.

165. Ala, A., Walker, A.P., Ashkan, K., Dooley, J.S. and Schilsky, M.L. (2007) Wilson's disease. *Lancet*, **369**, 397-408.

166. Roberts, E.A. and Schilsky, M.L. (2008) Diagnosis and treatment of Wilson disease: An update. *Hepatology*, **47**, 2089-2111.

167. Killian, J.K., Kim, S.Y., Miettinen, M., Smith, C., Merino, M., Tsokos, M., Quezado, M., Smith, W.I., Jahromi, M.S., Xekouki, P. *et al.* (2013) Succinate dehydrogenase mutation underlies global epigenomic divergence in gastrointestinal stromal tumor. *Cancer Discov.*, **3**, 648-657.

168. Figueroa, M.E., Abdel-Wahab, O., Lu, C., Ward, P.S., Patel, J., Shih, A., Li, Y., Bhagwat, N., Vasanthakumar, A., Fernandez, H.F. *et al.* (2010) Leukemic IDH1 and IDH2 mutations result in a hypermethylation phenotype, disrupt TET2 function, and impair hematopoietic differentiation. *Cancer Cell*, **18**, 553-567.

169. Yang, H., Lin, H., Xu, H., Zhang, L., Cheng, L., Wen, B., Shou, J., Guan, K., Xiong, Y. and Ye, D. (2014) TET-catalyzed 5-methylcytosine hydroxylation is dynamically regulated by metabolites. *Cell Res.*, **24**, 1017-1020.

170. Ye, D., Xiong, Y. and Guan, K.-L. (2012) The mechanisms of IDH mutations in tumorigenesis. *Cell Res.*, **22**, 1102-1104.

171. Dang, L., White, D.W., Gross, S., Bennett, B.D., Bittinger, M.A., Driggers, E.M., Fantin, V.R., Jang, H.G., Jin, S., Keenan, M.C. *et al.* (2009) Cancer-associated IDH1 mutations produce 2-hydroxyglutarate. *Nature*, **462**, 739-744.

172. Ward, P.S., Patel, J., Wise, D.R., Abdel-Wahab, O., Bennett, B.D., Coller, H.A., Cross, J.R., Fantin, V.R., Hedvat, C.V., Perl, A.E. *et al.* (2010) The common feature of leukemia-associated IDH1 and IDH2 mutations is a neomorphic enzyme activity converting α-ketoglutarate to 2-hydroxyglutarate. *Cancer Cell*, **17**, 225-234.

173. Xiao, M., Yang, H., Xu, W., Ma, S., Lin, H., Zhu, H., Liu, L., Liu, Y., Yang, C., Xu, Y. *et al.* (2012) Inhibition of α-KG-dependent histone and DNA demethylases by fumarate and succinate that are accumulated in mutations of FH and SDH tumor suppressors. *Genes Dev.*, **26**, 1326-1338.

174. Schulze, A. and Harris, A.L. (2012) How cancer metabolism is tuned for proliferation and vulnerable to disruption. *Nature*, **491**, 364-373.

175. Xu, W., Yang, H., Liu, Y., Yang, Y., Wang, P., Kim, S.-H., Ito, S., Yang, C., Wang, P., Xiao, M.-T. *et al.* (2011) Oncometabolite 2-hydroxyglutarate is acompetitive inhibitor of α-ketoglutarate-dependent dioxygenases. *Cancer Cell*, **19**, 17-30.

176. Jin, S.-G., Jiang, Y., Qiu, R., Rauch, T.A., Wang, Y., Schackert, G., Krex, D., Lu, Q. and Pfeifer, G.P. (2011) 5-hydroxymethylcytosine is strongly depleted in human cancers but its levels do not correlate with IDH1 mutations. *Cancer Res.*, **71**, 7360-7365.

177. Shen, L., Song, C.X., He, C. and Zhang, Y. (2014) Mechanism and function of oxidative reversal of DNA and RNA methylation. *Annu. Rev. Biochem*, **83**, 585-614.

178. Song, C.-X. and He, C. (2013) Potential functional roles of DNA demethylation intermediates. *Trends Biochem. Sci*, **38**, 480-484.

179. Spruijt, Cornelia G., Gnerlich, F., Smits, Arne H., Pfaffeneder, T., Jansen, Pascal W.T.C., Bauer, C., Münzel, M., Wagner, M., Müller, M., Khan, F. *et al.* (2013) Dynamic readers for 5-(hydroxy)methylcytosine and its oxidized derivatives. *Cell*, **152**, 1146-1159.

180. Mellén, M., Ayata, P., Dewell, S., Kriaucionis, S. and Heintz, N. (2012) MeCP2 binds to 5hmC enriched within active genes and accessible chromatin in the nervous system. *Cell*, **151**, 1417-1430.

181. Yildirim, O., Li, R., Hung, J.-H., Chen, Poshen B., Dong, X., Ee, L.-S., Weng, Z., Rando, Oliver J. and Fazzio, Thomas G. (2011) Mbd3/NURD complex regulates expression of 5-hydroxymethylcytosine marked genes in embryonic stem cells. *Cell*, **147**, 1498-1510.

182. Frauer, C., Hoffmann, T., Bultmann, S., Casa, V., Cardoso, M.C., Antes, I. and Leonhardt, H. (2011) Recognition of 5-hydroxymethylcytosine by the Uhrf1 SRA domain. *PLoS One*, **6**, e21306.

183. Iurlaro, M., Ficz, G., Oxley, D., Raiber, E.-A., Bachman, M., Booth, M.J., Andrews, S., Balasubramanian, S. and Reik, W. (2013) A screen for hydroxymethylcytosine and formylcytosine binding proteins suggests functions in transcription and chromatin regulation. *Genome Biol.*, **14**, 1-11.

184. Sun, Z., Dai, N., Borgaro, Janine G., Quimby, A., Sun, D., Corrêa, Ivan R., Jr., Zheng, Y., Zhu, Z. and Guan, S. (2015) A sensitive approach to map genome-wide 5-hydroxymethylcytosine and 5-formylcytosine at single-base resolution. *Mol. Cell*, **57**, 750-761.

185. Jin, S.-G., Zhang, Z.-M., Dunwell, Thomas L., Harter, Matthew R., Wu, X., Johnson, J., Li, Z., Liu, J., Szabó, Piroska E., Lu, Q. *et al.* (2016) Tet3 reads 5-carboxylcytosine through its CXXC domain and is a potential guardian against neurodegeneration. *Cell Reports*, **14**, 493-505.

186. Kraemer, K.H., Patronas, N.J., Schiffmann, R., Brooks, B.P., Tamura, D. and DiGiovanna, J.J. (2007) Xeroderma pigmentosum, trichothiodystrophy and Cockayne syndrome: A complex genotype–phenotype relationship. *Neuroscience*, **145**, 1388-1396.

187. Borgesius, N.Z., de Waard, M.C., van der Pluijm, I., Omrani, A., Zondag, G.C., van der Horst, G.T., Melton, D.W., Hoeijmakers, J.H., Jaarsma, D. and Elgersma, Y. (2011) Accelerated age-related cognitive decline and neurodegeneration, caused by deficient DNA repair. *J. Neurosci.*, **31**, 12543-12553.

188. Bartsch, H. and Nair, U.J. (2014), *Cancer and Inflammation Mechanisms*. John Wiley & Sons, Inc., pp. 61-74.

189. Liu, X., Lovell, M.A. and Lynn, B.C. (2005) Development of a method for quantification of acrolein−deoxyguanosine adducts in DNA using isotope dilution-capillary LC/MS/MS and its application to human brain tissue. *Anal. Chem.*, **77**, 5982-5989.

190. Moldovan, G.-L. and D'Andrea, A.D. (2009) How the fanconi anemia pathway guards the genome. *Annu. Rev. Genet.*, **43**, 223-249.

191. D'Andrea , A.D. (2010) Susceptibility pathways in Fanconi's anemia and breast cancer. *New Engl. J. Med.*, **362**, 1909-1919.

192. Kottemann, M.C. and Smogorzewska, A. (2013) Fanconi anaemia and the repair of Watson and Crick DNA crosslinks. *Nature*, **493**, 356-363.

193. Tischkowitz, M.D. and Hodgson, S.V. (2003) Fanconi anaemia. *J. Med. Genet.*, **40**, 1-10.

194. Finkel, T. and Holbrook, N.J. (2000) Oxidants, oxidative stress and the biology of ageing. *Nature*, **408**, 239-247.

195. Shuker, D.E.G. and Margison, G.P. (1997) Nitrosated glycine derivatives as a potential source of O^6-methylguanine in DNA. *Cancer Res.*, **57**, 366-369.

196. Stenner, F., Liewen, H., Zweifel, M., Weber, A., Tchinda, J., Bode, B., Samaras, P., Bauer, S., Knuth, A. and Renner, C. (2008) Targeted therapeutic approach for an anaplastic thyroid cancer *in vitro* and *in vivo*. *Cancer Sci.*, **99**, 1847-1852.

197. Van Hecke, T., Vanden Bussche, J., Vanhaecke, L., Vossen, E., Van Camp, J. and De Smet, S. (2014) Nitrite curing of chicken, pork, and beef inhibits oxidation but does not affect *N*-nitroso compound (NOC)-specific DNA adduct formation during *in vitro* digestion. *J. Agric. Food. Chem.*, **62**, 1980-1988.

198. Cupid, B.C., Zeng, Z.T., Singh, R. and Shuker, D.E.G. (2004) Detection of O^6-carboxymethyl-2'-deoxyguanosine in DNA following reaction of nitric oxide with glycine and in human blood DNA Using a quantitative immunoslot blot assay. *Chem. Res. Toxicol.*, **17**, 294-300.

199. Harrison, K.L., Jukes, R., Cooper, D.P. and Shuker, D.E.G. (1999) Detection of concomitant formation of O^6-carboxymethyl- and O^6-methyl-2'-deoxyguanosine in DNA exposed to nitrosated glycine derivatives using a combined immunoaffinity/HPLC method. *Chem. Res. Toxicol.*, **12**, 106-111.

200. Wang, H., Cao, H. and Wang, Y. (2010) Quantification of N^2-carboxymethyl-2'-deoxyguanosine in calf thymus DNA and cultured human kidney epithelial cells by capillary high-performance liquid chromatography-tandem mass spectrometry coupled with stable isotope dilution method. *Chem. Res. Toxicol.*, **23**, 74-81.

201. Tricker, A.R. and Preussmann, R. (1991) Carcinogenic *N*-nitrosamines in the diet-occurrence, formation, mechanisms and carcinogenic potential. *Mutat. Res.*, **259**, 277-289.

202. Lijinsky, W. (1999) *N*-Nitroso compounds in the diet. *Mutat. Res.*, **443**, 129-138.

203. Hecht, S.S. (1999) DNA adduct formation from tobacco-specific *N*-nitrosamines. *Mutat. Res.*, **424**, 127-142.

204. Hecht, S.S. and Hoffmann, D. (1988) Tobacco-specific nitrosamines, an important group of carcinogens in tobacco and tobacco smoke. *Carcinogenesis*, **9**, 875-884.

205. Yalcin, E. and de la Monte, S. (2016) Tobacco nitrosamines as culprits in disease: mechanisms reviewed. *J. Physiol. Biochem.*, **72**, 107-120.

206. Sanner, T. and Grimsrud, T.K. (2015) Nicotine: carcinogenicity and effects on response to cancer treatment – a review. *Front. Oncol.*, **5**.

207. Bolzán, A.D. and Bianchi, M.S. (2002) Genotoxicity of Streptozotocin. *Mutat. Res.*, **512**, 121-134.

208. Eileen Dolan, M. (1997) Inhibition of DNA repair as a means of increasing the antitumor activity of DNA reactive agents. *Adv. Drug Del. Rev.*, **26**, 105-118.

209. Tricker, A.R. (1997) *N*-nitroso compounds and man: sources of exposure, endogenous formation and occurrence in body fluids. *Eur. J. Cancer Prev.*, **6**, 226-268.

210. Wang, J. and Wang, Y. (2009) Chemical synthesis of oligodeoxyribonucleotides containing *N*3-and O^4-carboxymethylthymidine and their formation in DNA. *Nucleic Acids Res.*, **37**, 336-345.

211. Mirvish, S.S. (1995) Role of *N*-nitroso compounds (NOC) and *N*-nitrosation in etiology of garstric, esophageal, nasopharyngeal and bladder-cancer and contribution to cancer of known exposures to NOC. *Cancer Lett.*, **93**, 17-48.

212. Lundberg, J.O., Weitzberg, E., Cole, J.A. and Benjamin, N. (2004) Nitrate, bacteria and human health. *Nat Rev Micro*, **2**, 593-602.

213. Lundberg, J.O., Weitzberg, E. and Gladwin, M.T. (2008) The nitrate-nitrite-nitric oxide pathway in physiology and therapeutics. *Nat. Rev. Drug Discov.*, **7**, 156-167.

214. Lundberg, J.O. and Weitzberg, E. (2013) Biology of nitrogen oxides in the gastrointestinal tract. *Gut*, **62**, 616-629.

215. Kobayashi, J. (2017) Effect of diet and gut environment on the gastrointestinal formation of *N*-nitroso compounds: a review. *Nitric Oxide*.

216. Fahrer, J. and Kaina, B. (2013) O^6-methylguanine-DNA methyltransferase in the defense against *N*-nitroso compounds and colorectal cancer. *Carcinogenesis*, **34**, 2435-2442.

217. Harrison, K.L., Fairhurst, N., Challis, B.C. and Shuker, D.E.G. (1997) Synthesis, characterization, and immunochemical detection of O^6-(carboxymethyl)-2'-deoxyguanosine: A DNA adduct formed by nitrosated glycine derivatives. *Chem. Res. Toxicol.*, **10**, 652-659.

218. Wang, J. and Wang, Y. (2010) Synthesis and characterization of oligodeoxyribonucleotides containing a site-specifically incorporated N^6-carboxymethyl-2'-deoxyadenosine or N^4-carboxymethyl-2'-deoxycytidine. *Nucleic Acids Res.*, **38**, 6774-6784.

219. Zurlo, J., Curphey, T.J., Hiley, R. and Longnecker, D.S. (1982) Identification of 7-carboxymethylguanine in DNA from pancreatic acinar cells exposed to azaserine. *Cancer Res.*, **42**, 1286-1288.

220. Yu, Y., Wang, J., Wang, P. and Wang, Y. (2016) Quantification of azaserine-induced carboxymethylated and methylated DNA lesions in cells by nanoflow liquid chromatography-nanoelectrospray ionization tandem mass spectrometry coupled with the stable isotope-dilution method. *Anal. Chem.*, **88**, 8036-8042.

221. Gottschalg, E., Scott, G.B., Burns, P.A. and Shuker, D.E.G. (2007) Potassium diazoacetate-induced *p53* mutations in vitro in relation to formation of O^6-carboxymethyl- and O^6-methyl-2'-deoxyguanosine DNA adducts: relevance for gastrointestinal cancer. *Carcinogenesis*, **28**, 356-362.

222. Lewin, M.H., Bailey, N., Bandaletova, T., Bowman, R., Cross, A.J., Pollock, J., Shuker, D.E.G. and Bingham, S.A. (2006) Red meat enhances the colonic formation of the DNA adduct O^6-carboxymethyl guanine: Implications for colorectal cancer. *Cancer Res.*, **66**, 1859-1865.

223. O'Driscoll, M., Macpherson, P., Xu, Y.Z. and Karran, P. (1999) The cytotoxicity of DNA carboxymethylation and methylation by the model carboxymethylating agent azaserine in human cells. *Carcinogenesis*, **20**, 1855-1862.

224. Wu, J., Wang, P., Li, L., Williams, N.L., Ji, D., Zahurancik, W.J., You, C., Wang, J., Suo, Z. and Wang, Y. (2017) Replication studies of carboxymethylated DNA lesions in human cells. *Nucleic Acids Res.*, **45**, 7276-7284.

225. You, C., Wang, P., Nay, S.L., Wang, J., Dai, X., O'Connor, T.R. and Wang, Y. (2016) Roles of Aag, Alkbh2, and Alkbh3 in the repair of carboxymethylated and ethylated thymidine lesions. *ACS Chem. Biol.*, **11**, 1332-1338.

226. Senthong, P., Millington, C.L., Wilkinson, O.J., Marriott, A.S., Watson, A.J., Reamtong, O., Eyers, C.E., Williams, D.M., Margison, G.P. and Povey, A.C. (2013) The nitrosated bile acid DNA lesion O^6-carboxymethylguanine is a substrate for the human DNA repair protein O^6-methylguanine-DNA methyltransferase. *Nucleic Acids Res.*, **41**, 3047-3055.

227. Correa, P. (1992) Human gastric carcinogenesis-a multistep and multifunctional process-1st American cancer society award lecture on cancer epidemiology and prevention. *Cancer Res.*, **52**, 6735-6740.

228. Hemeryck, L.Y., Van Hecke, T., Vossen, E., De Smet, S. and Vanhaecke, L. (2017) DNA adductomics to study the genotoxic effects of red meat consumption with and without added animal fat in rats. *Food Chem.*, **230**, 378-387.

229. Terasaki, M., Totsuka, Y., Nishimura, K., Mukaisho, K., Chen, K., Hattori, T., Takamura-Enya, T., Sugimura, T. and Wakabayashi, K. (2008) Detection of endogenous DNA adducts, O^6-carboxymethyl-2'-deoxyguanosine and 3-ethanesulfonic acid-2'-deoxycytidine, in the rat stomach after duodenal reflux. *Cancer Sci.*, **99**, 1741-1746.

Chapter 2 Comprehensive assessment of oxidatively induced modifications of DNA in a rat model of human Wilson's Disease

Introduction

Many endogenous and exogenous chemical events may produce DNA damage, including assault from reactive oxygen species (ROS) (1,2). ROS are routinely generated in cells as a consequence of metabolic activity and exposure to various environmental agents. Under physiological conditions, transition metal ion-mediated Fenton reaction constitutes a major endogenous source of ROS, and aberrant accumulation of transition metal ions may elicit deleterious effects on cells. Elevated ROS could lead to DNA damage directly, or indirectly via byproducts of lipid peroxidation (LPO). In this vein, hydroxyl radical can directly react with DNA to yield a myriad of DNA lesions, including the bulky 8,5′-cyclopurine-2′-deoxynucleosides (cPu) (3,4). Byproducts of LPO could react with DNA to generate exocyclic adducts, including 1,N^6-etheno-2′-deoxyadenosine (εdA) and 1,N^2-etheno-2′-deoxyguanosine (εdG) (5,6). Multiple lines of evidence showed that these DNA lesions in mammalian cells, tissues and blood may serve as potential biomarkers of oxidative stress (7-14).

Some oxidatively induced DNA modifications are also exploited by mammalian cells to regulate gene expression. In this context, Fe^{2+}- and 2-oxoglutarate (2-OG)-dependent ten-eleven translocation (TET) family dioxygenases were recently found to be involved in sequential oxidation of 5-methyl-2′-deoxycytidine (5-mdC) to yield 5-hydroxymethyl-2′-deoxycytidine (5-HmdC), 5-formyl-2′-deoxycytidine (5-FodC), and 5-

carboxyl-2′-deoxycytidine (5-CadC) (15-20). Subsequent excision of 5-FodC and 5-CadC from DNA by thymine DNA glycosylase (TDG), coupled with restoration of an unmethylated 2′-deoxycytidine by base-excision repair (BER) pathway, may facilitate active DNA cytosine demethylation in mammals (16,21). In addition, 5-hmdC could be recognized by some specific cellular proteins (22-25), suggesting that the oxidized derivatives of 5-mdC may also serve as epigenetic marks on their own.

Transition metal ion homeostasis is essential for normal cellular function and excess accumulation of metal ions, such as iron or copper, may result in diseases. In this vein, Wilson's disease (WD) is an autosomal recessive genetic disorder arising from mutations in the P-type ATPase gene, *ATP7B*, and patients suffering from this disease are manifested by defective excretion of copper ions into bile (26,27). This leads to accumulation of copper in the body with progressive damage in liver, brain and kidneys (26,27). The Long-Evans Cinnamon (LEC) rat, which was found in a colony of healthy Long-Evans Agouti (LEA) rat, harbors a partial deletion at the 3′ end of the *Atp7b* gene and shares many clinical attributes of Wilson's disease in humans, including excess copper accumulation in the liver along with spontaneous acute liver failure and progressive liver damage with extensive hepatic cholangiofibrosis (28). Therefore, the LEC rat serves as an excellent animal model for studying the pathophysiology of human Wilson's disease.

Increased copper content and elevated levels of ROS and oxidative DNA damage have been observed in liver tissues of LEC rats (10,29). However, it remains unclear whether abnormal copper accumulation perturbs epigenetic signaling by modulating the

formation of 5-HmdC. In light of our previous finding that 5-HmdC could be induced from oxidation of 5-mdC in synthetic duplex DNA by Fenton-type reagent (Cu^{2+}/H_2O_2/ascorbate) *in vitro* (30), we reasoned that increased copper accumulation might also elicit higher levels of 5-HmdC *in vivo*. On the other hand, the Jumonji C domain-containing histone demethylases (JHDMs), which are also Fe^{2+}- and 2-OG-dependent dioxygenases, were previously shown to be perturbed by exposure to carcinogenic heavy metals, including nickel, chromium, and possibly arsenic (31-33). The replacement of iron in the active site of JHDMs by nickel, and depletion of ascorbic acid, a crucial cofactor of these enzymes, from chromium or arsenic exposure, could attenuate the demethylase activity of JHDMs in cells (31-33). Likewise, other Fe^{2+}- and 2-OG-dependent dioxygenases, including hypoxia inducible factor (HIF)-prolyl hydroxylase PHD2 and DNA repair enzymes ALKBH2/3, could also be inhibited by nickel ion (31,34). Therefore, accumulation of copper in Wilson's disease may compromise enzymatic activities of Tet proteins *in vivo*, thereby resulting in lower 5-HmdC levels.

Herein, we comprehensively assessed the effect of abnormal copper accumulation on oxidatively induced DNA modifications in liver and brain tissues of LEC and LEA rats by LC-MS/MS combined with the stable isotope-dilution technique. The goal was to gain a better understanding of genetic and epigenetic alterations arising from aberrant copper accumulation.

Materials and methods

Materials & animals

All chemicals and enzymes, unless otherwise specified, were purchased from Sigma-Aldrich (St. Louis, MO) and New England Biolabs (Ipswich, WA), respectively. Stable isotope-labeled compounds were obtained from Cambridge Isotope Labs (Cambridge, MA). *Erythro*-9-(2-hydroxy-3-nonyl)adenine (EHNA) hydrochloride was from Tocris Bioscience (Ellisville, MO). LEA and LEC rats (14-16 week old) were bred in a Core Facility at Einstein as described previously (10). The stable isotope-labeled *S*-cdA, *S*-cdG and 5-HmdC were synthesized previously (10,30). The εdA and εdG as well as their stable isotope-labeled counterparts were synthesized following procedures published previously (35,36).

Extraction and Enzymatic Digestion of DNA

Genomic DNA was extracted from rat tissues by using a high-salt method (10). The liver and brain tissues of LEA/LEC rats were grounded into fine powders under liquid nitrogen in a mortar. A 100-μL lysis buffer, containing 20 mM Tris (pH 8.1), 20 mM EDTA, 400 mM NaCl, 1% SDS (w/v) and 10-15 μL of proteinase K (20 mg/mL), was added to the powdered tissue with incubation in a water bath at 55°C overnight. Saturated NaCl solution (0.5 volume) was subsequently added to the mixture, which was vortexed for 1 min and incubated at 55°C for another 15 min. The resulting mixture was centrifuged at 13000 rpm for 30 min. Nucleic acids were precipitated from the supernatant by ethanol. The RNA in the nucleic acid mixture was digested by 3 μL RNase A (10 mg/mL) and 2 μL RNase T1 (25 units/μL) at 37°C overnight, followed by

extraction with an equal volume of chloroform/isoamyl alcohol (24:1, v/v). The DNA was precipitated from the aqueous layer by ethanol, re-dissolved in water and quantified by UV spectrophotometry.

The DNA sample (10 μg) was digested with 1 unit of nuclease P1 and 0.00125 unit of phosphodiesterase II in a 15-μL buffer containing 300 mM sodium acetate (pH 5.6), 10 mM $ZnCl_2$ and 2.5 nmol of EHNA, which served as an inhibitor of adenine deaminase to minimize deamination of dA to 2′-deoxyinosine (10). After incubation at 37°C for 48 hr, to the mixture were added 1.0 unit of alkaline phosphatase, 0.0025 unit of phosphodiesterase I, and 20 μL of buffer containing 500 mM Tris-HCl (pH 8.9). After a 2-hr incubation at 37°C, the digestion mixture was neutralized with 1 M formic acid, and uniformly ^{15}N-labeled *S*-cdA, *S*-cdG, εdA and εdG internal standards were added to the mixture. The enzymes in the digestion mixture were removed by extraction with chloroform/isoamyl alcohol (24:1, v/v), and the resulting aqueous layer was subjected to off-line HPLC enrichment.

For quantification of 5-HmdC and 5-mdC, [1,3-$^{15}N_2$-2′-D]-5-HmdC and [1′,2′,3′,4′,5′-$^{13}C_5$]-5-mdC were added to the enzymatic digestion mixture of 50 ng of genomic DNA. The enzymes in digestion mixture were again removed by extraction with chloroform/isoamyl alcohol (24:1, v/v), and the resulting aqueous layer was subjected directly to LC-MS/MS analysis on an LTQ linear ion trap mass spectrometer (Thermo Fisher Scientific).

HPLC enrichment

The HPLC separation was performed on a Beckman HPLC system with pump module 125 and UV detector module 126. An Alltima HP-C18 column (4.6 × 250 mm, 5 μm in particle size, 300 Å in pore size, Grace Davison, Deerfield, IL) was used to enrich oxidatively induced DNA lesions from the aforementioned nucleoside mixture. The mobile phases were 10 mM ammonium formate (Solution A) and methanol (Solution B). A gradient of 42 min 0% B, 1 min 0-2% B, 17 min 2% B, 1 min 2-5% B, 9 min 5% B, 10 min 5-13% B, 20 min 13% B, and 50 min 13-60% B was used, and the flow rate was 1 mL/min. The HPLC fractions containing *S*-cdG (33.5-38.0 min), *S*-cdA (66.0-70.0 min), and εdA + εdG (81.5-87.5 min) were pooled individually and dried in a Speed-vac. The dried samples were then reconstituted in water for NanoLC-NSI/MS^2 analysis.

NanoLC-NSI/MS^2 analysis

The NanoLC-NSI-MS/MS analysis was conducted on a TSQ Vantage triple quadrupole mass spectrometer (Thermo Fisher Scientific) equipped with a nano-electrospray ionization source and coupled with an EASY nLC II (Thermo Fisher Scientific). HPLC separation was carried out using a homemade trapping column (150 μm × 40 mm) and an analytical column (75 μm × 200 mm), both packed with Magic C18 AQ (200 Å, 5 μm, Michrom BioResources, Auburn, CA). Mobile phase A was 0.1% formic acid in H_2O and mobile phase B was 0.1% formic acid in acetonitrile. Initially, the sample was loaded onto the trapping column with mobile phase A at a flow rate of 2.5 μL/min. The analytes were eluted using a 40-min linear gradient of 0-40% mobile phase B at a flow rate of 300 nL/min. The TSQ Vantage mass spectrometer was operated in the

positive-ion mode, where the spray voltage was 1.8 kV and the temperature for ion-transport tube was 275°C. The instrument was set up in multiple-reaction monitoring (MRM) mode, with MRM transitions being listed in Table S1. The sensitivities for detecting all modified nucleosides were optimized by varying the collision energy (Table A1). The amounts of oxidative stress-induced DNA modifications (in moles) in nucleoside mixtures were calculated from area ratios of peaks found in selected-ion chromatograms (SICs) for the analytes over their corresponding isotope-labeled standards, the amounts of the labeled standards added (in moles) and the calibration curves (Figure A2.2). The final levels of the modified nucleosides, in terms of the numbers of modified nucleosides per 10^7 nucleosides, were calculated by dividing the amounts of individual modified nucleosides with the total amount of nucleosides (in moles) in the digested DNA.

Capillary LC-tandem MS analyses of 5-HmdC and 5-mdC

The LC-MS^3 quantification of 5-HmdC was conducted on an LTQ linear ion trap mass spectrometer (Thermo Fisher Scientific) coupled with an Agilent 1200 capillary HPLC pump, as described previously (37). The LC-MS^2 measurement of 5-mdC was performed on the same instrument. The HPLC separation was conducted using a 0.5 × 250 mm Zorbax SB-C18 column (5 μm in particle size, Agilent Technologies). A solution of 2 mM ammonium bicarbonate in water (pH 7.0, solution A) and methanol (solution B) were employed as mobile phases. A gradient of 5 min 0-20% B and 25 min 20-70% B was used for separating analytes, and the flow rate was 8.0 μL/min. The voltage for electrospray was 5.0 kV, and the ion-transport tube was maintained at a

temperature of 275°C. The isolation width for precursor ion selection was 3 *m/z* units, the normalized collision energy was 35, the activation Q was 0.25, and the activation time was 30 ms. The levels of 5-HmdC and 5-mdC were calculated with the method described above for the oxidative stress-induced DNA lesions.

Biochemical assay of Tet1-mediated oxidation of 5-mdC in duplex DNA

The Tet1-mediated 5-mdC oxidation assay was conducted with the use of the 5mC Tet1 Oxidation Kit (Wisegene, IL, USA) and a 5-mdC-containing duplex DNA, d(AGCTC(5-mdC)GGTCA)/d(GTGACCGGAGCTG), following procedures reported previously (38) with slight modifications. Briefly, 20 pmol of the aforementioned duplex DNA was incubated with 0.4 μL of mouse Tet1 protein, along with a reaction buffer containing 50 mM HEPES (pH 8.0), 100 mM sodium chloride, 2 mM ascorbic acid, 1 mM 2-oxoglutarate, 1 mM ATP, 1 mM DTT, along with 75 μM ammonium iron(II) sulfate and various concentrations of copper sulfate (at Cu^{2+}/Fe^{2+} molar ratios of 0, 0.25, 0.50, 1.0, 2.0 and 5.0) in a total volume of 50 μL. After incubation at 37°C for 10 min, the reaction mixtures were immediately frozen on dry ice. The enzyme in the mixture was removed using chloroform extraction. The resulting aqueous layer was subjected directly to LC-MS and MS^2 on an LTQ linear ion trap mass spectrometer to identify reaction products and to quantify conversions of 5-mdC to its oxidation products. A 0.5 × 250 mm Zorbax SB-C18 column was employed for the separation and the flow rate was 8.0 μL/min. 1,1,1,3,3,3-Hexafluoroisopropanol (HFIP, pH adjusted to 7.0 with triethylamine, solution A) and methanol (solution B) were employed as mobile phases, and a gradient of 5 min of 0-20% B and 35 min of 20-40% B was used. The voltage for

electrospray was 4.0 kV and the ion-transport tube of the mass spectrometer was set at 300°C. The MS^2 and higher-resolution "ultra-zoom-scan" MS were acquired for the $[M - 3H]^{3-}$ ions of the initial 11mer 5-mdC-containing ODN and corresponding oxidized 5-mdC products. The intensities of the monoisotopic and M + 1 isotopic peaks were employed for calculating fractions of 5-mdC oxidation product in the reaction mixtures.

Results

NanoLC-NSI/MS^2 method for quantifying oxidative stress-induced DNA lesions in rat tissues

Relatively large amounts of unmodified nucleosides and buffer salts are present in the enzymatic digestion mixture of tissue DNA, which can significantly interfere with the detection of low levels of DNA lesions. To overcome this, we employed off-line HPLC separation to enrich DNA lesions of interest from the digestion mixtures prior to NanoLC-NSI/MS^2 analysis. Relative to previously reported capillary LC-MS^3 methods (10), the low flow rate used for nanoflow LC (at 300 nL/min) further improved the sensitivity of analyte detection by improving the ionization efficiencies and transmission of ions from the ionization interface to the mass analyzer. Consequently, the amount of tissue DNA consumed in sample preparation was reduced from 80-100 μg to 10-20 μg.

Upon collisional activation, the $[M + H]^+$ ions of unlabeled εdA and εdG can eliminate a 2-deoxyribose moiety to yield the protonated nucleobase portion as the dominant fragment ions in MS/MS, i.e., the ions of *m/z* 160 and 176 for εdA and εdG, respectively (Figure 2.1A & 2.1B and Figure A2.1A). The collisional activation of $[M + H]^+$ ions of unlabeled *S*-cdA and *S*-cdG, on the other hand, gave fragment ions of *m/z* 164

and 180, respectively, which arise from cleavages of both the *N*-glycosidic bond and the C_4'-C_5' bond in the 2-deoxyribose moiety (Figure 2.1C & 2.1D and Figure A2.1B) (39). The nearly identical elution time for the analytes and their stable isotope-labeled counterparts, along with their specific MRM transitions, allowed for unambiguous identification and reliable quantification of oxidative stress-induced lesions in rat tissue DNA (calibration curves shown in Figure A2.2).

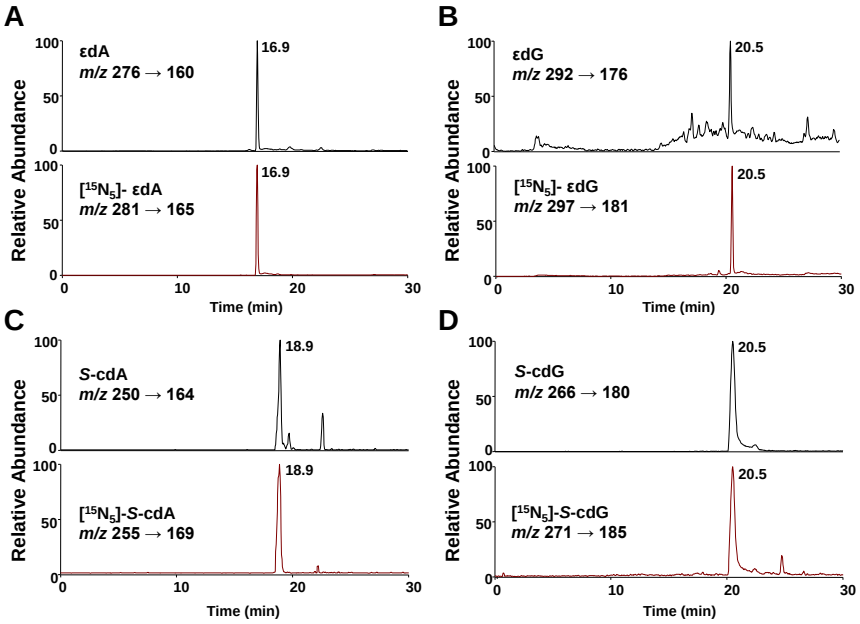


Figure 2.1.Representative NanoLC-NSI/MS^2 results for the quantifications of εdA (A), εdG (B), *S*-cdA (C) and *S*-cdG (D) in DNA of rat tissues. Shown are the selected-ion chromatograms (SICs) for monitoring the indicated MRM transitions for the analytes (top trace) and the isotope-labeled standards (bottom trace).

Levels of oxidative stress-induced DNA lesions in liver and brain tissues of LEA and LEC rats

With the NanoLC-NSI/MS^2 method, we were able to measure the levels of cPus and LPO-induced exocyclic DNA lesions in rat liver and brain tissues with low-μg quantities of DNA. Our quantification results revealed that *S*-cdA, *S*-cdG, εdA and εdG levels in LEA rat liver tissues were 12.0, 20.2, 2.3 and 1.1 lesions per 10^7 nucleosides, respectively (Figure 2.2 & Table A2.2). The corresponding levels of these lesions were 26.8, 44.5, 3.0 and 1.6 adducts per 10^7 nucleosides, respectively, in DNA from LEC rat liver tissues (Figure 2.2 & Table A2.2). Thus, the levels of all four oxidative stress-induced DNA lesions were significantly higher in liver tissues of LEC than LEA rats,

which is in agreement with markedly increased liver copper content and liver injury in LEC rats (28). Consistent with the absence of gross neurological defects in LEC rats (40), the levels of oxidative stress-induced DNA lesions in brain tissues of LEC and LEA rats were similar.

Our quantification results also showed that *S*-cdA and *S*-cdG (12.0-44.5 lesions per 10^7 nucleosides) are present endogenously in rat liver tissues at much higher levels than εdA and εdG (1.1-4.4 lesions per 10^7 nucleosides, Figure 2.2 and Table A2.2). Similarly, the magnitudes of increases in the levels of *S*-cdA and *S*-cdG (~2.2-fold), arising from aberrant copper accumulation in liver tissues of LEC versus LEA rats, were more pronounced than those for εdA and εdG (~1.3-fold, Figure 2.2 & Table A2.2). These results suggested more efficient formation and/or less facile repair of direct ROS-induced cPu lesions than εdA and εdG, which arise from byproducts of LPO.

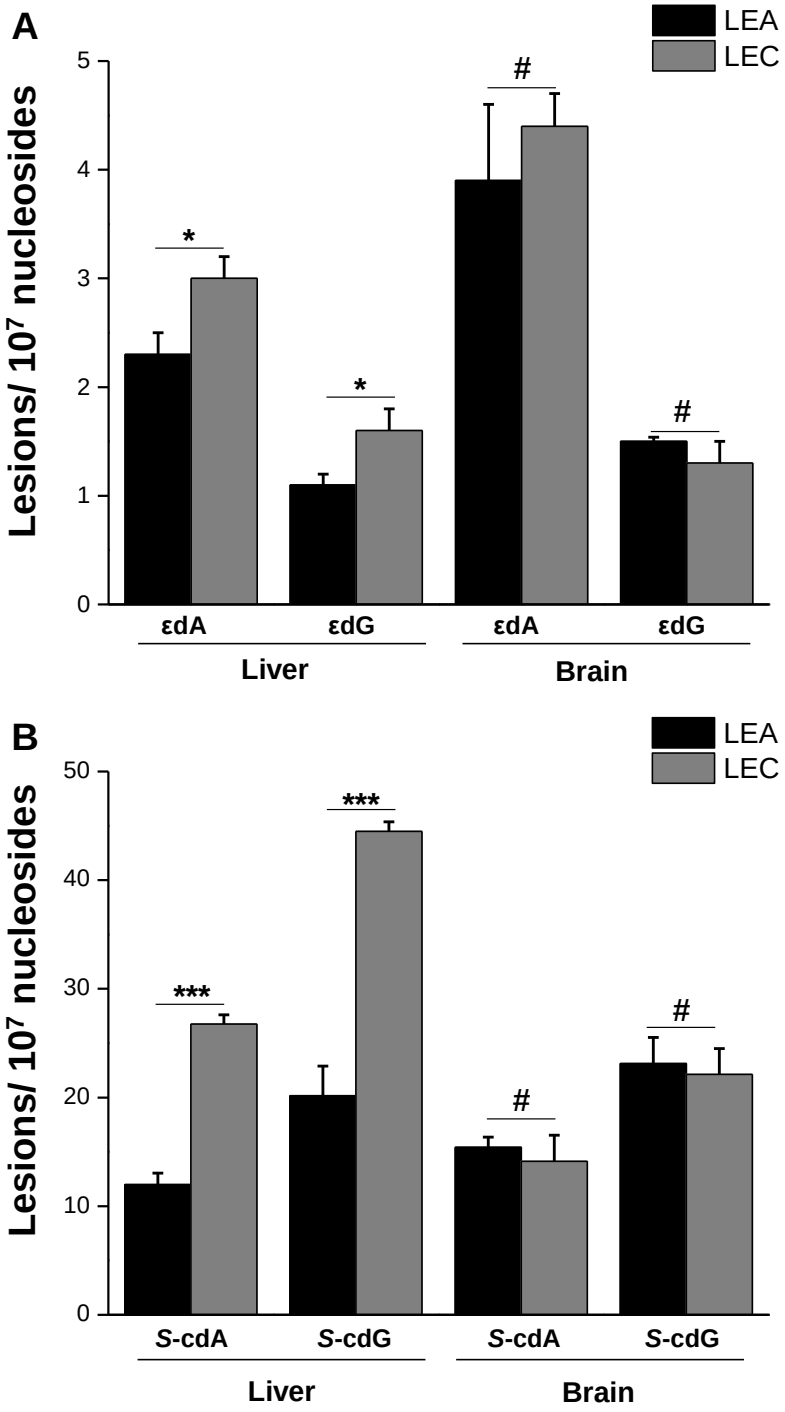

A
LEA
LEC
Lesions/ 10^7 nucleosides
0
1
2
3
4
5
*
*
#
#
εdA
εdG
εdA
εdG
Liver
Brain
B
LEA
LEC
Lesions/ 10^7 nucleosides
0
10
20
30
40
50
***
***
#
#
S-cdA
S-cdG
S-cdA
S-cdG
Liver
Brain

Figure 2.2.Quantification results for the levels of εdA and εdG (A), as well as *S*-cdA and *S*-cdG (B) in liver tissues of LEA (n = 6) and LEC (n = 5) rats as well as in brain tissues of LEA (n = 3) and LEC (n = 3) rats. The data represent the mean and standard deviation of the measurement results. The *P* values were calculated using unpaired two-tailed Student's *t*-test. #, $P > 0.05$; *, $P < 0.05$; **, $P < 0.01$; ***, $P < 0.001$.

The levels of 5-HmdC and 5-mdC in liver and brain tissues of LEA and LEC rats

5-HmdC is considered as a key nexus in DNA cytosine demethylation in mammalian cells that can either be passively diluted through DNA replication or actively converted to dC through further oxidation (i.e. to 5-FodC and 5-CadC) and action by TDG-mediated BER process (16,21,41). On the basis of our previous finding that Cu^{2+}/H_2O_2/ascorbate could induce oxidation of 5-mdC to 5-HmdC in synthetic duplex DNA *in vitro*, we initially hypothesized that copper accumulation may also stimulate 5-HmdC formation in liver tissues of LEC rats. However, our quantification data revealed significantly lower levels of 5-HmdC in liver tissues of LEC rats than LEA rats (at 176 and 339 modifications per 10^6 nucleosides, respectively. Figure 2.3A & Figure A2.3). The LC-MS/MS quantification results showed similar level of 5-mdC in liver of LEA and LEC rats (Figure 2.3B & Figure A2.3); thus, the lower level of 5-HmdC in liver of LEC rats was not attributed to alterations in 5-mdC levels. In line with the lack of difference in the prevalence of cPu and etheno DNA lesions in brain tissues of LEA and LEC rats, we found no appreciable difference in 5-HmdC levels in DNA extracted from brain of LEA and LEC rats (Figure 2.3A & Table A2.2).

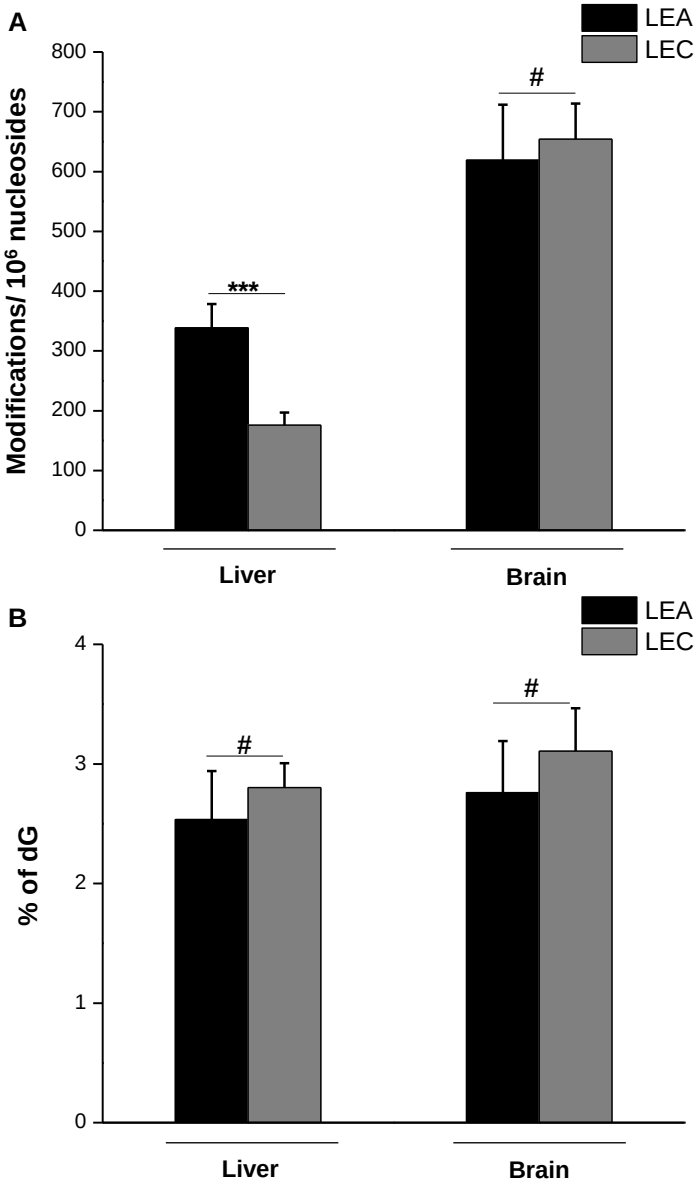


Figure 2.3.Quantification results for the levels of 5-HmdC (A) and 5-mdC (B) in LEA rat liver tissues (n = 6), LEC rat liver tissues (n = 5), LEA rat brain tissues (n = 3) and LEC rat brain tissues (n = 3). The data represent the mean and standard deviation of the measurement results. The *P* values were calculated using unpaired two-tailed Student's *t*-test. #, $P > 0.05$; *, $P < 0.05$; **, $P < 0.01$; ***, $P < 0.001$.

Biochemical assay for Tet1-mediated oxidation of 5-mdC in duplex DNA

The above results prompted us to reason that decreased levels of 5-HmdC in liver tissues of LEC rats might result from inhibition of Tet enzymes by elevated levels of copper ions. To explore this, we examined how the presence of Cu^{2+} ion affects the TET1-mediated oxidation of 5-mdC in duplex DNA *in vitro* (Figure 2.4A & Figure A2.4) (38). "Ultra-zoom-scan" MS-based quantification results revealed 5-HmdC and 5-FodC as the major Tet1 oxidation products of 5-mdC in double-stranded DNA. Addition of Cu^{2+} ion to the reaction mixture significantly reduced the overall catalytic efficiencies of Tet1 in all samples with Cu^{2+} treatment compared to the reaction without Cu^{2+} (Figure 2.4B). In particular, we observed that the inhibition of Tet1-mediated formation of 5-FodC is dependent on the concentration of Cu^{2+} (Figure 2.4B). Moreover, the remaining TET1 activity in Cu^{2+}-treated samples was largely similar to the control samples without addition of Fe^{2+} or Cu^{2+}, suggesting that only a portion of the Tet1 protein was initially charged with Fe^{2+}, and Cu^{2+} may not displace Fe^{2+} already incorporated in the active center of the Tet1 enzyme. In this context, it is worth noting the difference between the Tet1 protein used in the *in vitro* biochemical assay and the Tet proteins in liver tissues of LEC rats. The Tet1 protein used for the *in vitro* assay was purified from host cells that were not exposed to high concentrations of copper. Therefore, the catalytic center of the protein is expected to be occupied, in part, by Fe^{2+} which, as noted above, may not be readily replaced with Cu^{2+} during the *in vitro* reaction. In the hepatocytes of LEC rats, the Tet proteins are folded in an environment with elevated concentrations of Cu^{2+}, and the resulting Cu^{2+}-bound Tet proteins are not expected to be active (*vide infra*).

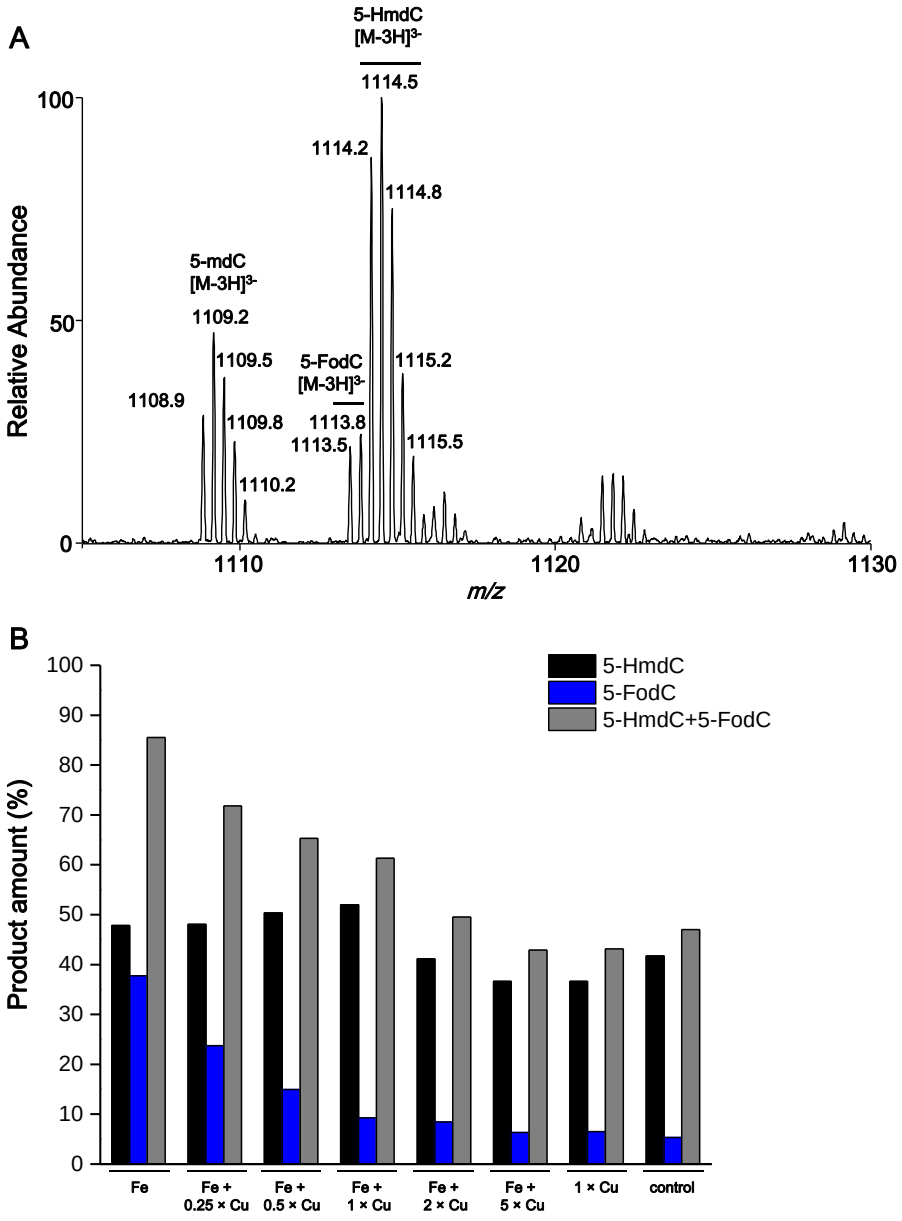

A
5-HmdC
[M-3H]3-
1114.5
1114.2
1114.8
100
50
0
Relative Abundance
5-mdC
[M-3H]3-
1109.2
1109.5
1108.9
1109.8
1110.2
5-FodC
[M-3H]3-
1113.8
1113.5
1115.2
1115.5
1110
1120
1130
m/z
B
5-HmdC
5-FodC
5-HmdC+5-FodC
Product amount (%)
100
90
80
70
60
50
40
30
20
10
0
Fe
Fe +
0.25 × Cu
Fe +
0.5 × Cu
Fe +
1 × Cu
Fe +
2 × Cu
Fe +
5 × Cu
1 × Cu
control

Figure 2.4.(A) Representative LC-MS data for monitoring the Tet1-mediated oxidation of 5-mdC in a duplex DNA, d(AGCTC(5-mdC)GGTCA)/d(GTGACCGGAGCTG). Shown are the higher resolution "ultra-zoom-scan" MS results for monitoring the $[M - 3H]^{3-}$ ions of the initial 5-mdC-bearing DNA and its oxidation products. (B) Quantification results for the formation of 5-HmdC and 5-FodC in Tet-mediated oxidation of 5-mdC in the presence of a reaction buffer containing 75 μM Fe^{2+} and various concentrations of Cu^{2+} (at Cu^{2+}/Fe^{2+} molar ratios of 0, 0.25, 0.50, 1.0, 2.0 and 5.0). A control reaction was also conducted in the presence of 75 μM Cu^{2+} alone (1× Cu).

Discussion

In the present study, we employed a novel NanoLC-NSI/MS^2 coupled with the stable isotope-dilution method for the first comprehensive assessment of oxidatively induced modifications of DNA. These included nucleoside modifications induced directly by ROS (cdA and cdG), indirectly by ROS (εdA and εdG from byproducts of LPO), and enzymatically from Tet-catalyzed 5-mdC oxidation. This method offers unambiguous chemical specificity for analyte identification based on the co-elution of the analyte with its stable isotope-labeled standard and the characteristic fragment ions observed in the MS/MS or MS/MS/MS (Figure 2.1). Although the ROS-induced cyclopurine lesions were quantified in our previous work (10), in the present study we were able to rigorously compare the levels of direct ROS-induced cyclopurine lesions with the LPO-induced εdA and εdG lesions in DNA isolated from the tissues of the same animals and based on measurements made on the same analytical platform. Our results revealed for the first time that, relative to LPO-induced εdA and εdG lesions, the direct ROS-induced *S*-cdA and *S*-cdG were present at much higher levels in liver and brain tissues of LEA and LEC rats, and were stimulated to a greater extent by aberrant accumulation of copper ions in liver tissues of LEC rats (Figure 2.2).

We found significantly lower levels of 5-HmdC in DNA isolated from the liver tissues of LEC than LEA rats (Figure 2.3A), though no appreciable differences were observed for the levels of 5-mdC (Figure 2.3B). This result is seemingly incongruent with our previous *in vitro* data concerning the dose-dependent induction of 5-HmdC by Fenton-type reagent (30). However, results from our *in vitro* biochemical assay suggested

that aberrant accumulation of copper may directly perturb the TET-mediated oxidation of 5-mdC to 5-HmdC. In this vein, Ni^{2+} ion is known to be able to replace Fe^{2+} from the catalytic center of other Fe^{2+}- and 2-OG-dependent dioxygenases (31,34). The stability of bivalent transition metal ion complexes follows the Irving-Williams order, i.e. $Mn^{2+} < Fe^{2+} < Co^{2+} < Ni^{2+} < Cu^{2+} > Zn^{2+}$, irrespective of the nature of the ligand (42). In addition, Cu^{2+} was previously shown to be capable of substituting Fe^{2+} from the DNA repair enzyme, AlkB, another Fe^{2+}/2-OG-dependent dioxygenase (43). Thus, Cu^{2+} may occupy the catalytic center of TET1 in lieu of Fe^{2+}. The catalytic cycle mediated by the Fe^{2+}/2-OG-dependent dioxygenases, including TET proteins, involves Fe^{4+} (44), an oxidation state that cannot be adopted by Cu^{2+}. Thus, Cu^{2+} may occupy the Fe^{2+}-binding site of TET enzymes and disrupt their catalytic activities because of the incapability of Cu^{2+} to undergo further oxidization. Viewing that aberrant epigenetic regulation of gene expression is associated with cancer development (45), our results also suggest that abnormal copper accumulation-induced dysfunction of TET enzymes may contribute, in part, to progressive hepatic injury in Wilson's disease.

Aside from TET enzymes, other members of the Fe(II)- and 2-OG-dependent dioxygenase family may also act as potential molecular targets for copper toxicity. *Escherichia coli* AlkB protein, which is an ortholog of human ALKBH2 and ALKBH3, were shown to be capable of repairing etheno DNA lesions (46,47). Thus, compromised ALKBH repair activity arising from elevated copper content may also account, in part, for greater accumulation of etheno DNA lesions in liver tissues of LEC rats relative to LEA rats. As observed for Ni^{2+} ion (31,33), elevated copper accumulation may also

inhibit the Fe^{2+}/2-OG-dependent dioxygenases involved in histone demethylation, which may play roles in hepatic damage in human Wilson's disease.

In summary, we employed a sensitive LC-MS/MS and MS^3 coupled with the stable isotope-dilution method for simultaneous quantification of oxidative stress-induced cPus and etheno DNA lesions, as well as 5-HmdC and 5-mdC epigenetic marks in tissue DNA. Our results illustrated, for the first time, relative levels of ROS- and LPO-induced DNA adducts *in vivo*, which supported the implications of oxidative DNA damage in pathogenesis of Wilson's disease and revealed the relative contributions of these two subgroups of oxidatively induced DNA lesions (i.e., the direct ROS-induced cdA and cdG vs. LPO-induced εdA and εdG) to this process. Moreover, assessment of 5-HmdC and 5-mdC levels in DNA, in combination with results of TET1-mediated 5-mdC oxidation *in vitro*, suggest a role of copper-induced inhibition of TET enzymes and resultant perturbation of 5-HmdC epigenetic mark in the pathophysiology of Wilson's disease. Taken together, our data provide mechanistic insights into copper toxicity *in vivo*, where accumulation of copper may compromise genomic integrity by oxidative DNA damage and perturbation of epigenetic pathways of gene regulation.

References

1. Finkel, T. and Holbrook, N.J. (2000) Oxidants, oxidative stress and the biology of ageing. *Nature*, **408**, 239-247.

2. Friedberg, E.C., Walker, G.C., Siede, W., Wood, R.D., Schultz, R.A. and Ellenberger, T. (2006) *DNA Repair and Mutagenesis*. ASM Press, Washington, D.C.

3. Brooks, P.J. (2007) The case for 8,5'-cyclopurine-2'-deoxynucleosides as endogenous DNA lesions that cause neurodegeneration in xeroderma pigmentosum. *Neurosci.*, **145**, 1407-1417.

4. Wang, Y. (2008) Bulky DNA lesions induced by reactive oxygen species. *Chem. Res. Toxicol.*, **21**, 276-281.

5. Chung, F.L., Chen, H.J.C. and Nath, R.G. (1996) Lipid peroxidation as a potential endogenous source for the formation of exocyclic DNA adducts. *Carcinogenesis*, **17**, 2105-2111.

6. Marnett, L.J. (2000) Oxyradicals and DNA damage. *Carcinogenesis*, **21**, 361-370.

7. Chen, H.-J.C., Lin, G.-J. and Lin, W.-P. (2010) Simultaneous quantification of three lipid peroxidation-derived etheno adducts in human DNA by stable isotope dilution nanoflow liquid chromatography nanospray ionization tandem mass spectrometry. *Anal. Chem.*, **82**, 4486-4493.

8. Chen, H.-J.C. and Lin, W.-P. (2009) Simultaneous quantification of 1,N^2-propano-2'-deoxyguanosine adducts derived from acrolein and crotonaldehyde in human placenta and leukocytes by isotope dilution nanoflow LC nanospray ionization tandem mass spectrometry. *Anal. Chem.*, **81**, 9812-9818.

9. Wang, J., Clauson, C.L., Robbins, P.D., Niedernhofer, L.J. and Wang, Y. (2012) The oxidative DNA lesions 8,5'-cyclopurines accumulate with aging in a tissue-specific manner. *Aging Cell*, **11**, 714-716.

10. Wang, J., Yuan, B., Guerrero, C., Bahde, R., Gupta, S. and Wang, Y. (2011) Quantification of oxidative DNA lesions in tissues of Long-Evans Cinnamon rats by capillary high-performance liquid chromatography-tandem mass spectrometry coupled with stable isotope-dilution method. *Anal. Chem.*, **83**, 2201-2209.

11. Zhang, S., Villalta, P.W., Wang, M. and Hecht, S.S. (2006) Analysis of crotonaldehyde- and acetaldehyde-derived 1,N^2-propanodeoxyguanosine adducts in DNA from human tissues using liquid chromatography electrospray ionization tandem mass spectrometry. *Chem. Res. Toxicol.*, **19**, 1386-1392.

12. Mitra, D., Luo, X., Morgan, A., Wang, J., Hoang, M.P., Lo, J., Guerrero, C.R., Lennerz, J.K., Mihm, M.C., Wargo, J.A. *et al.* (2012) An ultraviolet-radiation-independent pathway to melanoma carcinogenesis in the red hair/fair skin background. *Nature*, **491**, 449-453.

13. Shaked, H., Hofseth, L.J., Chumanevich, A., Chumanevich, A.A., Wang, J., Wang, Y., Taniguchi, K., Guma, M., Shenouda, S., Clevers, H. *et al.* (2012) Chronic epithelial NF-κB activation accelerates APC loss and intestinal tumor initiation through iNOS up-regulation. *Proc. Natl. Acad. Sci. U. S. A.*, **109**, 14007-14012.

14. Tilstra, J.S., Robinson, A.R., Wang, J., Gregg, S.Q., Clauson, C.L., Reay, D.P., Nasto, L.A., St Croix, C.M., Usas, A., Vo, N. *et al.* (2012) NF-κB inhibition delays DNA damage-induced senescence and aging in mice. *J. Clin. Invest.*, **122**, 2601-2612.

15. Pfaffeneder, T., Hackner, B., Truss, M., Muenzel, M., Mueller, M., Deiml, C.A., Hagemeier, C. and Carell, T. (2011) The discovery of 5-formylcytosine in embryonic stem cell DNA. *Angew. Chem.-Int. Ed.*, **50**, 7008-7012.

16. He, Y.-F., Li, B.-Z., Li, Z., Liu, P., Wang, Y., Tang, Q., Ding, J., Jia, Y., Chen, Z., Li, L. *et al.* (2011) Tet-mediated formation of 5-carboxylcytosine and its excision by TDG in mammalian DNA. *Science*, **333**, 1303-1307.

17. Ito, S., D'Alessio, A.C., Taranova, O.V., Hong, K., Sowers, L.C. and Zhang, Y. (2010) Role of Tet proteins in 5mC to 5hmC conversion, ES-cell self-renewal and inner cell mass specification. *Nature*, **466**, 1129-U1151.

18. Ito, S., Shen, L., Dai, Q., Wu, S.C., Collins, L.B., Swenberg, J.A., He, C. and Zhang, Y. (2011) Tet proteins can convert 5-methylcytosine to 5-formylcytosine and 5-carboxylcytosine. *Science*, **333**, 1300-1303.

19. Kriaucionis, S. and Heintz, N. (2009) The nuclear DNA base 5-hydroxymethylcytosine is present in Purkinje neurons and the brain. *Science*, **324**, 929-930.

20. Tahiliani, M., Koh, K.P., Shen, Y., Pastor, W.A., Bandukwala, H., Brudno, Y., Agarwal, S., Iyer, L.M., Liu, D.R., Aravind, L. *et al.* (2009) Conversion of 5-methylcytosine to 5-hydroxymethylcytosine in mammalian DNA by MLL partner TET1. *Science*, **324**, 930-935.

21. Maiti, A. and Drohat, A.C. (2011) Thymine DNA glycosylase can rapidly excise 5-formylcytosine and 5-carboxylcytosine: potential implications for active demethylation of CpG sites. *J. Biol. Chem.*, **286**, 35334-35338.

22. Mellen, M., Ayata, P., Dewell, S., Kriaucionis, S. and Heintz, N. (2012) MeCP2 binds to 5hmC enriched within active genes and accessible chromatin in the nervous system. *Cell*, **151**, 1417-1430.

23. Yildirim, O., Li, R., Hung, J.H., Chen, P.B., Dong, X., Ee, L.S., Weng, Z., Rando, O.J. and Fazzio, T.G. (2011) Mbd3/NURD complex regulates expression of 5-hydroxymethylcytosine marked genes in embryonic stem cells. *Cell*, **147**, 1498-1510.

24. Spruijt, C.G., Gnerlich, F., Smits, A.H., Pfaffeneder, T., Jansen, P.W., Bauer, C., Munzel, M., Wagner, M., Muller, M., Khan, F. *et al.* (2013) Dynamic readers for 5-(hydroxy)methylcytosine and its oxidized derivatives. *Cell*, **152**, 1146-1159.

25. Frauer, C., Hoffmann, T., Bultmann, S., Casa, V., Cardoso, M.C., Antes, I. and Leonhardt, H. (2011) Recognition of 5-hydroxymethylcytosine by the Uhrf1 SRA domain. *PLoS One*, **6**, e21306.

26. Ala, A., Walker, A.P., Ashkan, K., Dooley, J.S. and Schilsky, M.L. (2007) Wilson's disease. *Lancet*, **369**, 397-408.

27. Roberts, E.A. and Schilsky, M.L. (2008) Diagnosis and treatment of Wilson disease: An update. *Hepatol.*, **47**, 2089-2111.

28. Li, Y., Togashi, Y., Sato, S., Emoto, T., Kang, J.H., Takeichi, N., Kobayashi, H., Kojima, Y., Une, Y. and Uchino, J. (1991) Spontaneous hepatic copper accumulation in Long-Evans Cinnamon rats with hereditary hepatitis. A model of Wilson's disease. *J. Clin. Invest.*, **87**, 1858-1861.

29. Nair, J., Strand, S., Frank, N., Knauft, J., Wesch, H., Galle, P.R. and Bartsch, H. (2005) Apoptosis and age-dependant induction of nuclear and mitochondrial etheno-DNA adducts in Long-Evans Cinnamon (LEC) rats: enhanced DNA damage by dietary curcumin upon copper accumulation. *Carcinogenesis*, **26**, 1307-1315.

30. Cao, H. and Wang, Y. (2007) Quantification of oxidative single-base and intrastrand cross-link lesions in unmethylated and CpG-methylated DNA induced by Fenton-type reagents. *Nucleic Acids Res.*, **35**, 4833-4844.

31. Chen, H., Giri, N.C., Zhang, R., Yamane, K., Zhang, Y., Maroney, M. and Costa, M. (2010) Nickel ions inhibit histone demethylase JMJD1A and DNA repair enzyme ABH2 by replacing the ferrous iron in the catalytic centers. *J. Biol. Chem.*, **285**, 7374-7383.

32. Chervona, Y., Arita, A. and Costa, M. (2012) Carcinogenic metals and the epigenome: understanding the effect of nickel, arsenic, and chromium. *Metallomics*, **4**, 619-627.

33. Chervona, Y. and Costa, M. (2012) The control of histone methylation and gene expression by oxidative stress, hypoxia, and metals. *Free Radic. Biol. Med.*, **53**, 1041-1047.

34. Chen, H. and Costa, M. (2009) Iron- and 2-oxoglutarate-dependent Dioxygenases: an emerging group of molecular targets for nickel toxicity and carcinogenicity. *BioMetals*, **22**, 191-196.

35. Chen, H.J.C., Chiang, L.C., Tseng, M.C., Zhang, L.L., Ni, J.S. and Chung, F.L. (1999) Detection and quantification of 1,N^6-ethenoadenine in human placental DNA by mass spectrometry. *Chem. Res. Toxicol.*, **12**, 1119-1126.

36. Garcia, C.C.M., Freitas, F.P., Di Mascio, P. and Medeiros, M.H.G. (2010) Ultrasensitive simultaneous quantification of 1,N^2-etheno-2'-deoxyguanosine and 1,N^2-propano-2'-deoxyguanosine in DNA by an online liquid chromatography-electrospray tandem mass spectrometry assay. *Chem. Res. Toxicol.*, **23**, 1245-1255.

37. Liu, S., Wang, J., Su, Y., Guerrero, C., Zeng, Y., Mitra, D., Brooks, P.J., Fisher, D.E., Song, H. and Wang, Y. (2013) Quantitative assessment of Tet-induced oxidation products of 5-methylcytosine in cellular and tissue DNA. *Nucleic Acids Res.*, **41**, 6421-6429.

38. Fu, L., Guerrero, C.R., Zhong, N., Amato, N.J., Liu, Y., Liu, S., Cai, Q., Ji, D., Jin, S.-G., Niedernhofer, L.J. *et al.* (2014) Tet-mediated formation of 5-hydroxymethylcytosine in RNA. *J. Am. Chem. Soc.*, **136**, 11582-11585.

39. Jaruga, P., Birincioglu, M., Rodriguez, H. and Dizdaroglu, M. (2002) Mass spectrometric assays for the tandem lesion 8,5'-cyclo-2'-deoxyguanosine in mammalian DNA. *Biochemistry*, **41**, 3703-3711.

40. Ahn, T.B., Cho, S.S., Kim, D.W. and Jeon, B.S. (2005) Absence of nigrostriatal degeneration in LEC rats up to 20 weeks of age. *Neurol. Res.*, **27**, 409-411.

41. Kohli, R.M. and Zhang, Y. (2013) TET enzymes, TDG and the dynamics of DNA demethylation. *Nature*, **502**, 472-479.

42. Irving, H. and Williams, R.J.P. (1953) The stability of transition-metal complexes. *J. Chem. Soc.*, 3192-3210.

43. Bleijlevens, B., Shivarattan, T., Sedgwick, B., Rigby, S.E. and Matthews, S.J. (2007) Replacement of non-heme Fe(II) with Cu(II) in the α-ketoglutarate dependent DNA repair enzyme AlkB: spectroscopic characterization of the active site. *J. Inorg. Biochem.*, **101**, 1043-1048.

44. Lu, X., Zhao, B.S. and He, C. (2015) TET family proteins: Oxidation activity, interacting molecules, and functions in diseases. *Chem. Rev.*, **115**, 2225-2239.

45. Lund, A.H. and van Lohuizen, M. (2004) Epigenetics and cancer. *Genes Dev.*, **18**, 2315-2335.

46. Delaney, J.C., Smeester, L., Wong, C., Frick, L.E., Taghizadeh, K., Wishnok, J.S., Drennan, C.L., Samson, L.D. and Essigmann, J.M. (2005) AlkB reverses etheno DNA lesions caused by lipid oxidation *in vitro* and *in vivo*. *Nat. Struct. Mol. Biol.*, **12**, 855-860.

47. Frick, L.E., Delaney, J.C., Wong, C., Drennan, C.L. and Essigmann, J.M. (2007) Alleviation of 1,N^6-ethanoadenine genotoxicity by the *Escherichia coli* adaptive response protein AlkB. *Proc. Natl. Acad. Sci. USA*, **104**, 755-760.

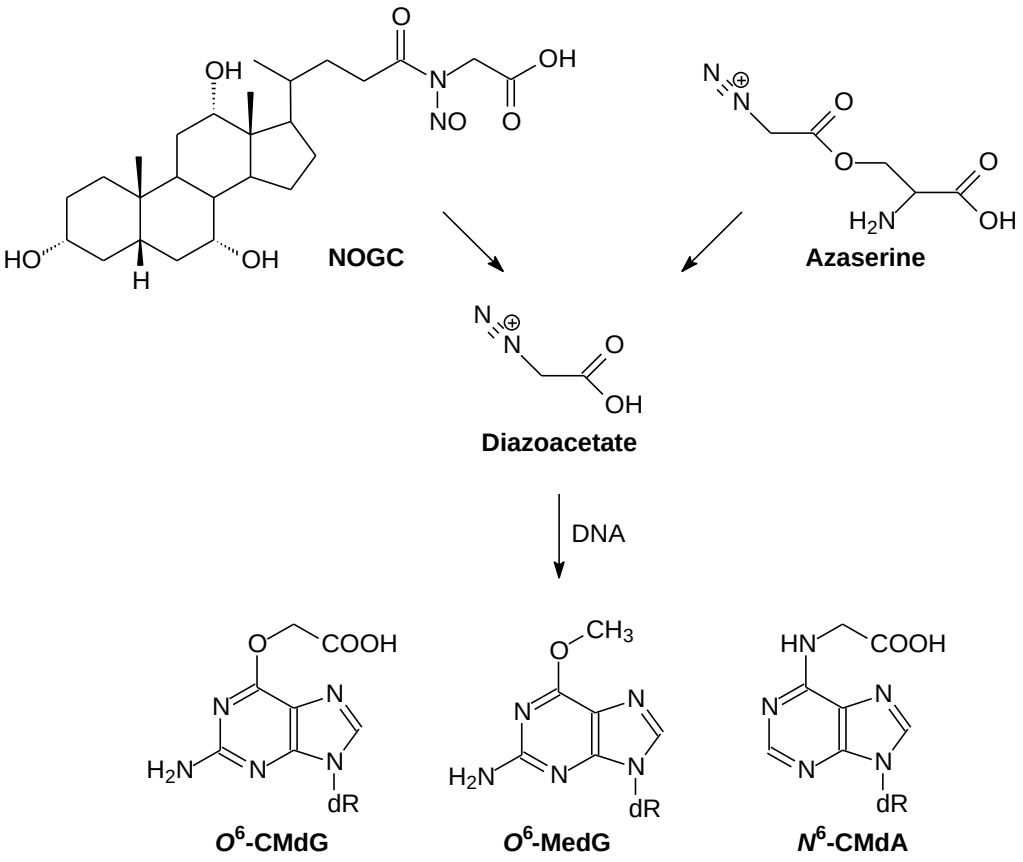
Chapter 3 Quantification of azaserine-induced carboxymethylated and methylated DNA lesions in cells by nanoflow liquid chromatography-nanoelectrospray ionization tandem mass spectrometry coupled with the stable isotope-dilution method

Introduction

Human genome is continuously assaulted by a variety of endogenous and exogenous toxicants which can give rise to DNA damage and compromise genomic integrity (1). In this vein, *N*-nitroso compounds (NOCs) are present in food, tobacco, and pharmaceutical products (2,3). Despite the prevalence of exogenous sources of NOCs, it was estimated that endogenous sources constitute 45-75% of total NOC exposure in humans (2). In a widely accepted model for the etiology of gastric cancer, DNA damage emanating from intragastric nitrosation is considered an important factor contributing to early stages of disease development (4). In support of this hypothesis, results from a recent European Prospective Investigation into Cancer and Nutrition, which encompassed more than 500,000 individuals and 314 incident cases of gastric cancer that had occurred after an average of 6.6 years of follow-up, showed a significant association between endogenous NOC level and the risk of non-cardia gastric cancer (5). In this vein, elevated red meat intake in humans was found to elicit a 3-fold increase in fecal NOC levels (6).

After metabolic activation, some NOCs can lead to carboxymethylation, and to a lesser degree, methylation of DNA (3). *N*-nitrosoglycocholic acid (NOGC), an *N*-nitroso bile acid conjugate, was previously found to be mutagenic in *Salmonella typhimurium*

and in diploid human lymphoblasts (7), and carcinogenic to laboratory animals (8). Incubation of calf thymus DNA with NOGC *in vitro* was shown to induce the carboxymethylation of the *N*3 of adenine as well as the *N*7 and O^6 of guanine, which is accompanied with the methylation of the O^6 of guanine (9). In addition, *N*-(N^6-acetyl-L-prolyl)-*N*-nitrosoglycine was found to induce O^6-carboxymethyl-2′-deoxyguanosine (O^6-CMdG) and, to a lower degree, O^6-methyl-2′-deoxyguanosine (O^6-MedG, Scheme 1) in DNA (10,11). Aside from NOCs, DNA carboxymethylation can also occur in cells upon exposure to azaserine (10-12), a pancreatic carcinogen (13). DNA carboxymethylation induced by the aforementioned agents is thought to arise from a common reactive intermediate, diazoacetate (Scheme 3.1) (3,14). Diazoacetate can decompose to yield carboxymethyldiazonium and methyldiazonium ions, which result in the carboxymethylation and methylation of DNA, respectively (3,14). Aside from guanine and adenine, cytosine and thymine in DNA can also be carboxymethylated by diazoacetate (15,16).



Scheme 3.1.Formation of diazoacetate and its induction of O^6-CMdG, O^6-MedG, and N^6-CMdA.

If not repaired, carboxymethylated DNA lesions may compromise the flow of genetic information by inhibiting DNA replication and transcription, and induce mutations in these processes. Gottschalg *et al.* (14) observed that the replication of diazoacetate-treated, human *p53* gene-containing plasmid in yeast cells could give rise to remarkably similar mutation profiles (types and frequencies of mutations) at non-CpG sites as those of *p53* gene found in human stomach and colorectal cancers. In particular, diazoacetate could induce nearly equal frequencies of transition and transversion

mutations, which differ from the predominant GC→AT transition mutations (>80%) induced by a DNA methylating agent (i.e. *N*-methyl-*N*-nitrosourea) (14). Preferential formation of O^6-CMdG over O^6-MedG was observed for isolated DNA treated with various DNA carboxymethylating agents and for human cells treated with diazoacetate (10,17). These findings, along with the fact that O^6-MedG induces predominantly GC→AT transition mutation (18), indicate that DNA carboxymethylation, rather than methylation, may contribute to the mutations of *p53* gene found in gastrointestinal cancer (14). Recent replication and transcription studies with the use of plasmids housing a site-specifically inserted DNA lesion showed that both O^4- and *N*3-carboxymethylthymidine could substantially block DNA replication and transcription in cells, and induce mutations in these processes (19-21). On the other hand, N^4-carboxymethyl-2′-deoxycytidine and N^6-carboxymethyl-2′-deoxyadenosine don't constitute strong blocks to DNA replication in *Escherichia coli* cells, and the replication across these lesions is highly accurate (20).

The potential involvement of NOCs and the resulting DNA carboxymethylation in human gastrointestinal carcinogenesis calls for robust analytical methods for the unambiguous identification and accurate quantification of carboxymethylated DNA lesions. In this context, ^{32}P-postlabeling assay (22), immunoslot blot assay (23) and immunoaffinity enrichment coupled with HPLC with fluorescence detection (10,11) were employed for measuring the levels of O^6-CMdG and O^6-MedG *in vitro* and *in vivo*. Owing to advances in instrumentation and sample preparation methods, mass spectrometry has become widely employed for the detection of DNA adducts by

providing structural and quantitative information (24,25). In this regard, solid-phase extraction followed by LC-MS/MS analysis on a triple-quadrupole mass spectrometer was previously employed for the quantification of O^6-CMdG and O^6-MedG, directly or after converting them to the corresponding modified nucleobases with acid hydrolysis at elevated temperature (17,26). Although neither approach provided adequate sensitivity for detecting these modified nucleosides in human urine samples (26), LC-MS/MS analysis of the acid-hydrolyzed samples facilitated the successful detection of O^6-CMdG and O^6-MedG in DNA isolated from cultured human cells treated with diazoacetate (17).

In this study, we developed a highly sensitive nano-flow liquid chromatography-nanoelectrospray ionization tandem mass spectrometry (nLC-nESI-MS^3) coupled with the stable isotope-dilution method for the simultaneous quantification of N^6-CMdA, O^6-CMdG and O^6-MedG (Scheme 3.1) in genomic DNA extracted from cells treated with azaserine. We decided to assess the formation of O^6-CMdG and O^6-MedG because their measurements will allow for the comparison of the levels of DNA lesions formed from *in-vivo* carboxymethylation and methylation. We chose to include N^6-CMdA in our analysis because our previous LC-MS/MS analysis suggests that this lesion is produced at a much higher level than O^6-CMdG in diazoacetate-treated calf thymus DNA (16).

Experimental section

Materials & cell lines

All chemicals and enzymes, unless otherwise specified, were purchased from Sigma-Aldrich (St. Louis, MO) or New England Biolabs (Ipswich, WA). Stable isotope-labeled compounds were obtained from Cambridge Isotope Laboratories (Cambridge,

MA). *Erythro*-9-(2-hydroxy-3-nonyl)adenine (EHNA) hydrochloride was from Tocris Bioscience (Ellisville, MO). GM04429 human skin fibroblasts deficient in xeroderma pigmentosum complementation group A (XPA) were kindly provided by Prof. Gerd P. Pfeifer. The human colorectal carcinoma HCT-116 cells were purchased from ATCC (Manassas, VA).

Preparation of standards

N^6-CMdA was synthesized previously (16). [$^{13}C_2$,^{15}N]-N^6-CMdA was prepared following the same procedures as those for the preparation of the unlabeled counterpart except that glycine ethyl ester was replaced with [$^{13}C_2$,^{15}N]-glycine ethyl ester, and the latter was synthesized from the commercially available [$^{13}C_2$,^{15}N]-glycine. Exact mass measurement (Agilent 6210 ESI-TOF MS) gave *m/z* 313.1185 for the $[M + H]^+$ ion of the [$^{13}C_2$,^{15}N]-N^6-CMdA, which is consistent with the calculated *m/z* of 313.1189.

O^6-CMdG was prepared following published procedures (11), and [D_2]-O^6-CMdG was synthesized by using the same procedures except that [D_2]-methyl glycolate, synthesized from the commercially available [D_2]-glycolic acid, was used in lieu of methyl glycolate. Exact mass measurement yielded *m/z* 328.1231 for the $[M + H]^+$ ion of the [D_2]-O^6-CMdG, which is in keeping with the calculated *m/z* of 328.1226.

O^6-MedG was synthesized according to a previously reported method (27), and the similar procedures were employed for the synthesis of [D_3]-O^6-MedG except that CD_3OD was used for incorporating the -OCD_3 group. Exact mass measurement gave *m/z* 285.1397 for the $[M + H]^+$ ion of the [D_3]-O^6-MedG, which is consistent with the calculated *m/z* of 285.1391.

Cell culture and azaserine treatment

XPA-deficient GM04429 human skin fibroblast cells and human colorectal carcinoma HCT-116 cells were cultured at 37°C in 5% CO_2 atmosphere in ATCC-recommended medium containing 10% fetal bovine serum and 100 IU/ml of penicillin. Cells (1~1.5 × 10^6) were seeded in 75 cm^2 flasks in complete medium. After 24 h, the cells were treated with different concentrations of azaserine (i.e. 0, 50, 150 and 450 μM). After 4 h of treatment, the cells were detached by using trypsin-EDTA and harvested by centrifugation. The cell pellets were subsequently washed twice with phosphate-buffered saline (PBS) to remove residual medium and azaserine.

Extraction and enzymatic digestion of nuclear DNA

Genomic DNA was extracted by using a high-salt method (28). A lysis buffer (70 μL), which contained 20 mM Tris (pH 8.1), 20 mM EDTA, 400 mM NaCl, 1% SDS (w/v), and 10 μL of proteinase K (20 mg/mL), was added to the cell pellet and incubated at 55°C overnight. Saturated NaCl solution (0.5 volume) was subsequently added to the digestion mixture, which was then vortexed briefly and incubated at 55°C for another 15 min. The resulting mixture was centrifuged at 13,000 rpm for 30 min, and the nucleic acids were precipitated from the supernatant with 2 volumes of ethanol. The RNA in the nucleic acid mixture was removed by digestion with 3 μL RNase A (10 mg/mL) and 2 μL RNase T1 (25 units/μL) at 37°C overnight followed by extraction with an equal volume of chloroform/isoamyl alcohol (24:1, v/v). The DNA was then precipitated from the aqueous layer with ethanol and centrifuged at 13,000 rpm for 10 min. The resulting DNA pellet was washed twice with 70% cold ethanol, allowed to air-dry at room temperature,

re-dissolved in doubly-distilled water and quantified by UV absorption measurement at 260 nm. Normally 15 μg DNA can be extracted from 1~1.5 × 10^6 cells.

The extracted cellular DNA (10 μg) was digested with 1 unit of nuclease P1 and 0.00125 unit of phosphodiesterase II in a 15-μL buffer containing 300 mM sodium acetate (pH 5.6), 10 mM $ZnCl_2$, and 2.5 nmol of EHNA, and to the mixture were added 80 fmol [D_2]-*O*^{6}-CMdG, 12 fmol [$^{13}C_2$,^{15}N]-*N*^{6}-CMdA and 8 fmol [D_3]-*O*^{6}-MedG. EHNA served as an inhibitor for adenine deaminase and minimized the deamination of dA to 2'-deoxyinosine (dI). The above mixture was incubated at 37°C for 48 h. To the mixture were then added 1.0 unit of alkaline phosphatase, 0.0025 unit of phosphodiesterase I, and a 20-μL buffer containing 0.5 M Tris-HCl (pH 8.9). After incubation at 37°C for 2 h, the digestion mixture was neutralized with 9.5 μL 1.0 M formic acid. The enzymes in the digestion mixture were subsequently removed by extraction with an equal volume of chloroform. The aqueous layer was concentrated to 100 μL and subjected to off-line HPLC enrichment.

HPLC enrichment

An Alltima HP C18 column (4.6 × 250 mm, 5 μm in particle size, 300 Å in pore size, Grace Inc., Deerfield, IL) was employed for the enrichment of *O*^{6}-CMdG, *O*^{6}-MedG and *N*^{6}-CMdA from the enzymatic digestion mixture. A solution of 10 mM ammonium formate (mobile phase A) and acetonitrile (mobile phase B) were used, and the gradient comprised of 0-2% B in 5 min, 2% B for 40 min and 2-40% B in 30 min, with the flow rate being 1 mL/min. The HPLC fractions in the retention time range of 22.5-27.5 min were pooled for *O*^{6}-CMdG and *N*^{6}-CMdA, and those fractions in 54.5-57.5 min were

combined for O^6-MedG (Figure B3.1). The eluents were dried in a Speed-vac, reconstituted in doubly distilled water and subjected to nLC-nESI-MS^3 analysis.

nLC-nESI-MS^3 analysis

Online nLC-nESI-MS^3 analyses were conducted on an LTQ-XL linear ion trap mass spectrometer (Thermo Fisher Scientific) equipped with a nanoelectrospray ionization source and coupled with an EASY-nLC II system (Thermo Fisher Scientific). HPLC separation was carried out by using a homemade trapping column (150 μm × 40 mm) and an analytical column (75 μm × 200 mm), both packed with Magic C18 AQ (200 Å, 5 μm, Michrom BioResource, Auburn, CA). Mobile phases A and B contained 0.1% formic acid in doubly distilled H_2O and acetonitrile, respectively. Initially, the sample was loaded onto the trapping column with mobile phase A at a flow rate of 2.5 μL/min for 6 min. The DNA lesions of interest were then eluted by using a 30-min linear gradient of 0-20% mobile phase B at a flow rate of 300 nL/min. The LTQ-XL mass spectrometer was operated in the positive-ion mode, the spray voltage was 2.0 kV, and the temperature for the ion transfer tube was maintained at 275°C. In MS^3 analysis, the widths for precursor ion selection were 3 and 2 *m/z* units in MS/MS and MS^3 modes, respectively. The normalized collision energy, activation Q and activation time were 35, 0.3, and 30 ms, respectively, in both MS/MS and MS^3. The limit of quantitation (LOQ), defined as the amount of analyte generating a signal-to-noise ratio (S/N) of 10 in the selected-ion chromatograms (SICs) plotted for the transitions used for quantification, were determined via three independent measurements conducted in three separate days (Table B3.1). The intra- and inter-day precision and accuracy (Table 3.1) were evaluated by analyzing

quality control samples of O^6-CMdG, O^6-MedG and N^6-CMdA at two different concentrations. The quality control samples were generated from calf thymus DNA spiked with unlabeled standard solutions, following the same sample preparation procedure as real cellular DNA samples (DNA digestion, chloroform extraction and offline HPLC enrichment). The precision was expressed as relative standard deviation (RSD), and the mean accuracy was expressed as percent recovery. The amounts of the carboxymethylated and methylated DNA lesions (in moles) in the nucleoside mixtures were calculated from the peak area ratios found in the SICs for the analytes over their corresponding stable isotope-labeled standards, the amounts of the labeled standards used (in moles) and the calibration curves (Figure B3.2). The final DNA lesion levels, in terms of numbers of lesions per 10^7 nucleosides, were calculated by dividing the amount of the DNA adducts with the amount of total nucleosides (in moles) in the digested DNA.

Results

Syntheses of unlabeled and stable isotope-labeled standards

We set out to establish an nLC-nESI-MS^3 coupled with the stable isotope-dilution method for the quantification of carboxymethylated dA and dG lesions in cellular DNA. To this end, we first synthesized standards for the unlabeled and stable isotope-labeled N^6-CMdA, O^6-CMdG and O^6-MedG, as described in the Experimental Section. In this regard, we did not observe any appreciable H/D exchange of [D_2]-O^6-CMdG at room temperature over a month, indicating that [D_2]-O^6-CMdG is a suitable internal standard for quantitation.

nLC-nESI-MS^3 for the quantifications of O^6-CMdG, N^6-CMdA, and O^6-MedG

With the above stable isotope-labeled standards, we developed a sensitive LC-MS^3 method for the accurate quantification of these lesions. In this method, we first digested the cellular DNA with a cocktail of 4 enzymes to liberate the lesions of interest as mononucleosides (See Experimental Section). The isotope-labeled O^6-CMdG, N^6-CMdA, and O^6-MedG were added to the DNA digestion mixture prior to the first step of DNA digestion and chloroform extraction, which corrected for the potential analyte loss during the subsequent steps of sample preparation. We then assessed the LOQ of the nLC-nESI-MS^3 method prior to the analyses of cellular DNA samples. When pure unlabeled standards were analyzed, the LOQs for O^6-CMdG, N^6-CMdA and O^6-MedG were determined to be 73.4, 11.5 and 6.2 amol, respectively (Table B3.1). We also assessed the intra- and inter-day precision and accuracy by analyzing three different

concentrations of standard solutions of O^6-CMdG, N^6-CMdA and O^6-MedG. It turned out that our method provides adequate precision and accuracy for the measurement of these three lesions (Table 3.1).

	Intra-day		Inter-day	
N^6-CMdA (nM)	**RSD (%)**	**Recovery (%)**	**RSD (%)**	**Recovery (%)**
0.020	**10.9**	**83.3**	**9.6**	**70.0**
0.028	**11.6**	**85.7**	**7.5**	**88.1**
O^6-CMdG (nM)	**RSD (%)**	**Recovery (%)**	**RSD (%)**	**Recovery (%)**
0.063	**5.4**	**92.3**	**16.6**	**86.9**
0.197	**20.5**	**75.6**	**7.9**	**82.7**
O^6-MedG (nM)	**RSD (%)**	**Recovery (%)**	**RSD (%)**	**Recovery (%)**
0.009	**20.4**	**84.6**	**6.9**	**77.2**
0.014	**8.5**	**76.0**	**18.5**	**80.9**

Table 3.1.Intra-day and inter-day precision and accuracy for the measurements of N^6-CMdA, O^6-CMdG and O^6-MedG, reported as Relative Standard Deviation (RSD) and Percent Recovery, respectively.

Relatively large amounts of unmodified nucleosides can significantly interfere with the detection of low levels of DNA lesions. Hence, we employed offline HPLC to enrich O^6-CMdG, N^6-CMdA and O^6-MedG from the DNA digestion mixtures prior to nLC-nESI-MS^3 analysis. In this context, due to the better sensitivity achieved in the positive- than the negative-ion mode, we quantified the carboxymethylated and methylated DNA lesions by using nLC-nESI-MS^3 in the positive-ion mode, where 0.1% formic acid (v/v) was added to the mobile phases to promote the protonation of the analytes. Upon collisional activation, the $[M + H]^+$ ions of O^6-CMdG, N^6-CMdA and O^6-MedG readily eliminate a neutral 2-deoxyribose to yield the protonated nucleobase as the most abundant fragment ion in MS^2, which is subsequently isolated and collisionally

activated for MS^3 analysis. In this vein, the cleavages of the $[M + H]^+$ ions of the nucleobase portion of O^6-CMdG and $[D_2]$-O^6-CMdG (*m/z* 210 and 212) led the formation of the major fragment ion of *m/z* 152, which stems from the neutral loss of the carboxymethyl functionality (Figure 3.1). The selected-ion chromatograms (SICs) for monitoring the *m/z* 326→210→152 and *m/z* 328→212→152 transitions revealed a peak at very similar retention time (21.7 min). This observation, together with the similar MS^3 for the analyte and the internal standard, provides unambiguous identification of O^6-CMdG. The excellent S/N observed in the SICs facilitates the accurate quantification of the level of this lesion.

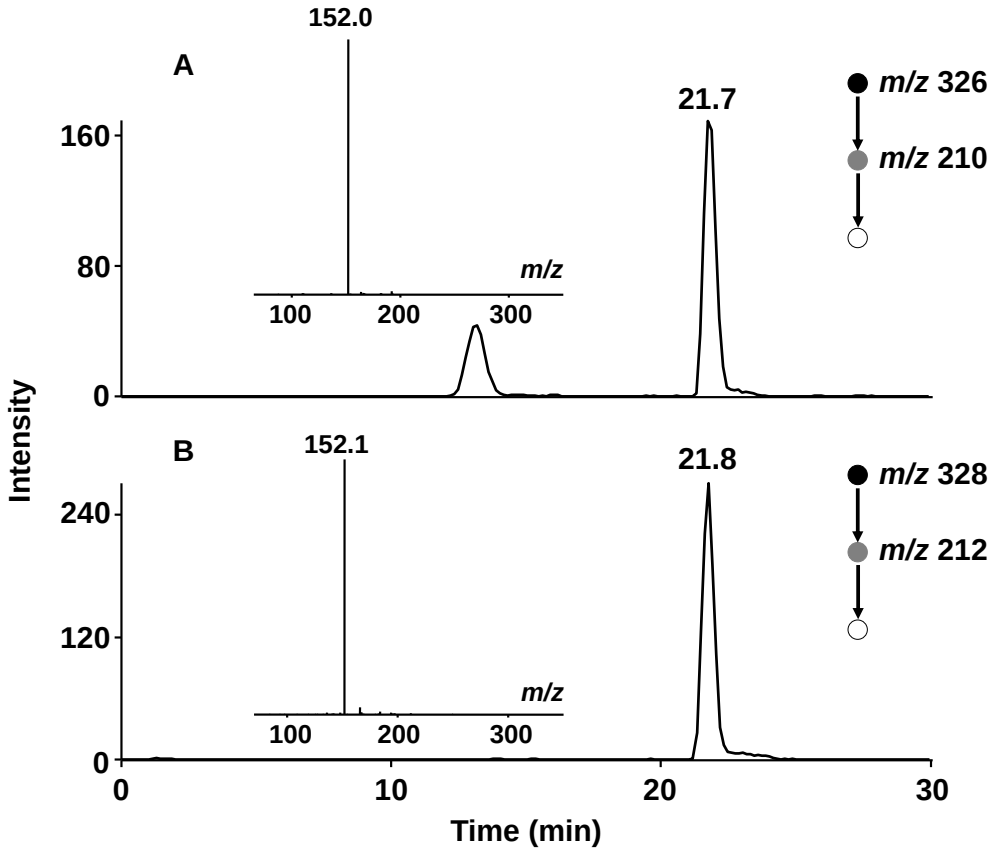


Figure 3.1.Representative selected-ion chromatograms (SICs) for monitoring the *m/z* 326→210→152 (A) and 328→212→152 (B) transitions for the $[M+H]^+$ ions of the unlabeled O^6-CMdG and $[D_2]$-O^6-CMdG, respectively, in the nucleoside mixture of genomic DNA extracted from the XPA-deficient human skin fibroblast cells treated with azaserine. Shown in the insets are the MS^3 spectra for the unlabeled and labeled O^6-CMdG.

Similar LC-MS^3 analysis was employed for the quantification of N^6-CMdA and O^6-MedG. In this context, it is of note that the collisional activation of the protonated nucleobase of N^6-CMdA (*m/z* 194) and [$^{13}C_2$,^{15}N]-N^6-CMdA (*m/z* 197) led to the facile neutral loss of a HCOOH and H^{13}COOH molecule from the carboxymethyl side chain to yield the ions of *m/z* 148 and *m/z* 150 in MS^3, respectively (Figure 3.2). On the other hand, MS^3 arising from the fragmentation of protonated nucleobase portions of O^6-MedG

and [D_3]-O^6-MedG led to neutral loss of an NH_3 molecule to give product ions of *m/z* 149 and *m/z* 152 for O^6-MedG and [D_3]-O^6-MedG in MS^3, respectively (Figure 3.3). The proposed fragmentation pathways for the three aforementioned DNA lesions are displayed in Supplementary Figure B3.3. Another set of representative SICs for the quantification of the three lesions were provided in the Supporting Information as qualifiers (Figure B3.4-B3.6).

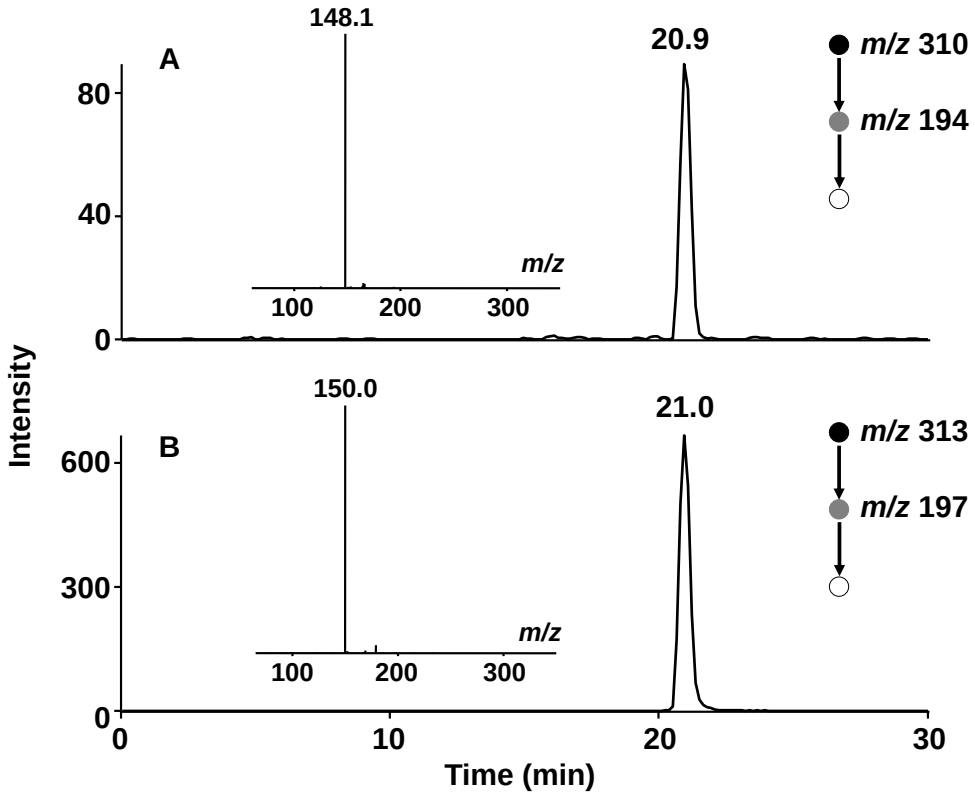


Figure 3.2.Representative SICs for monitoring the *m/z* 310→194→148 (A) and *m/z* 313→197→150 transitions (B) for the $[M+H]^+$ ions of the unlabeled N^6-CMdA and $[^{13}C_2,^{15}N]$-N^6-CMdA, respectively, in the nucleoside mixture of genomic DNA extracted from the XPA-deficient human skin fibroblast cells treated with azaserine. Shown in the insets are the positive-ion MS^3 spectra for the unlabeled and labeled N^6-CMdA.

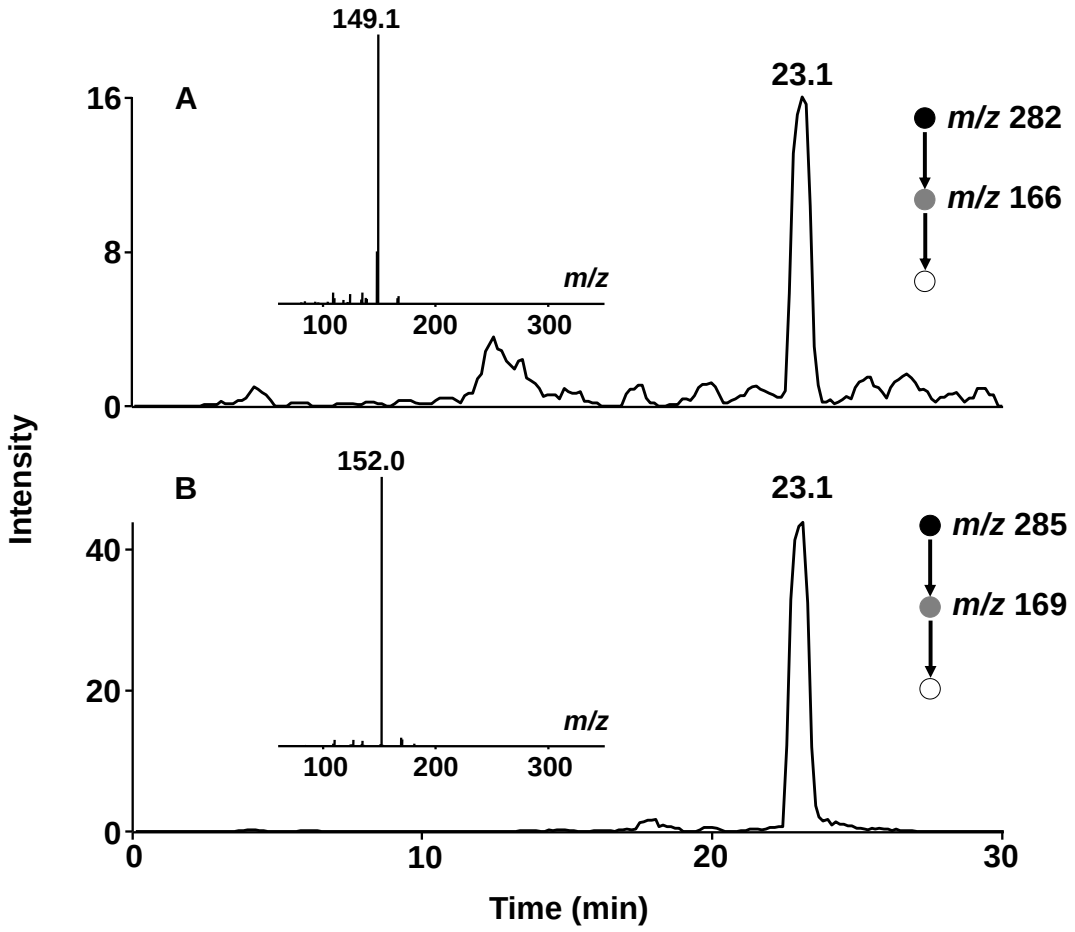


Figure 3.3.Representative SICs for monitoring the *m/z* 282→166→149 (A) and *m/z* 285→169→152 (B) transitions for the $[M+H]^+$ ions of unlabeled O^6-MedG and $[D_3]$-O^6-MedG, respectively, in the nucleoside mixture of genomic DNA extracted from the XPA-deficient human skin fibroblast cells treated with azaserine. Shown in the insets are the positive-ion MS^3 spectra for the unlabeled and labeled O^6-MedG.

Levels of O^6-CMdG, N^6-CMdA and O^6-MedG in azaserine-treated XPA-deficient GM04429 cells

With the above-described nLC-nESI-MS^3 method, we quantified the levels of O^6-CMdG, N^6-CMdA, and O^6-MedG in genomic DNA of XPA-deficient GM04429 human skin fibroblasts and HCT-116 human colorectal carcinoma cells treated with different

concentrations of azaserine. The quantification data revealed a dose-dependent formation of O^6-CMdG and O^6-MedG in both cell lines (Figure 3.4). The levels of O^6-CMdG and O^6-MedG in GM04429 cells increased from 0.054 to 4.95 and from 0.092 to 0.264 lesions per 10^7 nucleosides, respectively, when the dose of azaserine was increased from 0 to 450 μM (Figure 3.4, Table B3.2). Similarly, the levels of O^6-CMdG and O^6-MedG in HCT-116 cells elevated from 0.247 to 9.12 and from 0.07 to 0.52 lesions per 10^7 nucleosides, respectively, with the dose of azaserine increased from 0 to 450 μM (Figure 3.4, Table B3.2). Thus, azaserine treatment could predominantly induce DNA carboxymethylation rather than methylation *in vivo*, as reflected by the magnitude of increase in the levels of O^6-CMdG (by 4.9 and 8.9 lesions per 10^7 nucleosides, respectively, in GM04429 and HCT-116 cells) and O^6-MedG (by 0.172 and 0.45 lesions per 10^7 nucleosides, respectively, in GM04429 and HCT-116 cells, Figure 3.4A & 3.4B, Table B3.2). These results are in agreement with the previously reported findings made for isolated DNA treated with various DNA carboxymethylating agents (10), suggesting the more efficient generation and/or less efficient repair of the O^6-CMdG than the O^6-MedG. Moreover, all three lesions were detectable in control samples without azaserine treatment, indicating the existence of endogenous agents that can induce DNA carboxymethylation and methylation. The magnitude of increase in the levels of N^6-CMdA (by 0.18 lesions per 10^7 nucleosides) in XPA-deficient cells, arising from azaserine treatment, however, was not as prominent as that for O^6-CMdG (Figure 3.4A & 3.4C, Table B3.2). Moreover, no azaserine dose-dependent induction of N^6-CMdA was observed in genomic DNA extracted from azaserine treated HCT-116 cells (Figure 3.4A

& 3.4C, Table B3.2). These results, along with the lower levels of this lesion (Table B3.2) than O^6-CMdG, indicated the preferential formation of O^6-CMdG over N^6-CMdA and/or the presence of repair mechanism(s) for the facile removal of N^6-CMdA.

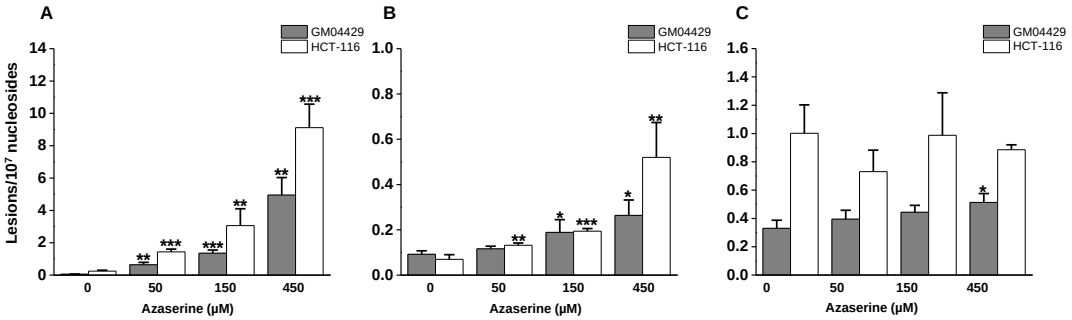


Figure 3.4.LC−MS^3 quantification results for O^6-CMdG (A), O^6-MedG (B) and N^6-CMdA (C) in DNA samples isolated from XPA-deficient human skin fibroblast cells and human colorectal carcinoma HCT-116 cells treated with different concentrations of azaserine. The data represent the means and standard deviations of results obtained from three independent experiments. *, $p < 0.05$; **, $p < 0.01$; ***, $p < 0.001$. The p values were calculated by using an unpaired two-tailed t-test.

Discussion

Owing to its sensitivity, accuracy and specificity, LC-MS/MS or MS^3 combined with the stable isotope-dilution technique constitutes a rigorous analytical method for the quantitation of DNA lesions in complex biological matrices (24,25). This technique is advantageous over other conventional methods for DNA adduct measurement (e.g. ^{32}P-postlabeling and immunoassay) as it allows for unequivocal identification and reliable quantitation of chemically modified nucleosides by providing structural information. In this method, the stable isotope-labeled standards of the lesions were added to the nucleoside mixture prior to enzymatic digestion. The determination of the levels of the lesions depends on the measurement of the molar ratios of the analytes over their corresponding internal standards, which is not affected by the variation in experimental conditions during sample preparation and LC-MS analysis.

Compared to the previously reported LC/MS-based quantification of O^6-CMdG and O^6-MedG in selected-reaction monitoring (SRM) mode on a triple quadrupole mass spectrometer (17,26), our MS^3 detection mode in the LTQ XL linear ion trap mass spectrometer provided better specificity (MS^2 and MS^3 detection mode comparison, Figure B7-B12). Additionally, in contrast to the solid-phase extraction method previously used for analyte enrichment (17,26), the off-line HPLC enrichment method reported herein offered better sample cleanup by removing excess amount of unmodified nucleosides and buffer salts added during the enzymatic digestion (29), which further improved the sensitivity of our method. Moreover, to our knowledge, our technique is the first application of the nLC-nESI-MS^3 for the simultaneous quantification of multiple carboxymethylated and methylated DNA lesions in cellular DNA, which increased the sensitivity of the analysis by improving ionization efficiency and transmission of ions from the ionization source into the mass analyzer.

We found a dose-dependent induction of O^6-CMdG and O^6-MedG in genomic DNA of both XPA-deficient GM04429 cells and HCT-116 cells treated with azaserine, which validated our analytical method. The quantification data of N^6-CMdA in both cell lines provided evidence to support the azaserine-induced formation of this lesion *in vivo*, which was consistent with our previous *in vitro* data obtained from diazoacetate treated calf thymus DNA (16). In contrast to O^6-CMdG and O^6-MedG, statistically significant increase in the level of N^6-CMdA was only observed when XPA-deficient GM04429 cells, but not HCT-116 cells, were treated with the highest dose (i.e. 450 μM) of azaserine, indicating the existence of potential pathway for the facile repair of this lesion

in vivo. Along this line, Li *et al.* (30) observed that N^6-methyl-2′-deoxyadenosine (N^6-MedA) could be repaired by *Escherichia coli* AlkB through a direct reversal mechanism. Recent studies also revealed the presence of demethylase for N^6-MedA in DNA in *Drosophila melanogaster* and *Caenorhabditis elegans* (31,32). It is possible that these enzymes may also be involved in the repair of N^6-CMdA, owing to its structural similarity with N^6-MedA.

Taken together, we reported, for the first time, the simultaneous quantifications of O^6-CMdG, N^6-CMdA and O^6-MedG in cultured human skin fibroblasts and human colorectal carcinoma cells treated with azaserine using nLC-nESI-MS^3 with the stable isotope-dilution method. This method may serve as a useful tool for the future exploration of the repair of these lesions and for the investigation about the involvement of DNA carboxymethylation and methylation in the etiology of human gastrointestinal tumors.

References

1. Lindahl, T. (1993) Instability and decay of the primary structure of DNA. *Nature*, **362**, 709-715.

2. Tricker, A.R. (1997) N-nitroso compounds and man: sources of exposure, endogenous formation and occurrence in body fluids. *Eur. J. Cancer Prev.*, **6**, 226-268.

3. He, Y.F., Li, B.Z., Li, Z., Liu, P., Wang, Y., Tang, Q.Y., Ding, J.P., Jia, Y.Y., Chen, Z.C., Li, L. *et al.* (2011) Tet-mediated formation of 5-carboxylcytosine and its excision by TDG in mammalian DNA. *Science*, **333**, 1303-1307.

4. Correa, P. (1992) Human gastric carcinogenesis: a multistep and multifactorial process. *Cancer Res.*, **52**, 6735-6740.

5. Jakszyn, P., Bingham, S., Pera, G., Agudo, A., Luben, R., Welch, A., Boeing, H., Del Giudice, G., Palli, D., Saieva, C. *et al.* (2006) Endogenous versus exogenous exposure to *N*-nitroso compounds and gastric cancer risk in the European Prospective Investigation into Cancer and Nutrition (EPIC-EURGAST) study. *Carcinogenesis*, **27**, 1497-1501.

6. Bingham, S.A., Pignatelli, B., Pollock, J.R., Ellul, A., Malaveille, C., Gross, G., Runswick, S., Cummings, J.H. and O'Neill, I.K. (1996) Does increased endogenous formation of *N*-nitroso compounds in the human colon explain the association between red meat and colon cancer? *Carcinogenesis*, **17**, 515-523.

7. Puju, S., Shuker, D.E., Bishop, W.W., Falchuk, K.R., Tannenbaum, S.R. and Thilly, W.G. (1982) Mutagenicity of N-nitroso bile acid conjugates in *Salmonella typhimurium* and diploid human lymphoblasts. *Cancer Res.*, **42**, 2601-2604.

8. Busby, W.F., Jr., Shuker, D.E., Charnley, G., Newberne, P.M., Tannenbaum, S.R. and Wogan, G.N. (1985) Carcinogenicity in rats of the nitrosated bile acid conjugates *N*-nitrosoglycocholic acid and *N*-nitrosotaurocholic acid. *Cancer Res.*, **45**, 1367-1371.

9. Shuker, D.E. and Margison, G.P. (1997) Nitrosated glycine derivatives as a potential source of O^6-methylguanine in DNA. *Cancer Res.*, **57**, 366-369.

10. Harrison, K.L., Jukes, R., Cooper, D.P. and Shuker, D.E. (1999) Detection of concomitant formation of O^6-carboxymethyl- and O^6-methyl-2'-deoxyguanosine in DNA exposed to nitrosated glycine derivatives using a combined immunoaffinity/HPLC method. *Chem. Res. Toxicol.*, **12**, 106-111.

11. Harrison, K.L., Fairhurst, N., Challis, B.C. and Shuker, D.E. (1997) Synthesis, characterization, and immunochemical detection of O^6-(carboxymethyl)-2'-deoxyguanosine: a DNA adduct formed by nitrosated glycine derivatives. *Chem. Res. Toxicol.*, **10**, 652-659.

12. Zurlo, J., Curphey, T.J., Hiley, R. and Longnecker, D.S. (1982) Identification of 7-carboxymethylguanine in DNA from pancreatic acinar cells exposed to azaserine. *Cancer Res.*, **42**, 1286-1288.

13. Longnecker, D.S. and Curphey, T.J. (1975) Adenocarcinoma of the pancreas in azaserine-treated rats. *Cancer Res.*, **35**, 2249-2258.

14. Gottschalg, E., Scott, G.B., Burns, P.A. and Shuker, D.E. (2007) Potassium diazoacetate-induced *p53* mutations in vitro in relation to formation of O^6-carboxymethyl- and O^6-methyl-2'-deoxyguanosine DNA adducts: relevance for gastrointestinal cancer. *Carcinogenesis*, **28**, 356-362.

15. Wang, J. and Wang, Y. (2009) Chemical synthesis of oligodeoxyribonucleotides containing *N*3- and O^4-carboxymethylthymidine and their formation in DNA. *Nucleic Acids Res.*, **37**, 336-345.

16. Wang, J. and Wang, Y. (2010) Synthesis and characterization of oligodeoxyribonucleotides containing a site-specifically incorporated N^6-carboxymethyl-2'-deoxyadenosine or N^4-carboxymethyl-2'-deoxycytidine. *Nucleic Acids Res.*, **38**, 6774-6784.

17. Vanden Bussche, J., Moore, S.A., Pasmans, F., Kuhnle, G.G.C. and Vanhaecke, L. (2012) An approach based on ultra-high pressure liquid chromatography-tandem mass spectrometry to quantify O^6-methyl and O^6-carboxymethylguanine DNA adducts in intestinal cell lines. *J. Chromatogr. A*, **1257**, 25-33.

18. Altshuler, K.B., Hodes, C.S. and Essigmann, J.M. (1996) Intrachromosomal probes for mutagenesis by alkylated DNA bases replicated in mammalian cells: a comparison of the mutagenicities of O^4-methylthymine and O^6-methylguanine in cells with different DNA repair backgrounds. *Chem. Res. Toxicol.*, **9**, 980-987.

19. You, C., Wang, J., Dai, X. and Wang, Y. (2015) Transcriptional inhibition and mutagenesis induced by *N*-nitroso compound-derived carboxymethylated thymidine adducts in DNA. *Nucleic Acids Res.*, **43**, 1012-1018.

20. Yuan, B., Wang, J., Cao, H., Sun, R. and Wang, Y. (2011) High-throughput analysis of the mutagenic and cytotoxic properties of DNA lesions by next-generation sequencing. *Nucleic Acids Res.*, **39**, 5945-5954.

21. You, C., Wang, P., Nay, S.L., Wang, J., Dai, X., O'Connor, T.R. and Wang, Y. (2016) Roles of Aag, Alkbh2, and Alkbh3 in the Repair of Carboxymethylated and Ethylated Thymidine Lesions. *ACS Chem. Biol.*, **DOI:** 10.1021/acschembio.1026b00085.

22. Terasaki, M., Totsuka, Y., Nishimura, K., Mukaisho, K., Chen, K., Hattori, T., Takamura-Enya, T., Sugimura, T. and Wakabayashi, K. (2008) Detection of endogenous DNA adducts, O^6-carboxymethyl-2'-deoxyguanosine and 3-ethanesulfonic acid-2'-deoxycytidine, in the rat stomach after duodenal reflux. *Cancer Sci.*, **99**, 1741-1746.

23. Cupid, B.C., Zeng, Z., Singh, R. and Shuker, D.E. (2004) Detection of O^6-carboxymethyl-2'-deoxyguanosine in DNA following reaction of nitric oxide with glycine and in human blood DNA using a quantitative immunoslot blot assay. *Chem. Res. Toxicol.*, **17**, 294-300.

24. Tretyakova, N., Villalta, P.W. and Kotapati, S. (2013) Mass spectrometry of structurally modified DNA. *Chem. Rev.*, **113**, 2395-2436.

25. Liu, S. and Wang, Y. (2015) Mass spectrometry for the assessment of the occurrence and biological consequences of DNA adducts. *Chem. Soc. Rev.*, **44**, 7829-7854.

26. Da Pieve, C., Sahgal, N., Moore, S.A. and Velasco-Garcia, M.N. (2013) Development of a liquid chromatography/tandem mass spectrometry method to investigate the presence of biomarkers of DNA damage in urine related to red meat consumption and risk of colorectal cancer. *Rapid Commun. Mass Spectrom.*, **27**, 2493-2503.

27. Fathi, R., Goswami, B., Kung, P.P., Gaffney, B.L. and Jones, R.A. (1990) Synthesis of 6-substituted 2'-deoxyguanosine derivatives using trifluoroacetic-anhydride in pyridine. *Tetrahedron Lett.*, **31**, 319-322.

28. Wang, J., Yuan, B., Guerrero, C., Bahde, R., Gupta, S. and Wang, Y. (2011) Quantification of oxidative DNA lesions in tissues of Long-Evans Cinnamon rats by capillary high-performance liquid chromatography-tandem mass spectrometry coupled with stable isotope-dilution method. *Anal. Chem.*, **83**, 2201-2209.

29. Hong, H., Cao, H., Wang, Y. and Wang, Y. (2006) Identification and quantification of a guanine-thymine intrastrand cross-link lesion induced by Cu(II)/H_2O_2/ascorbate. *Chem. Res. Toxicol.*, **19**, 614-621.

30. Li, D., Delaney, J.C., Page, C.M., Yang, X., Chen, A.S., Wong, C., Drennan, C.L. and Essigmann, J.M. (2012) Exocyclic carbons adjacent to the N^6 of adenine are targets for oxidation by the *Escherichia coli* adaptive response protein AlkB. *J. Am. Chem. Soc.*, **134**, 8896-8901.

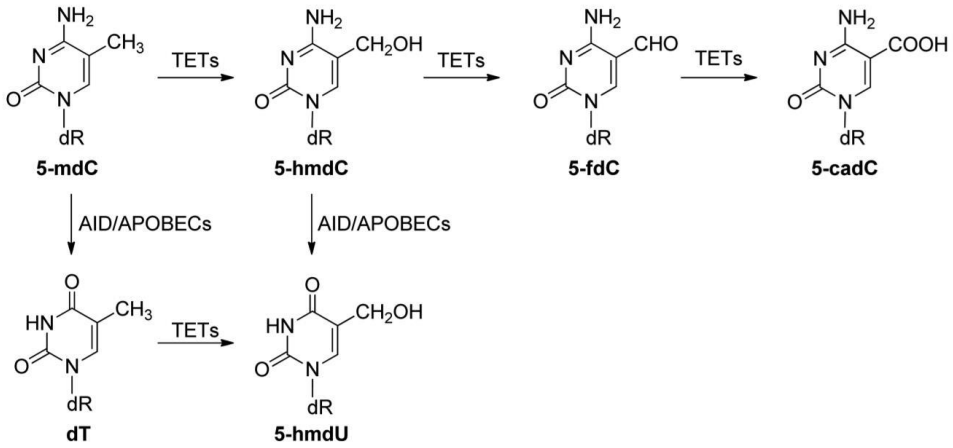
31. Greer, E.L., Blanco, M.A., Gu, L., Sendinc, E., Liu, J., Aristizabal-Corrales, D., Hsu, C.H., Aravind, L., He, C. and Shi, Y. (2015) DNA methylation on N^6-adenine in *C. elegans*. *Cell*, **161**, 868-878.

32. Zhang, G., Huang, H., Liu, D., Cheng, Y., Liu, X., Zhang, W., Yin, R., Zhang, D., Zhang, P., Liu, J. *et al.* (2015) N^6-methyladenine DNA modification in Drosophila. *Cell*, **161**, 893-906.

Chapter 4 LC-MS/MS for the investigation of the altered levels of 5-hmdC in cancer cells

Introduction

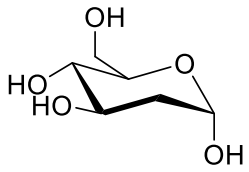
Previous studies demonstrated that the methyl group in 5-mdC, a DNA epigenetic marker, could be oxidized sequentially by Fe(II)- and 2-oxoglutarate (2-OG)-dependent ten-eleven translocation (TET) family dioxygenases, leading to the formation of 5-hmdC, 5-fdC and 5-cadC (Scheme 1) (1-3). In addition, the removal of 5-fdC and 5-cadC via the base excision repair (BER) pathway may play an important role in active cytosine demethylation in mammalian systems, which is different from the passive dilution of 5-mdC at CpG site after DNA replication (4-7). 5-hmdC may also undergo deamination to generate 5-hmdU (8,9). Furthermore, TET enzymes were found to catalyze directly the oxidation of thymidine to yield 5-hmdU in DNA of mouse embryonic stem cells (mESCs) (Scheme 4.1) (10). 5-hmC, 5-fC and 5-caC may serve as epigenetic marks in addition to being intermediates for active cytosine demethylation in mammals (6,11-16).



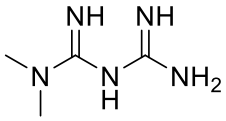
Scheme 4.1.TET-mediated oxidation of 5-mdC.

The depletion of global 5-hmC levels in cancer cells compared to normal cells has been observed in a variety of human cancers including leukemia as well as brain, breast, liver, lung, pancreatic and prostate cancers (7,17,18). Previous studies demonstrated that cancer-related gain-of-function mutations in isocitrate dehydrogenase genes *IDH1* and *IDH2* lead to formation of the oncometabolite (*R*)-2-hydroxyglutarate ((*R*)-2-HG) instead of production of 2-oxogluterate (2-OG), a co-substrate that is required for Tet-mediated oxidation of 5-mdC. In addition, mutations in two tricarboxylic acid (TCA) cycle genes, fumarate hydratase (*FH*) and succinate dehydrogenase (*SDH*), can result in aberrant accumulation of their substrates, fumarate and succinate, respectively. Owing to their structural similarity to 2-OG, (*R*)-2-HG, succinate and fumarate can act as competitive inhibitors of 2-OG-dependent TET enzymes, giving rise to decreased levels of 5-hmC in certain cancers (19-27). However, Jin *et al*. (28) observed an IDH mutation-independent depletion of 5-hmdC in multiple types of human cancers. In this study, levels of 5hmdC were observed to decrease by 5-fold and even more than 30-fold in squamous cell lung

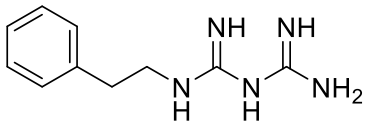
cancers and brain tumors, respectively, compared to their corresponding normal tissues (28). These data indicated the existence of alternative mechanism(s) involved in the loss of 5-hmdC in cancer cells. In this vein, lower concentration of molecular oxygen, due to hypoxia in expanding cancer cells and tissues, was recently found to suppress directly the activities of TET enzymes, giving rise to lower 5-hmdC levels (29). Taken together, the above-mentioned data provided insights into the involvement of aberrant metabolism in perturbation of epigenetic regulation. Nevertheless, it remains unclear whether other mechanism(s) also contributes to the diminished levels of 5-hmdC in cancer. Since cancer cells produce ATP predominantly through the aerobic glycolysis pathway due to the Warburg effect (30,31). it is crucial to explore whether accumulated glycolytic or other types of metabolites can impede TET activity in cancer cells. Here we applied a nanoflow LC-nanoelectrospray ionization-MS^3 (nLC-nESI-MS^3) quantification of 5-hmdC in different cancer cells treated with a glycolysis inhibitor, 2-deoxy-D-glucose (2-DG), or activators of AMP-activated protein kinase (AMPK), including phenformin, metformin and 5-aminoimidazole-4-carboxamide ribonucleoside (AICAR) (Scheme 4.2). The goal is to gain insights into the relationship between aberrant metabolism and the levels of 5-hmdC in cancer cells.



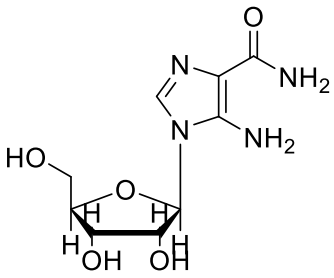
2-DG



metformin



phenformin



AICAR

Scheme 4.2.structures of 2-DG, metformin, phenformin and AICAR.

Experimental procedures

Materials and Cell Lines

All chemicals and enzymes, unless otherwise specified, were purchased from Sigma-Aldrich (St. Louis, MO) or New England Biolabs (Ipswich, WA). Stable isotope-labeled compounds were obtained from Cambridge Isotope Laboratories (Cambridge, MA). AICAR was purchased from TCI America (Portland, OR). GM00637 human skin fibroblasts were kindly provided by Prof. Gerd P. Pfeifer. Other cell lines, i.e. HEK293T human embryonic kidney cells, HeLa human cervical carcinoma cells, HCT-116 human colorectal carcinoma cells, U2OS bone osteosarcoma cells and MDA-MB-231 human breast adenocarcinoma cells were purchased from ATCC (Manassas, VA). The stable isotope-labeled 5-hmdC and 5-mdC were synthesized previously (15,32).

Cell culture and drug treatment

Cells were cultured at 37°C in 5% CO_2 atmosphere in ATCC-recommended medium containing 10% fetal bovine serum and 100 IU/mL of penicillin. Cells (2.5×10^6) were seeded in 6-well plates in complete medium. After 24 h, the cells were treated with 8 mM 2-DG, 2 mM phenformin, 10 mM metformin or 1 mM AICAR. After 24 h of treatment, the cells were detached by using trypsin-EDTA and harvested by centrifugation. The cell pellets were subsequently washed twice with phosphate-buffered saline (PBS) to remove residual medium and drugs.

Extraction and enzymatic digestion of nuclear DNA

The procedures for cellular DNA extraction and enzymatic digestion were similar as previously described (15). In this regard, a high-salt method was employed for the

extraction of genomic DNA (33). A lysis buffer (50 μL) containing 20 mM Tris (pH 8.1), 20 mM EDTA, 400 mM NaCl, 1% SDS (w/v), and 10 μL of proteinase K (20 mg/mL) was added to the cell pellet and incubated at 55°C overnight. Saturated sodium chloride solution (0.5 volume) was then added to the digestion mixture, and the mixture was vortexed for 1 min and incubated at 55°C for another 15 min. The resulting digestion mixture was centrifuged at 13000 rpm for 30 min, and the nucleic acids were precipitated from the supernatant with 2 volumes of ethanol. The RNA in the precipitated nucleic acids was removed by digestion with 3 μL of RNase A (10 mg/mL) and 2 μL of RNase T1 (25 units/μL) at 37°C overnight followed by extraction with an equal volume of chloroform/isoamyl alcohol (24:1, v/v). The DNA was then precipitated from the aqueous layer with 2 volumes of ethanol and centrifuged at 13000 rpm for 10 min. The resulting DNA pellet was washed with 70% cold ethanol twice, allowed to air dry at room temperature, dissolved in doubly distilled water, and quantified by UV absorption measurement at 260 nm. The cellular DNA (1 μg) was digested with 0.1 unit of nuclease P1 and 0.000125 unit of phosphodiesterase II in a 4.5-μL buffer containing 300 mM sodium acetate (pH 5.6), 10 mM $ZnCl_2$, and 2.5 nmol of EHNA. The above mixture was incubated at 37°C for 48 h. To the mixture were then added 0.1 unit of alkaline phosphatase, 0.00025 unit of phosphodiesterase I, and a 6-μL buffer containing 0.5 M Tris-HCl (pH 8.9). After incubation at 37°C for 2 h, the digestion mixture was neutralized with 1.0 M formic acid. [1,3-$^{15}N_2$-2'-D]-5-hmdC and [1',2',3',4',5'-$^{13}C_5$]-5mdC were added to the enzymatic digestion mixture of 50-100 ng of cellular DNA. The

enzymes in the digestion mixture were removed by extraction with chloroform, and the resulting aqueous layer was subjected directly to LC-MS/MS analysis.

nLC-nESI-MS^3 analysis of 5-hmdC

Online nLC-nESI-MS^3 analyses of 5-hmdC were performed on an LTQ-XL linear ion trap mass spectrometer (Thermo Fisher Scientific) equipped with a nanoelectrospray ionization source and coupled with an EASY nLC II system (Thermo Fisher Scientific), as described previously (15). HPLC separation was conducted by employing a home-made trapping column (150 μm × 40 mm) packed with porous graphitic carbon and an analytical column (75 μm × 200 mm) packed with Magic C18 AQ (200 Å, 5 μm, Michrom BioResource, Auburn, CA). Mobile phases A and B were 0.1% formic acid in doubly distilled H_2O and acetonitrile, respectively. Initially, the sample was loaded onto the trapping column with mobile phase A at a flow rate of 2.5 μL/min in 6 min. The modified nucleosides of interest were then eluted by using a 30-min linear gradient of 0−50% mobile phase B at a flow rate of 300 nL/min. The LTQ-XL mass spectrometer was operated in the positive-ion mode, the voltage for electrospray was 2.0 kV, and the temperature for the ion transfer tube was 275 °C. The widths for precursor ion selection were 3 and 2 *m*/*z* units in MS/MS and MS^3 modes, respectively. The normalized collision energy, activation Q, and activation time were 42, 0.25, and 30 ms in MS/MS as well as 27, 0.25, and 30 ms in MS^3, respectively.

LC-MS analysis of 5-mdC and 2'-deoxyguanosine (dG)

LC-MS/MS and LC-MS/MS/MS quantifications of 5-mdC and dG were described previously (15,34). The amounts of 5-mdC and dG (in moles) in the nucleoside mixtures

were calculated from area ratios of peaks found in selected-ion chromatograms (SICs) for the analytes over their corresponding isotope-labeled standards, the amounts of the labeled standards added (in moles), and the calibration curves. The levels of 5-mdC (presented % of dG) were calculated by comparing the moles of 5-mdC relative to the moles of dG.

Results and Discussion

LC-MS quantifications of 5-hmdC and 5-mdC in cellular DNA

We first developed a sensitive nLC-nESI-MS^3 with the stable-isotope dilution method for the accurate quantification of 5-hmdC. In this method, we first digested the cellular DNA with a cocktail of 4 enzymes to release the lesions of interest as mononucleosides (see Experimental Procedures). The stable isotope-labeled 5-hmdC was added to the DNA digestion mixture prior to the chloroform extraction, which corrected for the potential analyte loss during the sample preparation. Upon collisional activation, the $[M + H]^+$ ion of 5-hmdC readily eliminates its 2-deoxyribose moiety to yield the protonated nucleobase as the most abundant product ion in MS^2, which is subsequently isolated and collisionally activated for MS^3 analysis. In this vein, the cleavages of the $[M + H]^+$ ions of the protonated nucleobase portion of 5-hmdC and [1,3-$^{15}N_2$-2'-D]-5-hmdC (*m/z* 142 and 144) gave rise to the generation of the major fragment ion of *m/z* 124 and 126, respectively, which originate from the facile neutral loss of a water molecule from the hydroxymethyl side chain (Figure 4.1). The very close retention time of 5-hmdC and

its labeled standard, together with the similar MS^3 for the analyte and the internal standard as well as the excellent signal-to-noise ratio (S/N), provides unambiguous identification and accurate quantification of the levels of this modified nucleoside.

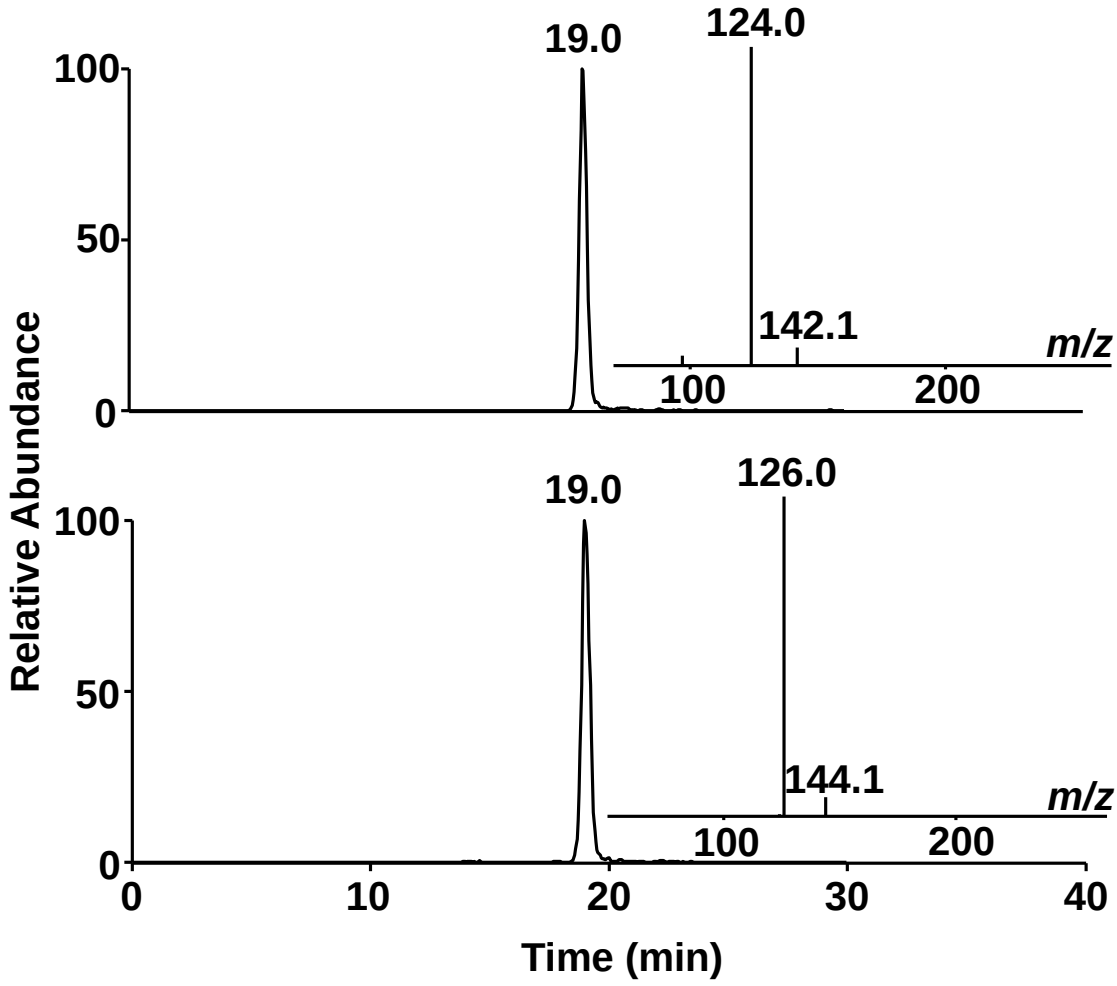


Figure 4.1.Representative selected-ion chromatograms (SICs) for monitoring the *m/z* 258 → 142 → 124 (top) and 261 → 144 → 126 (bottom) transitions for the $[M + H]^+$ ions of the unlabeled 5-hmdC and [1,3-$^{15}N_2$-2'-D]-5-hmdC, respectively, in the nucleoside mixture of genomic DNA extracted from cells. Shown in the insets are the MS^3 spectra for the unlabeled and labeled 5-hmdC.

Similar LC-MS/MS and MS/MS/MS methods were employed for the quantifications of 5-mdC and dG. In this vein, collisional activation of the protonated 5-mdC (*m/z* 242) and [1',2',3',4',5'-$^{13}C_5$]-5-mdC (*m/z* 247) resulted in the neutral loss of the 2-deoxyribose portion to yield the ions of *m/z* 126 in MS^2 (Figure 4.2). MS^3 arising from the fragmentation of protonated nucleobase portions of dG and [$^{15}N_5$]-dG led to neutral loss of an NH_3 molecule to give product ions of *m/z* 135 and *m/z* 139 for dG and [$^{15}N_5$]-dG in MS^3, respectively (Figure 4.3). The proposed fragmentation pathways for the three aforementioned nucleosides are displayed in Figure 4.4.

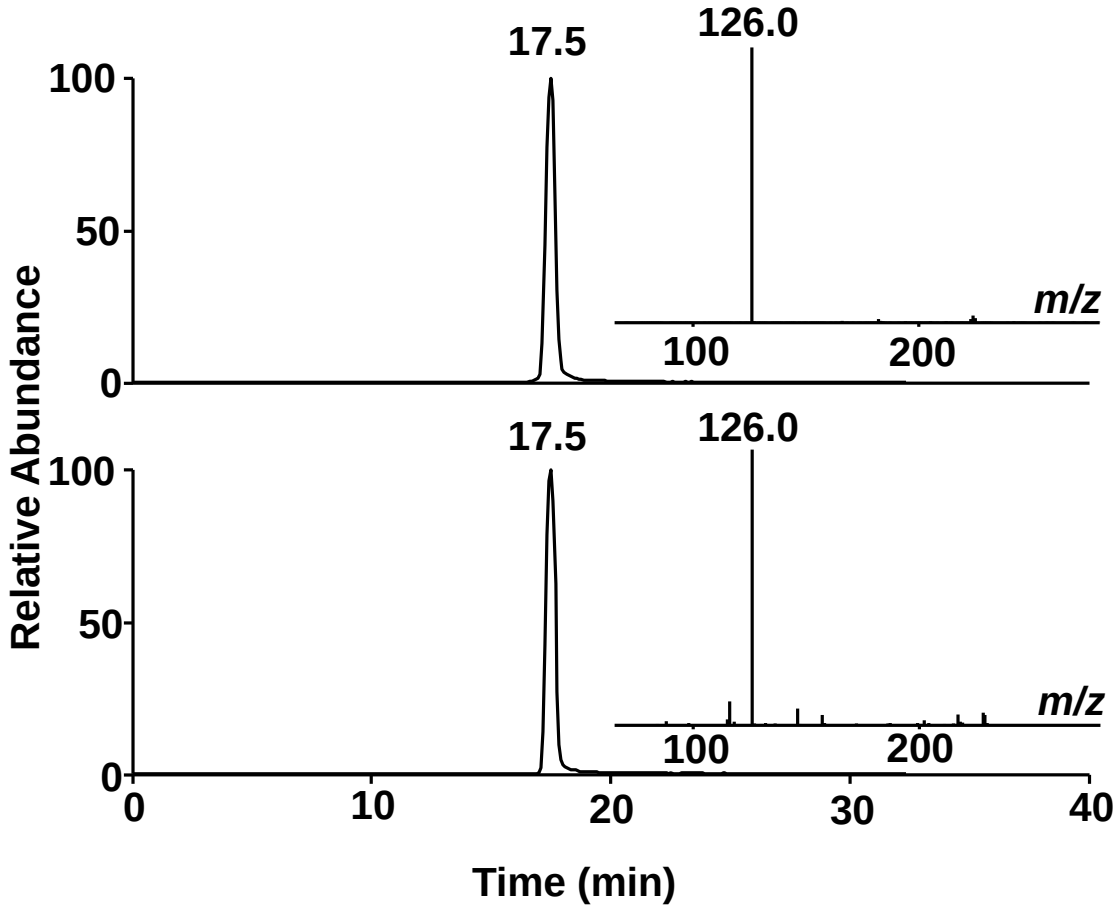


Figure 4.2.Representative selected-ion chromatograms (SICs) for monitoring the *m/z* 242 → 126 (top) and 247 → 126 (bottom) transitions for the $[M + H]^+$ ions of the unlabeled 5-mdC and [1',2',3',4',5'-$^{13}C_5$]-5mdC, respectively, in the nucleoside mixture of genomic DNA extracted from cells. Shown in the insets are the MS^2 spectra for the unlabeled and labeled 5-mdC.

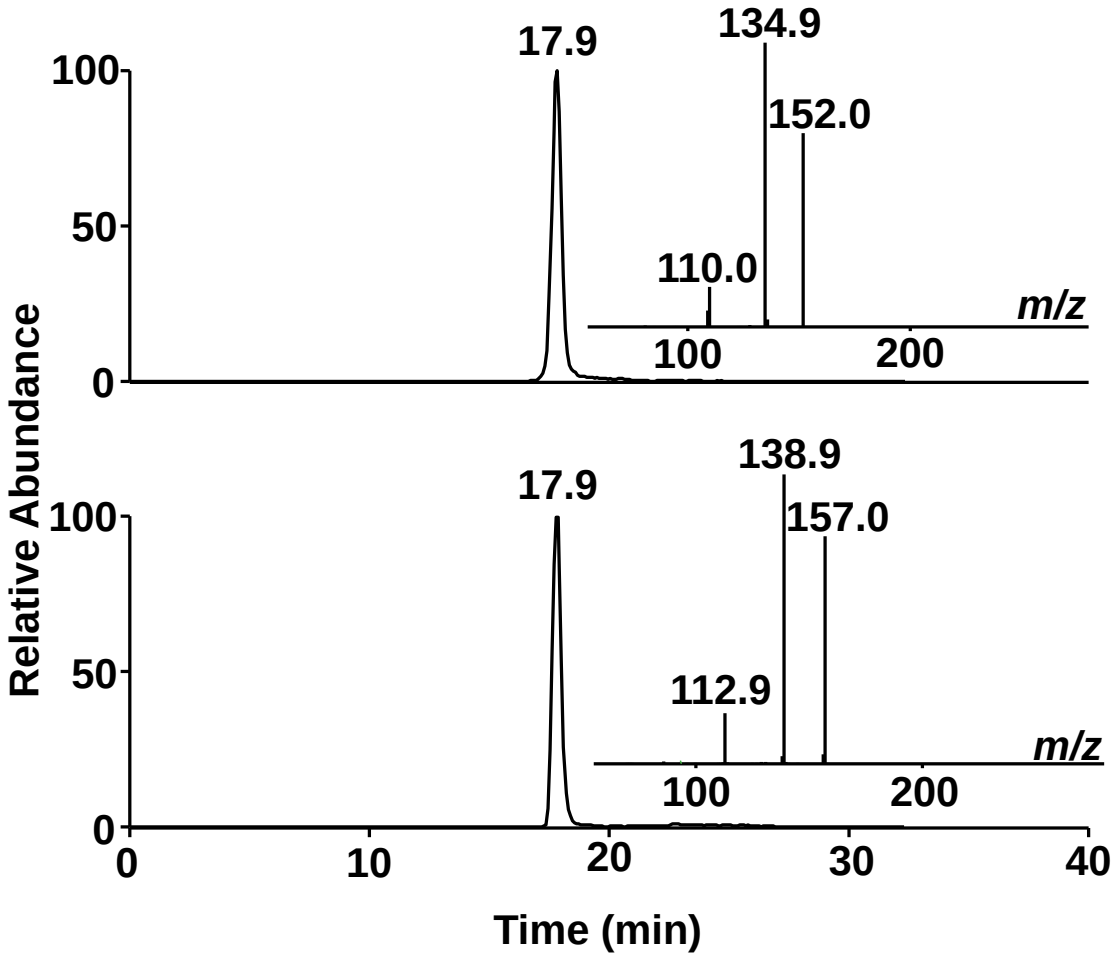


Figure 4.3.Representative selected-ion chromatograms (SICs) for monitoring the *m/z* 268 → 152 → 135 (top) and 273 → 157 → 139 (bottom) transitions for the $[M + H]^+$ ions of the unlabeled dG and $[^{15}N_5]$-dG, respectively, in the nucleoside mixture of genomic DNA extracted from cells. Shown in the insets are the MS^3 spectra for the unlabeled and labeled dG.

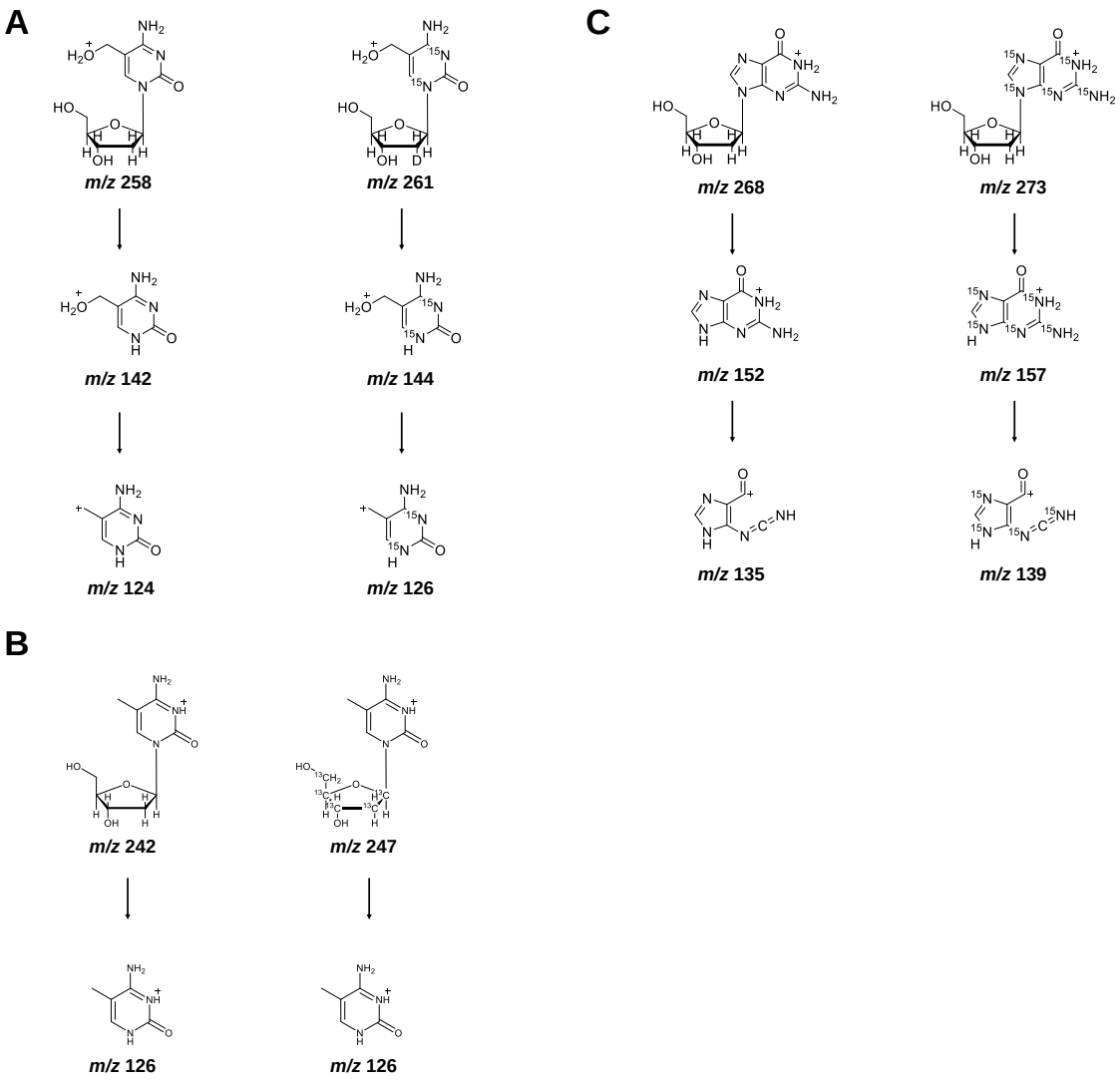


Figure 4.4.Proposed fragmentation pathways for unlabeled and labeled 5-hmdC (A), 5-mdC (B) and dG (C) in MS^n.

Glycolysis inhibition alters 5-hmdC levels in cancer cells

With the above-described nLC-nESI-MS^3 method, we firstly quantified the levels of 5-hmdC in genomic DNA of HeLa human cervical carcinoma cells and HCT-116 human colorectal carcinoma cells as well as two non-cancerous GM00637 human skin fibroblasts and HEK293 human embryonic kidney cells, after treatment with 8 mM of 2-DG for 24 h. 2-DG enters the cell through glucose transporter and can be phosphorylated by hexokinase (HK) to yield 2-deoxy-D-glucose-6-phosphate (2-DG-6-P). Since 2-DG-6-P is not a substrate for either phosphoglucose isomerase (PGI) or glucose-6-phosphate dehydrogenase (G6PD), both the glycolysis and the pentose phosphate pathways were inhibited (35-37). The quantification data revealed that the treatment with 2-DG induced a significant increase in the levels of 5-hmdC only in cancerous cell lines, but not in non-cancerous cells (Figure 4.5). Moreover, the increase in the levels of 5-hmdC in 2-DG-treated cancer cells was not due to the change in the levels of 5-mdC since no significant difference in levels of 5-mdC was observed in all 2-DG-treated cells compared to control groups (Figure 4.6). These results indicated that 2-DG-induced inhibition of glycolysis pathway may lead to altered epigenetic status in cancer cells by increasing the levels of 5-hmdC.

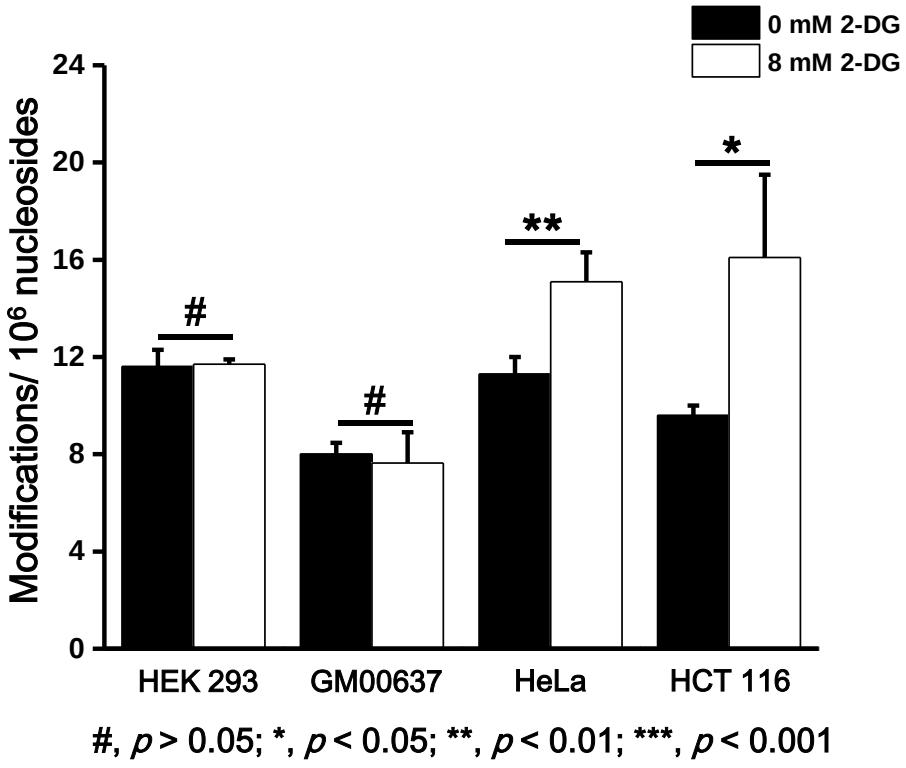


Figure 4.5.5-hmdC levels in cells treated with 8 mM 2-DG.

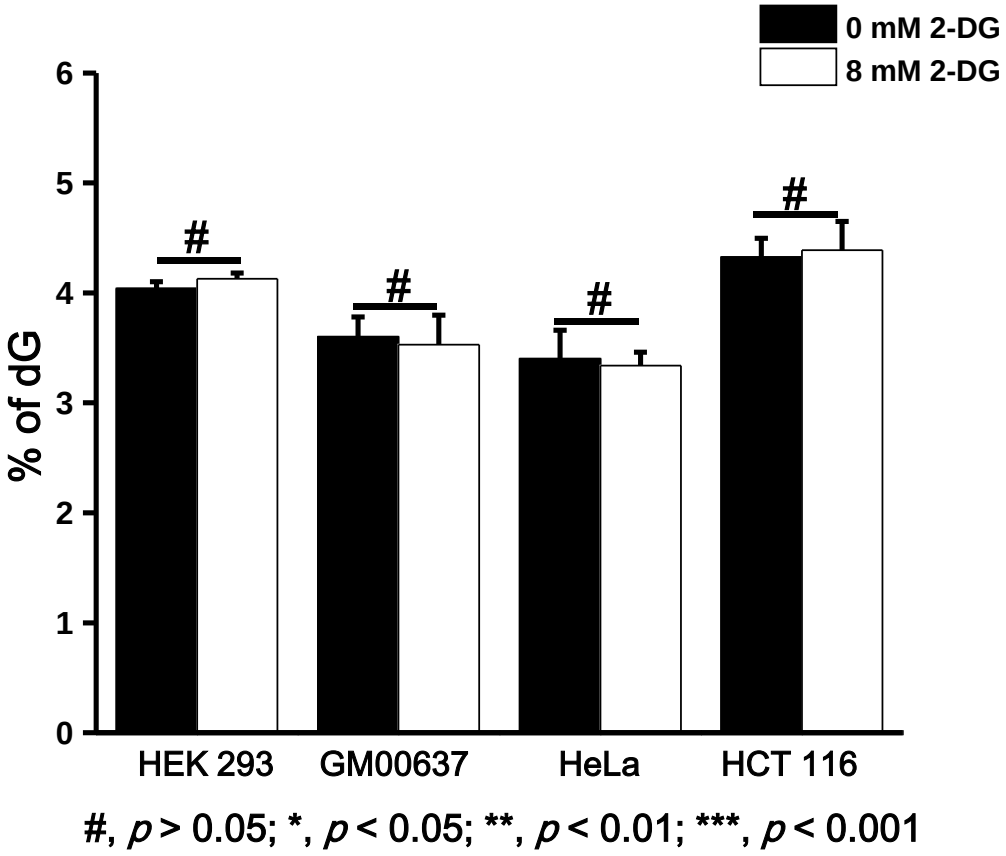


Figure 4.6.5-mdC levels in cells treated with 8 mM 2-DG.

AMPK activation led to elevated levels of 5-hmdC in cells

Previous studies demonstrated that 2-DG-triggered inhibition of glycolysis can also induce the activation of liver kinase B1 (LKB1)/ adenosine monophosphate-activated protein kinase (AMPK) pathway (26,38). The LKB1/AMPK serves as the sensor of energy metabolism, responsing to the metabolic stress-induced intracellular AMP/ATP ratios. AMPKγ forms a complex with AMPKα and β after binding to AMP. The AMPKα subunit is subsequently phosphorylated by LKB1, leading to the activation of AMPK pathway. The activated AMPK pathway induces enhanced glucose uptake and regulates downstream signaling associated with metabolic processes, leading to the restoration of the cellular energy balance (38-40). Multiple compounds were found to activate the AMPK pathway. For instance, the biguanide compounds, metformin and phenformin, can inhibit mitochondrial function, leading to diminished production of ATP, whereas AICAR is a nucleoside analog that can be uptaken into cells by adenosine transporters and phosphorylated to yield 5-aminoimidazole-4-carboxamide ribonucleoside (ZMP), a structural analog that mimics AMP (41-43). Thus, we also examined the impact of AMPK activation on the levels of 5-hmdC in LKB1-deficient HeLa cells (39) and LKB1-proficient HCT-116 cells (44). Quantification results illustrated that phenformin treament induced markedly elevated levels of 5-hmdC in LKB1-proficient HCT-116 cells; however, no increase in 5-hmdC level was observed in LKB1-deficient HeLa cells (Figure 4.7), suggesting a role of AMPK activation in alteration of the levels of 5-hmdC in cells.

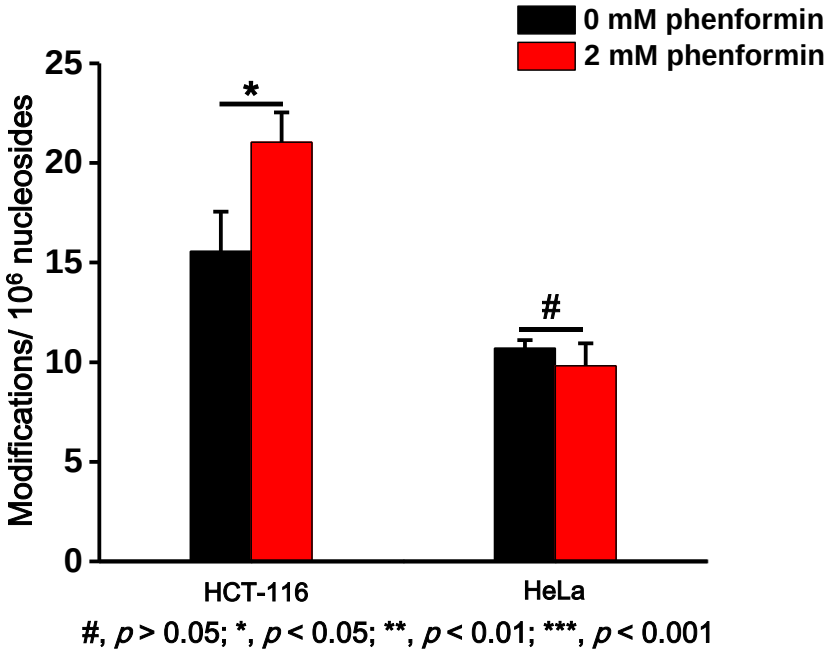


Figure 4.7.5-hmdC levels in cells treated with 2 mM phenformin.

5-hmdC levels were further measured in LKB1-proficient U2OS cells (45) and LKB1-deficient MDA-MB-231 cells (46) treated with three different AMPK activors, i.e. metformin, phenformin and AICAR. All three compounds can significantly elevate the levels of 5-hmdC in U2OS cells, but not in MDA-MB-231 cells (Figure 4.8). Interestingly, the same 5-hmdC upregulation effect of AMPK activators was found in noncancerous HEK293T cells (Figure 4.8), suggesting that the AMPK activation-induced 5-hmdC elevation may occur universally in all types of cells instead of only in cancer cell lines.

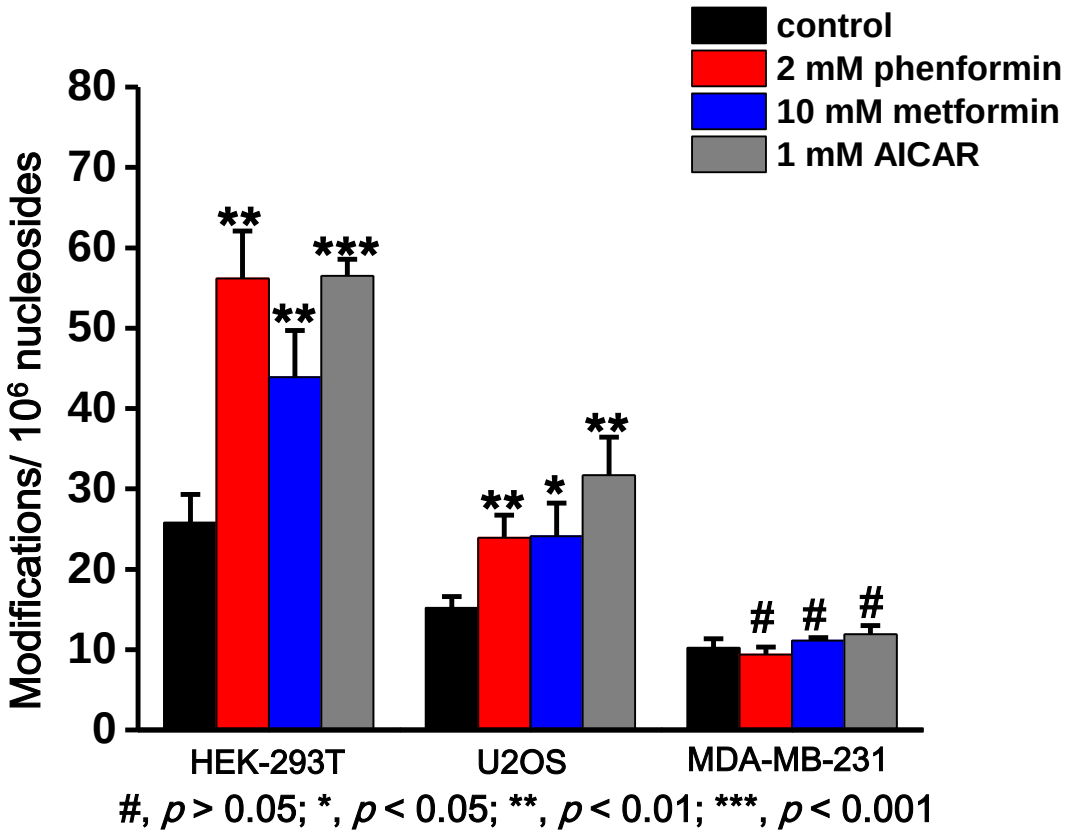


Figure 4.8.5-hmdC levels in cells treated with AMPK activators.

Discussion

In this chapter, we reported the use of nLC-nESI-MS^3 coupled with the stable isotope-dilution method for the quantification of DNA epigenetic marker 5-hmdC in a series of cultured human cancer and noncancerous cells treated with a glycolysis inhibitor (2-DG) or AMPK activators (metformin, phenformin and AICAR). Compared to our previously reported capillary LC-MS^3 technique (15), the method provided higher sensitivity of analysis due to the improvement in ionization efficiency and transmission of ions from the ionization source to the mass analyzer.

Depletion of 5-hmdC in cancer cells has already been considered as a useful biomarker for the detection and diagnosis of cancer. Although IDH1/2 mutation-induced inhibition of TET catlytic activity has been demonstrated to contribute to decreased levels of 5-hmdC in certain types of cancers, it is important to explore further other possible mechanisms about this phenomenon owing to the existence of IDH mutation-independent 5-hmdC depletion (28,47). As rapid proliferating cells, cancer cells mainly rely on rapid glucose uptake and glycolysis, even under normal oxygen conditions, to fulfill their high demand for ATP, a phenomenom known as Warburg effect. This universal property of most cancer cells prompted us to investigate whether aberrant metabolism contributes the alteration of the levels of 5-hmdC in cancer cells. Our quantification data demonstrated that, in cancer cells, perturbated glycolysis pathway induces elevated levels of 5-hmdC. Since 2-DG also indirectly activates the AMPK pathway by reducing ATP levels in cells via inhibition of glycolysis, the effect of AMPK activation on 5-hmdC alteration was further tested in different cancer cell lines as well as in noncancerous HEK293T cells.

Our data revealed that AMPK activation resulted in upregulation of 5-hmdC, not only in cancer cells, but also in HEK293T cells, suggesting that AMPK activation may play a important role in epigenetic regulation. Future work is needed to uncover the mechanism of this AMPK-induced 5-hmdC elevation in cells. One possible explanation is that AMPK can improve the catalytic activity of TET enzymes via direct phosphorylation. A previous study demonstrated that TET enzymes contain consensus sequence motifs for AMPK-mediated phosphorylation (48). It is of note that AMPK may also regulate 5-hmdC indirectly via other mechanisms. For instance, AMPK activation was also found to down-regulate glycolysis through the repression of mTOR and its downstream target HIF-1α, suggesting that AMPK activation-induced downregulation of glycolysis or mTOR itself may lead to altered epigenetic regulation (37,43,49-51). Other than AMPK-involved regulation of 5-hmdC, hypoxia can also participate in altering 5-hmdC levels in cancer cells. Recently Thienpont *et al*. (29) demonstrated that the lack of molecule oxygen leads to the reduced oxidative activity of TET enzymes, which contributes to up to half of hypermethylation events. In this study, the reduction in TET activity was found to be independent from hypoxia-related alterations in TET expression, proliferation, metabolism, hypoxia-inducible factor (HIF) activity or ROS, and depends directly on oxygen storage. Moreover, promoters of tumor suppressor genes are methylated at significantly higher levels in hypoxic tumor tissue of patients (29). In addition, Wise *et al*. (52) found that hypoxia promotes IDH-dependent carboxylation of 2-OG to yield citrate via a reverse direction of TCA cycle to support cell growth and viability. Moreover, the resulting increased IDH2-dependent carboxylation of 2-OG in hypoxia is

associated with a concomitant increase in 2-HG synthesis in cells even with wild-type IDH1 and IDH2. This finding indicated that cancer cells may produce 2-HG in hypoxia through a mechanism that is independent of IDH mutation, thereby attenuating the TET-mediated formation of 5-hmdC (52). Taken together, our analytical method will serve as a powerful tool for the future exploration of alterations of epigenetic regulations mediated by other metabolic pathways.

References

1. Tahiliani, M., Koh, K.P., Shen, Y.H., Pastor, W.A., Bandukwala, H., Brudno, Y., Agarwal, S., Iyer, L.M., Liu, D.R., Aravind, L. *et al.* (2009) Conversion of 5-methylcytosine to 5-hydroxymethylcytosine in mammalian DNA by MLL partner TET1. *Science*, **324**, 930-935.

2. Ito, S., Shen, L., Dai, Q., Wu, S.C., Collins, L.B., Swenberg, J.A., He, C. and Zhang, Y. (2011) Tet proteins can convert 5-methylcytosine to 5-formylcytosine and 5-carboxylcytosine. *Science*, **333**, 1300-1303.

3. He, Y.F., Li, B.Z., Li, Z., Liu, P., Wang, Y., Tang, Q.Y., Ding, J.P., Jia, Y.Y., Chen, Z.C., Li, L. *et al.* (2011) Tet-mediated formation of 5-carboxylcytosine and its excision by TDG in mammalian DNA. *Science*, **333**, 1303-1307.

4. Wu, H., D'Alessio, A.C., Ito, S., Wang, Z.B., Cui, K.R., Zhao, K.J., Sun, Y.E. and Zhang, Y. (2011) Genome-wide analysis of 5-hydroxymethylcytosine distribution reveals its dual function in transcriptional regulation in mouse embryonic stem cells. *Genes Dev.*, **25**, 679-684.

5. Lu, X.Y., Zhao, B.S. and He, C. (2015) TET family proteins: oxidation activity, interacting molecules, and functions in diseases. *Chem. Rev.*, **115**, 2225-2239.

6. Cimmino, L. and Aifantis, I. (2017) Alternative roles for oxidized mCs and TETs. *Curr. Opin. Genet. Dev.*, **42**, 1-7.

7. An, J., Rao, A. and Ko, M. (2017) TET family dioxygenases and DNA demethylation in stem cells and cancers. *Exp. Mol. Med.*, **49**, e323.

8. Guo, J.U., Su, Y.J., Zhong, C., Ming, G.L. and Song, H.J. (2011) Hydroxylation of 5-methylcytosine by TET1 promotes active DNA demethylation in the adult brain. *Cell*, **145**, 423-434.

9. Branco, M.R., Ficz, G. and Reik, W. (2012) Uncovering the role of 5-hydroxymethylcytosine in the epigenome. *Nat. Rev. Genet.*, **13**, 7-13.

10. Pfaffeneder, T., Spada, F., Wagner, M., Brandmayr, C., Laube, S.K., Eisen, D., Truss, M., Steinbacher, J., Hackner, B., Kotljarova, O. *et al.* (2014) Tet oxidizes thymine to 5-hydroxymethyluracil in mouse embryonic stem cell DNA. *Nat. Chem. Biol.*, **10**, 574-581.

11. Shen, L., Wu, H., Diep, D., Yamaguchi, S., D'Alessio, A.C., Fung, H.L., Zhang, K. and Zhang, Y. (2013) Genome-wide analysis reveals TET- and TDG-dependent 5-methylcytosine oxidation dynamics. *Cell*, **153**, 692-706.

12. Song, C.X., Szulwach, K.E., Dai, Q., Fu, Y., Mao, S.Q., Lin, L., Street, C., Li, Y.J., Poidevin, M., Wu, H. *et al.* (2013) Genome-wide profiling of 5-formylcytosine reveals its roles in epigenetic priming. *Cell*, **153**, 678-691.

13. Shen, L., Song, C.X., He, C. and Zhang, Y. (2014) Mechanism and function of oxidative reversal of DNA and RNA methylation. *Annu. Rev. Biochem*, **83**, 585-614.

14. Song, C.-X. and He, C. (2013) Potential functional roles of DNA demethylation intermediates. *Trends Biochem. Sci*, **38**, 480-484.

15. Yu, Y., Guerrero, C.R., Liu, S., Amato, N.J., Sharma, Y., Gupta, S. and Wang, Y. (2016) Comprehensive assessment of oxidatively induced modifications of DNA in a rat model of human Wilson's disease. *Mol. Cell. Proteomics*, **15**, 810-817.

16. Andy Madrid , L.A.P., Reid S Alisch. (2016) New hope: the emerging role of 5-hydroxymethylcytosine in mental health and disease. *Epigenomics*, **8**, 981-991.

17. Lu, X., Zhao, B.S. and He, C. (2015) TET family proteins: Oxidation activity, interacting molecules, and functions in diseases. *Chem. Rev.*, **115**, 2225-2239.

18. Ko, M., An, J., Pastor, W.A., Koralov, S.B., Rajewsky, K. and Rao, A. (2015) TET proteins and 5-methylcytosine oxidation in hematological cancers. *Immunol. Rev.*, **263**, 6-21.

19. Killian, J.K., Kim, S.Y., Miettinen, M., Smith, C., Merino, M., Tsokos, M., Quezado, M., Smith, W.I., Jahromi, M.S., Xekouki, P. *et al.* (2013) Succinate dehydrogenase mutation underlies global epigenomic divergence in gastrointestinal stromal tumor. *Cancer Discov.*, **3**, 648-657.

20. Figueroa, M.E., Abdel-Wahab, O., Lu, C., Ward, P.S., Patel, J., Shih, A., Li, Y., Bhagwat, N., Vasanthakumar, A., Fernandez, H.F. *et al.* (2010) Leukemic IDH1 and IDH2 mutations result in a hypermethylation phenotype, disrupt TET2 function, and impair hematopoietic differentiation. *Cancer Cell*, **18**, 553-567.

21. Yang, H., Lin, H., Xu, H., Zhang, L., Cheng, L., Wen, B., Shou, J., Guan, K., Xiong, Y. and Ye, D. (2014) TET-catalyzed 5-methylcytosine hydroxylation is dynamically regulated by metabolites. *Cell Res.*, **24**, 1017-1020.

22. Ye, D., Xiong, Y. and Guan, K.-L. (2012) The mechanisms of IDH mutations in tumorigenesis. *Cell Res.*, **22**, 1102-1104.

23. Dang, L., White, D.W., Gross, S., Bennett, B.D., Bittinger, M.A., Driggers, E.M., Fantin, V.R., Jang, H.G., Jin, S., Keenan, M.C. *et al.* (2009) Cancer-associated IDH1 mutations produce 2-hydroxyglutarate. *Nature*, **462**, 739-744.

24. Ward, P.S., Patel, J., Wise, D.R., Abdel-Wahab, O., Bennett, B.D., Coller, H.A., Cross, J.R., Fantin, V.R., Hedvat, C.V., Perl, A.E. *et al.* (2010) The common feature of leukemia-associated IDH1 and IDH2 mutations is a neomorphic enzyme activity converting α-ketoglutarate to 2-hydroxyglutarate. *Cancer Cell*, **17**, 225-234.

25. Xiao, M., Yang, H., Xu, W., Ma, S., Lin, H., Zhu, H., Liu, L., Liu, Y., Yang, C., Xu, Y. *et al.* (2012) Inhibition of α-KG-dependent histone and DNA demethylases by fumarate and succinate that are accumulated in mutations of FH and SDH tumor suppressors. *Genes Dev.*, **26**, 1326-1338.

26. Schulze, A. and Harris, A.L. (2012) How cancer metabolism is tuned for proliferation and vulnerable to disruption. *Nature*, **491**, 364-373.

27. Xu, W., Yang, H., Liu, Y., Yang, Y., Wang, P., Kim, S.-H., Ito, S., Yang, C., Wang, P., Xiao, M.-T. *et al.* (2011) Oncometabolite 2-hydroxyglutarate is acompetitive inhibitor of α-ketoglutarate-dependent dioxygenases. *Cancer Cell*, **19**, 17-30.

28. Jin, S.-G., Jiang, Y., Qiu, R., Rauch, T.A., Wang, Y., Schackert, G., Krex, D., Lu, Q. and Pfeifer, G.P. (2011) 5-hydroxymethylcytosine is strongly depleted in human cancers but its levels do not correlate with IDH1 mutations. *Cancer Res.*, **71**, 7360-7365.

29. Thienpont, B., Steinbacher, J., Zhao, H., D'Anna, F., Kuchnio, A., Ploumakis, A., Ghesquière, B., Van Dyck, L., Boeckx, B., Schoonjans, L. *et al.* (2016) Tumour hypoxia causes DNA hypermethylation by reducing TET activity. *Nature*, **537**, 63-68.

30. Vander Heiden, M.G., Cantley, L.C. and Thompson, C.B. (2009) Understanding the Warburg Effect: The Metabolic Requirements of Cell Proliferation. *Science*, **324**, 1029-1033.

31. Warburg, O., Wind, F. and Negelein, E. (1927) The metabolism of tumors in the body. *J Gen Physiol.*, **8**, 519-530.

32. Cao, H. and Wang, Y. (2007) Quantification of oxidative single-base and intrastrand cross-link lesions in unmethylated and CpG-methylated DNA induced by Fenton-type reagents. *Nucleic Acids Res.*, **35**, 4833-4844.

33. Wang, J., Yuan, B., Guerrero, C., Bahde, R., Gupta, S. and Wang, Y. (2011) Quantification of oxidative DNA lesions in tissues of Long-Evans Cinnamon rats by capillary high-performance liquid chromatography-tandem mass spectrometry coupled with stable isotope-dilution method. *Anal. Chem.*, **83**, 2201-2209.

34. Volz, D.C., Leet, J.K., Chen, A., Stapleton, H.M., Katiyar, N., Kaundal, R., Yu, Y. and Wang, Y. (2016) Tris(1,3-dichloro-2-propyl)phosphate Induces Genome-Wide Hypomethylation within Early Zebrafish Embryos. *Environ. Sci. Technol.*, **50**, 10255-10263.

35. Shafaee, A., Dastyar, D.Z., Islamian, J.P. and Hatamian, M. (2015) Inhibition of tumor energy pathways for targeted esophagus cancer therapy. *Metabolism*, **64**, 1193-1198.

36. Aghaee, F., Pirayesh Islamian, J. and Baradaran, B. (2012) Enhanced Radiosensitivity and Chemosensitivity of Breast Cancer Cells by 2-Deoxy-D-Glucose in Combination Therapy. *J. Breast Cancer*, **15**, 141-147.

37. Yu, L., Chen, X., Wang, L.T. and Chen, S.W. (2016) The sweet trap in tumors: aerobic glycolysis and potential targets for therapy. *Oncotarget*, **7**, 38908-38926.

38. van Veelen, W., Korsse, S.E., van de Laar, L. and Peppelenbosch, M.P. (2011) The long and winding road to rational treatment of cancer associated with LKB1/AMPK/TSC/mTORC1 signaling. *Oncogene*, **30**, 2289-2303.

39. Shaw, R.J., Kosmatka, M., Bardeesy, N., Hurley, R.L., Witters, L.A., DePinho, R.A. and Cantley, L.C. (2004) The tumor suppressor LKB1 kinase directly activates AMP-activated kinase and regulates apoptosis in response to energy stress. *Proc. Natl. Acad. Sci. U. S. A.*, **101**, 3329-3335.

40. Zadra, G., Batista, J.L. and Loda, M. (2015) Dissecting the Dual Role of AMPK in Cancer: From Experimental to Human Studies. *Mol. Cancer Res.*, **13**, 1059-1072.

41. Hardie, D.G. (2014) AMPK—Sensing Energy while Talking to Other Signaling Pathways. *Cell Metabolism*, **20**, 939-952.

42. Hardie, D.G. and Alessi, D.R. (2013) LKB1 and AMPK and the cancer-metabolism link - ten years after. *BMC Biol.*, **11**, 36.

43. Hardie, D.G. (2013) AMPK: A Target for Drugs and Natural Products With Effects on Both Diabetes and Cancer. *Diabetes*, **62**, 2164-2172.

44. Faubert, B., Boily, G., Izreig, S., Griss, T., Samborska, B., Dong, Z., Dupuy, F., Chambers, C., Fuerth, Benjamin J., Viollet, B. *et al.* (2013) AMPK Is a Negative Regulator of the Warburg Effect and Suppresses Tumor Growth In Vivo. *Cell Metabolism*, **17**, 113-124.

45. Goodwin, Jonathan M., Svensson, Robert U., Lou, Hua J., Winslow, Monte M., Turk, Benjamin E. and Shaw, Reuben J. (2014) An AMPK-Independent Signaling Pathway Downstream of the LKB1 Tumor Suppressor Controls Snail1 and Metastatic Potential. *Mol. Cell*, **55**, 436-450.

46. Zhou, J., Huang, W., Tao, R., Ibaragi, S., Lan, F., Ido, Y., Wu, X., Alekseyev, Y.O., Lenburg, M.E., Hu, G.f. *et al.* (2009) Inactivation of AMPK alters gene expression and promotes growth of prostate cancer cells. *Oncogene*, **28**, 1993-2002.

47. Pfeifer, G.P., Xiong, W., Hahn, M.A. and Jin, S.-G. (2014) The role of 5-hydroxymethylcytosine in human cancer. *Cell Tissue Res.*, **356**, 631-641.

48. Marin, T.L., Gongol, B., Zhang, F., Martin, M., Johnson, D.A., Xiao, H., Wang, Y., Subramaniam, S., Chien, S. and Shyy, J.Y.-J. (2017) AMPK promotes mitochondrial biogenesis and function by phosphorylating the epigenetic factors DNMT1, RBBP7, and HAT1. *Sci. Signal.*, **10**.

49. Inoki, K., Zhu, T. and Guan, K.-L. (2003) TSC2 Mediates Cellular Energy Response to Control Cell Growth and Survival. *Cell*, **115**, 577-590.

50. Mamane, Y., Petroulakis, E., LeBacquer, O. and Sonenberg, N. (2006) mTOR, translation initiation and cancer. *Oncogene*, **25**, 6416-6422.

51. Düvel, K., Yecies, J.L., Menon, S., Raman, P., Lipovsky, A.I., Souza, A.L., Triantafellow, E., Ma, Q., Gorski, R., Cleaver, S. *et al.* (2010) Activation of a Metabolic Gene Regulatory Network Downstream of mTOR Complex 1. *Mol. Cell*, **39**, 171-183.

52. Wise, D.R., Ward, P.S., Shay, J.E.S., Cross, J.R., Gruber, J.J., Sachdeva, U.M., Platt, J.M., DeMatteo, R.G., Simon, M.C. and Thompson, C.B. (2011) Hypoxia promotes isocitrate dehydrogenase-dependent carboxylation of α-ketoglutarate to citrate to support cell growth and viability. *Proc. Natl. Acad. Sci. U. S. A*, **108**, 19611-19616.

Chapter 5 Conclusions and Future Directions

LC-MS has been employed as a powerful tool for elucidating the structures as well as providing accurate and unambiguous quantification of analytes. The focus of this dissertation is placed on the development of analytical methods for reliable quantification of chemically modified DNA, i.e. oxidative stress-induced DNA lesions, the DNA epigenetic markers and carboxymethylated DNA adducts.

In chapter 2, I developed a nanoflow liquid chromatography-nanoelectrospray ionization-tandem mass spectrometry (nanoLC-NSI-MS^2) coupled with the isotope-dilution method for the simultaneous quantification of oxidatively induced DNA modifications. This method enabled measurement, in microgram quantities of DNA, of four oxidative stress-induced lesions, including direct ROS-induced cPus and two exocyclic adducts induced by byproducts of LPO, i.e. εdA and εdG. Analysis of liver tissues of Long-Evans Cinnamon (LEC) rats, which constitute an animal model of human Wilson's disease, and their healthy counterparts [i.e. Long-Evans Agouti (LEA) rats] showed significantly higher levels of all four DNA lesions in LEC than LEA rats. Moreover, cPus were present at much higher levels than εdA and εdG lesions. In contrast, the level of 5-hmdC was markedly lower in the liver tissues of LEC than LEA rats, though no differences were observed for the levels of 5-mdC. *In vitro* biochemical assay showed that Cu^{2+} ions could directly inhibit the activity of Tet enzymes. Together, these results suggest that aberrant copper accumulation may perturb genomic stability by

elevating oxidatively induced DNA lesions, and by altering epigenetic pathways of gene regulation.

In chapter 3, I developed a highly sensitive nLC-nESI-MS^3 method for the simultaneous quantification of N^6-CMdA, O^6-CMdG and O^6-MedG. We were able to measure the levels of these three lesions with the use of low-microgram quantities of DNA from cultured human skin fibroblasts and human colorectal carcinoma cells treated with azaserine, a DNA carboxymethylating agent. Our results revealed that both the levels of O^6-CMdG and O^6-MedG increased when the dose of azaserine was increased from 0 to 450 μM. In the meantime, significant elevation in levels of N^6-CMdA was only observed in human skin fibroblasts treated with 450 μM azaserine, suggesting the presence of repair mechanism(s) for the rapid clearance of this lesion *in vivo*. This is the first report about the application of nLC-nESI-MS^3 technique for the simultaneous quantification of O^6-CMdG, O^6-MedG and N^6-CMdA. The method reported here will be useful for the future investigations about the repair of the carboxymethylated DNA lesions and about the implications of these lesions in carcinogenesis.

In chapter 4, I applied an LC-MS^3 quantification of 5-hmdC in different cancer cells treated with a glycolysis inhibitor or AMPK activators to gain insights into the relationship between aberrant metabolism and the levels of 5-hmdC in cancer cells. Quantification data showed significantly increased levels of 5-hmdC in several cancer cell lines (HeLa and HCT-116) upon 2-deoxy-D-glucose (2-DG) treatment. The levels of 5-mdC in genomic DNA of these cells, however, were not affected by 2-DG treatment, indicating that the 2-DG-induced elevation in the levels of 5-hmdC was not attributed to

the changes in the levels of 5-mdC. In contrast, similar treatment of non-cancerous cells (GM00637 and HEK-293) did not lead to apparent changes in the levels of 5-hmdC. Moreover, treatment with commonly used AMPK activators led to significantly higher levels of 5-hmdC in HEK-293T, HCT-116 and U2OS cells. Nevertheless, no alteration in the levels of 5-HmdC was found in HeLa and MDA-MB-231 cells with or without AMPK activator treatment, which is in line with the lack of AMPK pathway in these two cell lines. These data suggested that the altered metabolism in cancer cells could contribute, in part, to the diminished levels of 5-hmdC observed in cancer cells.

The development of LC-MS-based method, for high-throughput, accurate and efficient detection and measurement of DNA lesions, will still be the top priority of future studies. In contrast to our current offline HPLC enrichment methods, online solid phase extraction (SPE) and online column switching system, coupled with high separation ability UPLC or nanoflow UPLC, will facilitate the rapid and direct quantification of DNA lesions without offline HPLC enrichment. Moreover, high-resolution Orbitrap mass spectrometers will be increasingly applied in future studies to quantify low levels DNA adducts in cellular and tissue samples due to their accurate mass measurement capability and high sensitivity. Systematic analysis of DNA adductome will be another main task in future studies since different types of lesions may contribute together to the etiology of certain type of cancer. Along this line, a standard, comprehensive and publicly available database of DNA adductome based on high-resolution MS analysis will significantly promote the application of DNA adductome in future clinical investigation. To explore the function of AMPK or other energy-

metabolism-related pathways in 5-hmdC regulation, overexpression of TET1/2/3 protein expression vector in mammalian cells, combined with proteomic analysis of AMPK-mediated phosphorylation, will reveal better the implications of AMPK pathway in modulating the level of 5-hmdC in cells.

Appendix A Supporting information for chapter 2

	Precursor ion *m/z*	Product ion *m/z*	Collision energy (V)
S-cdG	266	180	17
[$^{15}N_5$]-*S*-cdG	271	185	17
S-cdA	250	164	19
[$^{15}N_5$]-*S*-cdA	255	169	19
εdA	276	160	20
[$^{15}N_5$]-εdA	281	165	20
εdG	292	176	25
[$^{15}N_5$]-εdG	297	181	25

Table A.1.A list of MRM transitions employed for the quantifications of the five oxidative stress-induced DNA lesions and their corresponding stable isotope-labeled standards.

Levels (Modifications/10^7 Nucleosides)	Liver		Brain	
	LEA	LEC	LEA	LEC
εdA	2.3 ± 0.2	3.0 ± 0.2	3.9 ± 0.7	4.4 ± 0.3
εdG	1.1 ± 0.1	1.6 ± 0.2	1.5 ± 0.04	1.3 ± 0.2
S-cdA	12.0 ± 1.1	26.8 ± 0.8	15.4 ± 0.9	14.1 ± 2.4
S-cdG	20.2 ± 3.0	44.5 ± 0.9	23.1 ± 2.4	22.1 ± 2.4
5-HmdC (/10^6 nucleosides)	339 ± 40	176 ± 21	619 ± 93	654 ± 59
5-mdC (% of dG)	2.5 ± 0.4	2.8 ± 0.2	2.8 ± 0.4	3.1 ± 0.4

Table A.2.A summary of the levels of oxidatively induced DNA modifications as well as 5-mdC in the liver and brain tissues of rats. The data represent mean ± standard deviation of LC-MS/MS results for the analysis of liver tissues from 5 LEC or 6 LEA rats, and brain tissues of 3 LEA and 3 LEC rats.

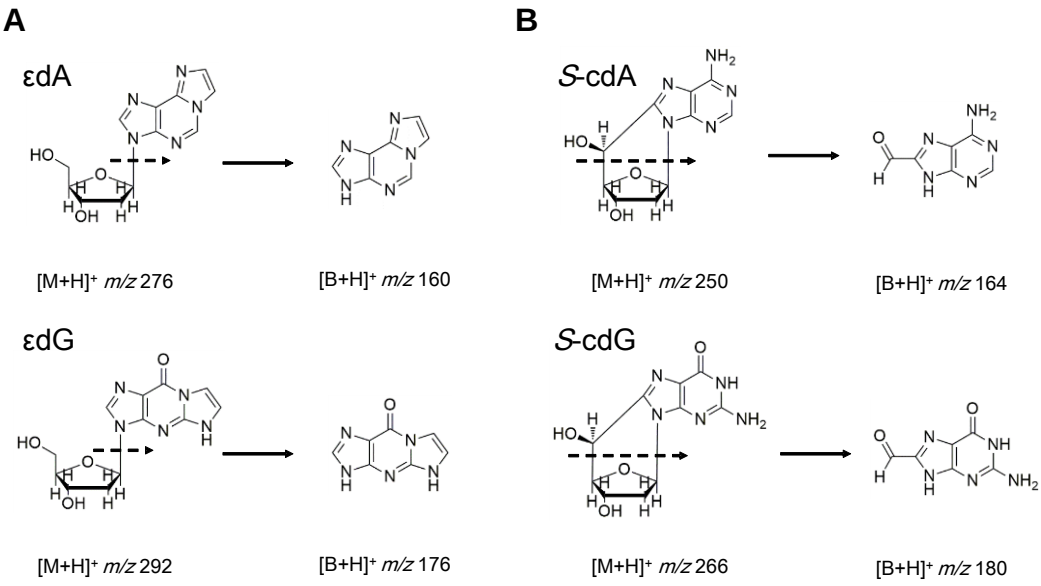


Figure A.1.The proposed fragmentation pathways for the $[M + H]^+$ ions of etheno DNA adducts (A) and cPus (B) lesions in MS/MS.

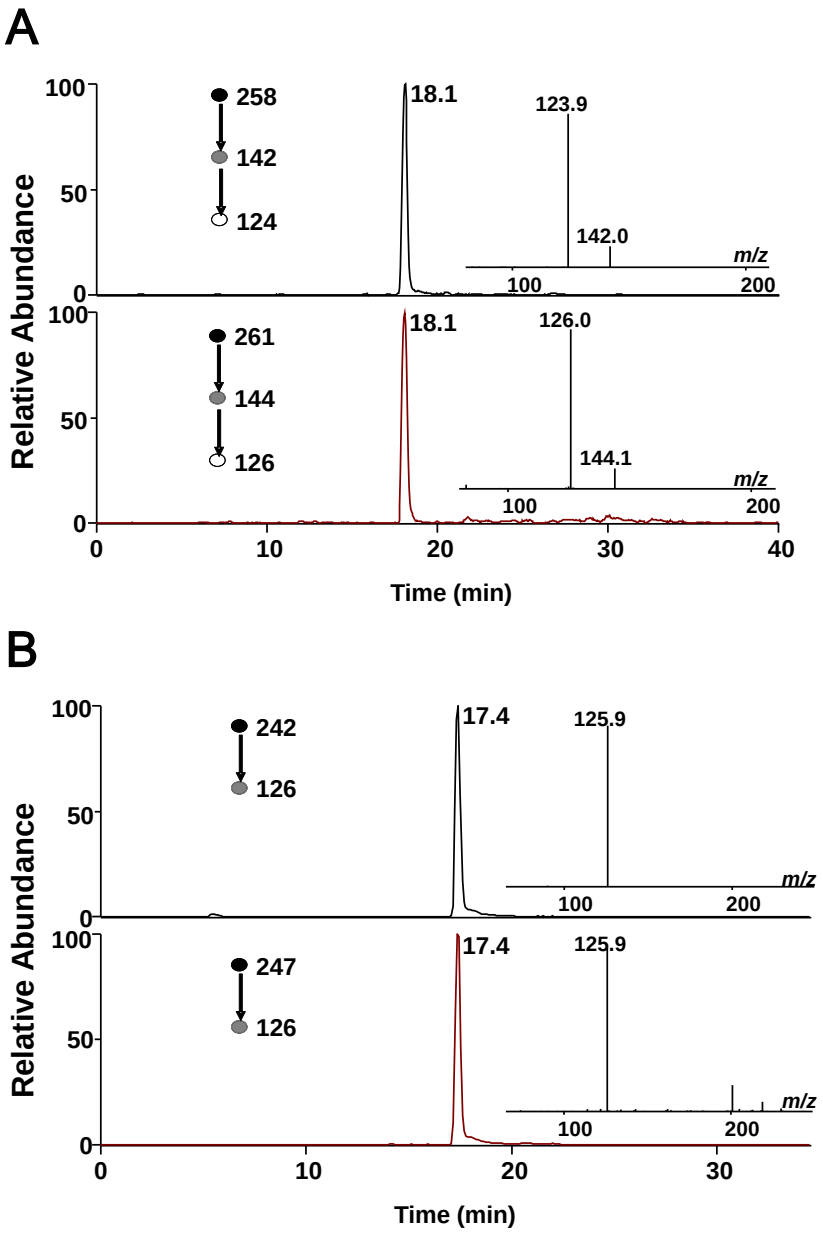


Figure A.2.Representative LC-MS^3 results for the quantifications of 5-HmdC (A) and 5-mdC (B) in rat tissues. Shown are the SICs for monitoring the indicated transitions for the analytes (top trace) and the labeled standards (bottom trace), and the inset shows the corresponding MS^3 spectra for the analytes and internal standards. The proposed fragmentation pathways for the $[M + H]^+$ ions of unlabeled and stable isotope-labeled nucleosides observed in MS^2 and MS^3 are shown on the right.

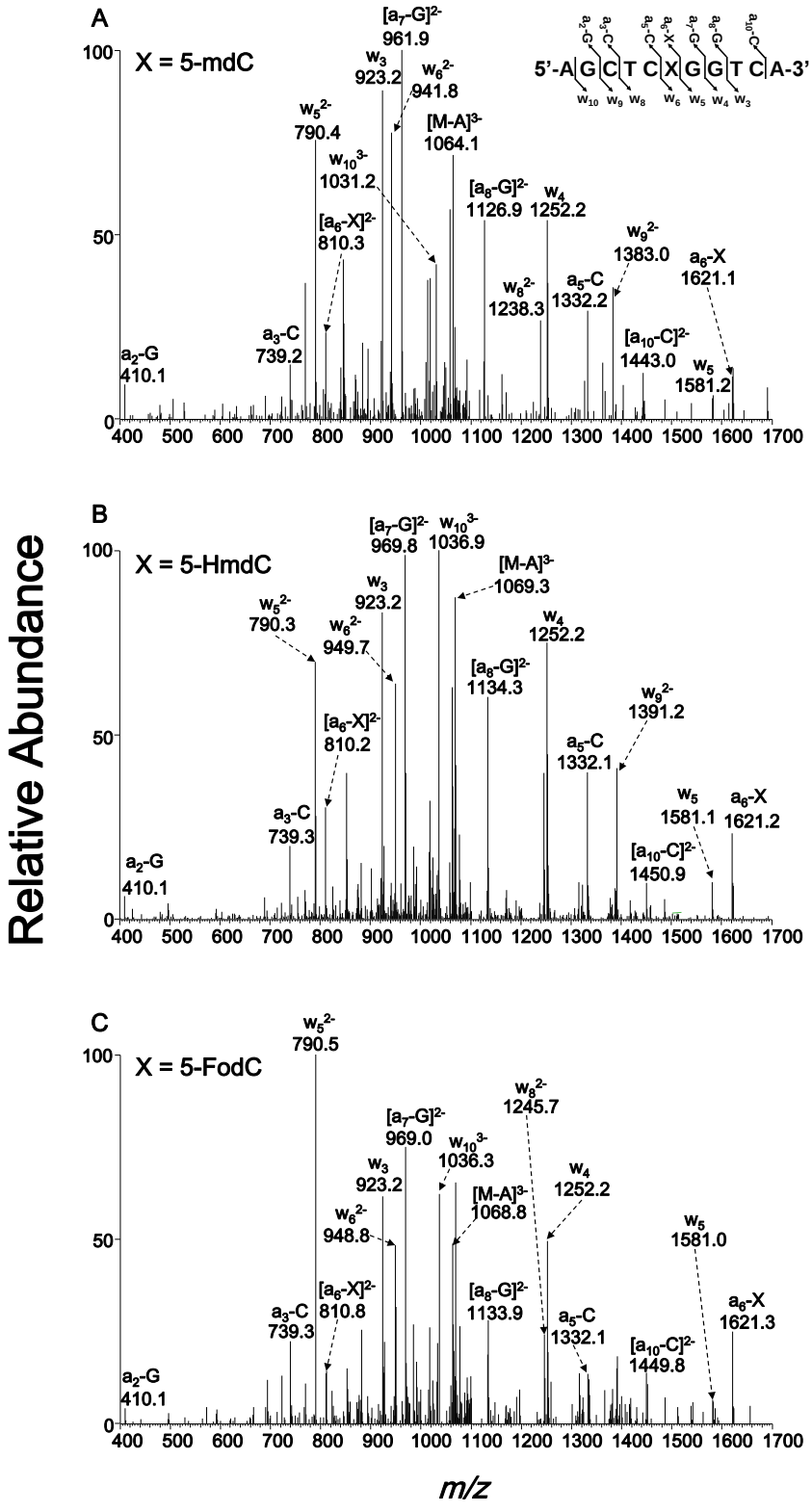

A
X = 5-mdC
5'-AGCTCXGGTCA-3'
[a7-G]2- 961.9
w3 923.2
w6 2- 941.8
w5 2- 790.4
[M-A]3- 1064.1
w10 3- 1031.2
[a8-G]2- 1126.9
w4 1252.2
[a6-X]2- 810.3
w9 2- 1383.0
a6-X 1621.1
w8 2- 1238.3
a5-C 1332.2
a3-C 739.2
[a10-C]2- 1443.0
a2-G 410.1
w5 1581.2
B
X = 5-HmdC
[a7-G]2- 969.8
w10 3- 1036.9
[M-A]3- 1069.3
w3 923.2
w5 2- 790.3
w6 2- 949.7
w4 1252.2
[a8-G]2- 1134.3
w9 2- 1391.2
[a6-X]2- 810.2
a5-C 1332.1
w5 1581.1
a6-X 1621.2
a3-C 739.3
[a10-C]2- 1450.9
a2-G 410.1
C
X = 5-FodC
w5 2- 790.5
w8 2- 1245.7
[a7-G]2- 969.0
w10 3- 1036.3
w3 923.2
w4 1252.2
[M-A]3- 1068.8
w6 2- 948.8
w5 1581.0
[a6-X]2- 810.8
[a8-G]2- 1133.9
a6-X 1621.3
a3-C 739.3
a5-C 1332.1
[a10-C]2- 1449.8
a2-G 410.1
Relative Abundance
m/z

Figure A.3.LC-MS^2 for monitoring the $[M - 3H]^{3-}$ ions of d(AGCTCXGGTCA) found in Tet1-catalyzed reaction mixture of the 11-mer duplex DNA, where 'X' is a 5-mdC, 5-HmdC or 5-FodC. Collisional activation of deprotonated ions of ODNs led to the loss of nucleobases (A, C, or G) and subsequent cleavages of the 3′ C-O bond of the same nucleoside to generate $[a_n - Base]$ and its complementary w_n ions.

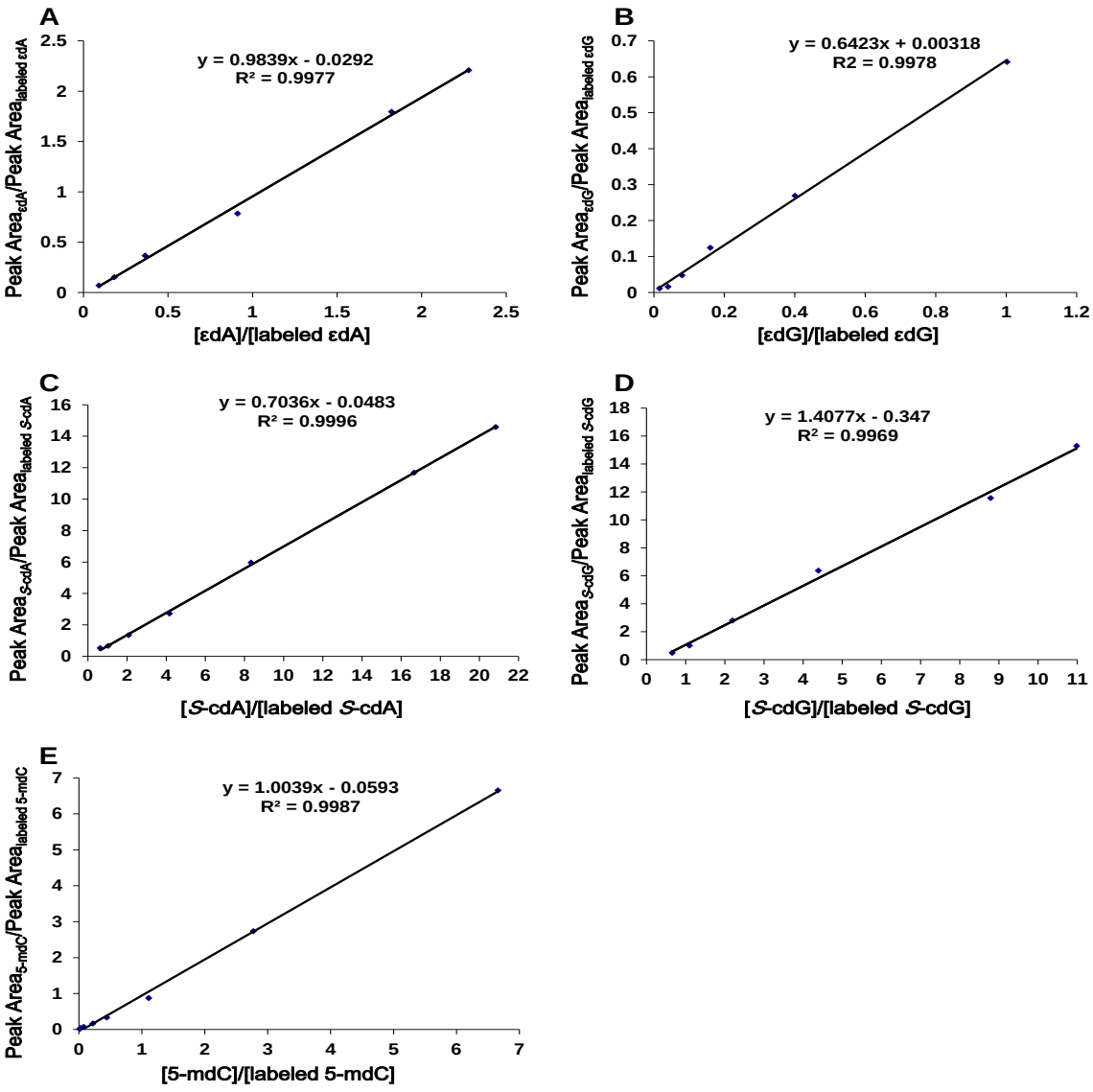


Figure A.4.Calibration curves for the quantification of εdA, εdG, *S*-cdA, *S*-cdG and 5-mdC by LC-MS with the stable isotope dilution method. Plotted are the ratios of areas of peaks found in the SICs for monitoring the transitions as shown in Figure 1 and S2B versus the molar ratios of the unlabeled nucleoside over that of the corresponding stable isotope-labeled standard.

Appendix B Supporting information for chapter 3

Lesions	LOQ (amol)
O^6-CMdG	73.4 ± 17.5
O^6-MedG	6.2 ± 1.6
N^6-CMdA	11.5 ± 2.8

Table B.1.The limits of quantitation (LOQ) for O^6-CMdG, N^6-CMdA, and O^6-MedG. The data represent the means and standard deviations of the results from three measurements of the unlabeled lesion standards in three separate days.

Lesions	Azaserine (μM)							
	0		50		150		450	
	GM04429	HCT-116	GM04429	HCT-116	GM04429	HCT-116	GM04429	HCT-116
O^6-CMdG	0.054 ± 0.009	0.247 ± 0.055	0.64 ± 0.15	1.436 ± 0.171	1.35 ± 0.20	3.06 ± 1.046	4.95 ± 1.08	9.12 ± 1.446
O^6-MedG	0.092 ± 0.015	0.070 ± 0.020	0.116 ± 0.012	0.132 ± 0.010	0.189 ± 0.056	0.194 ± 0.012	0.264 ± 0.068	0.52 ± 0.154
N^6-CMdA	0.33 ± 0.057	1.002 ± 0.20	0.395 ± 0.063	0.731 ± 0.15	0.444 ± 0.048	0.988 ± 0.30	0.513 ± 0.063	0.885 ± 0.035

Table B.2.A summary of the levels of O^6-CMdG, O^6-MedG and N^6-CMdA in GM04429 and HCT-116 cells treated with different concentrations of azaserine (in lesions per 10^7 nucleosides). The data represent the means and standard deviations of results from three independent experiments.

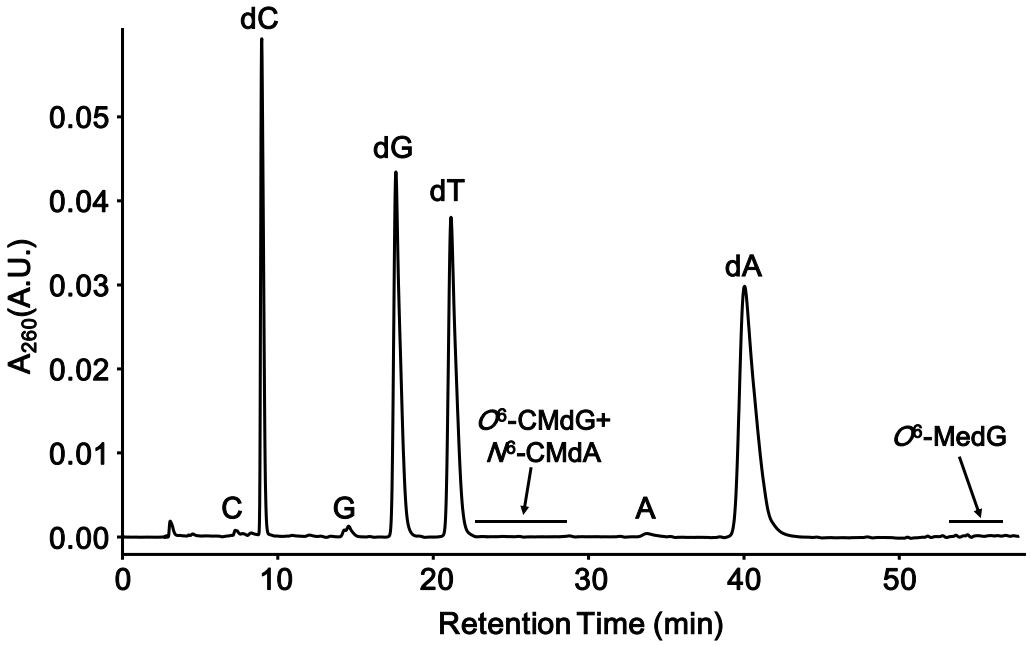


Figure B.1.A representative HPLC trace for the enrichment of O^6-CMdG, O^6-MedG, and N^6-CMdA from the nucleoside mixture arising from digestion of genomic DNA isolated from human skin fibroblasts treated with azaserine. ‘C’, ‘G’, ‘A’, ‘dC’, ‘dG’, ‘dT’, ‘dA’ represent cytidine, guanosine, adenosine, 2'-deoxycytidine, 2'-deoxyguanosine, thymidine, and 2'-deoxyadenosine, respectively.

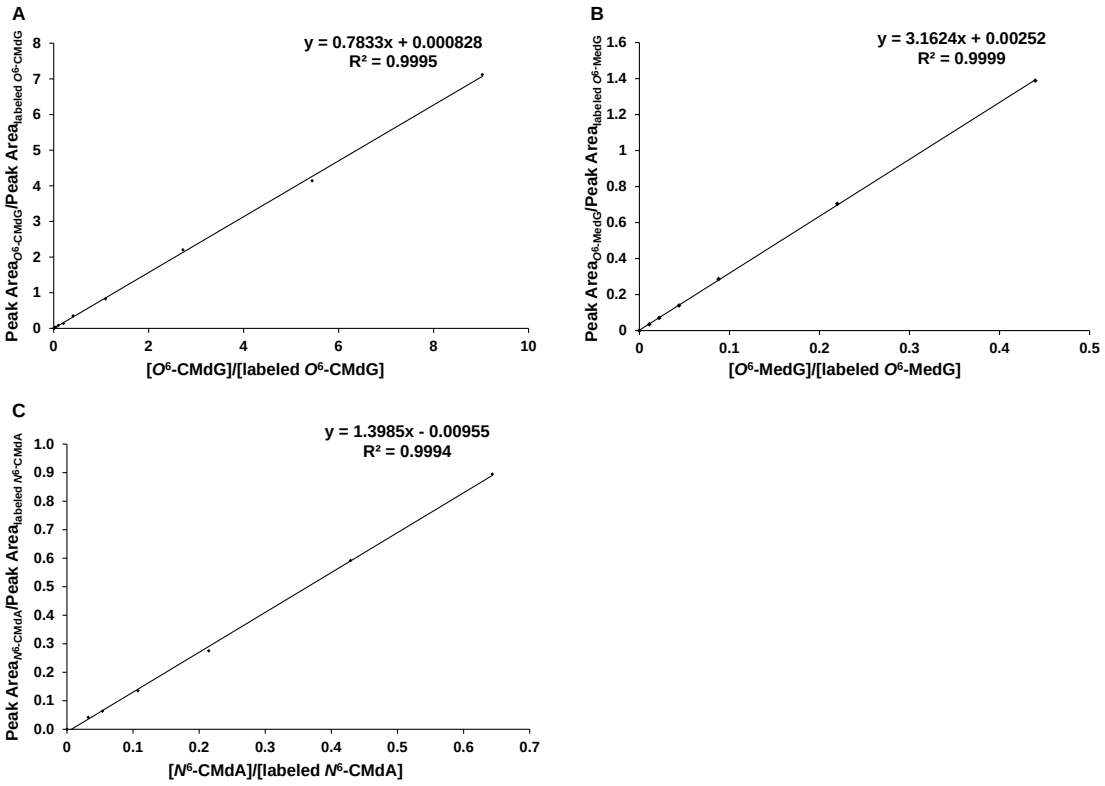


Figure B.2.Calibration curves for the quantitation of O^6-CMdG (A), O^6-MedG (B), and N^6-CMdA (C).

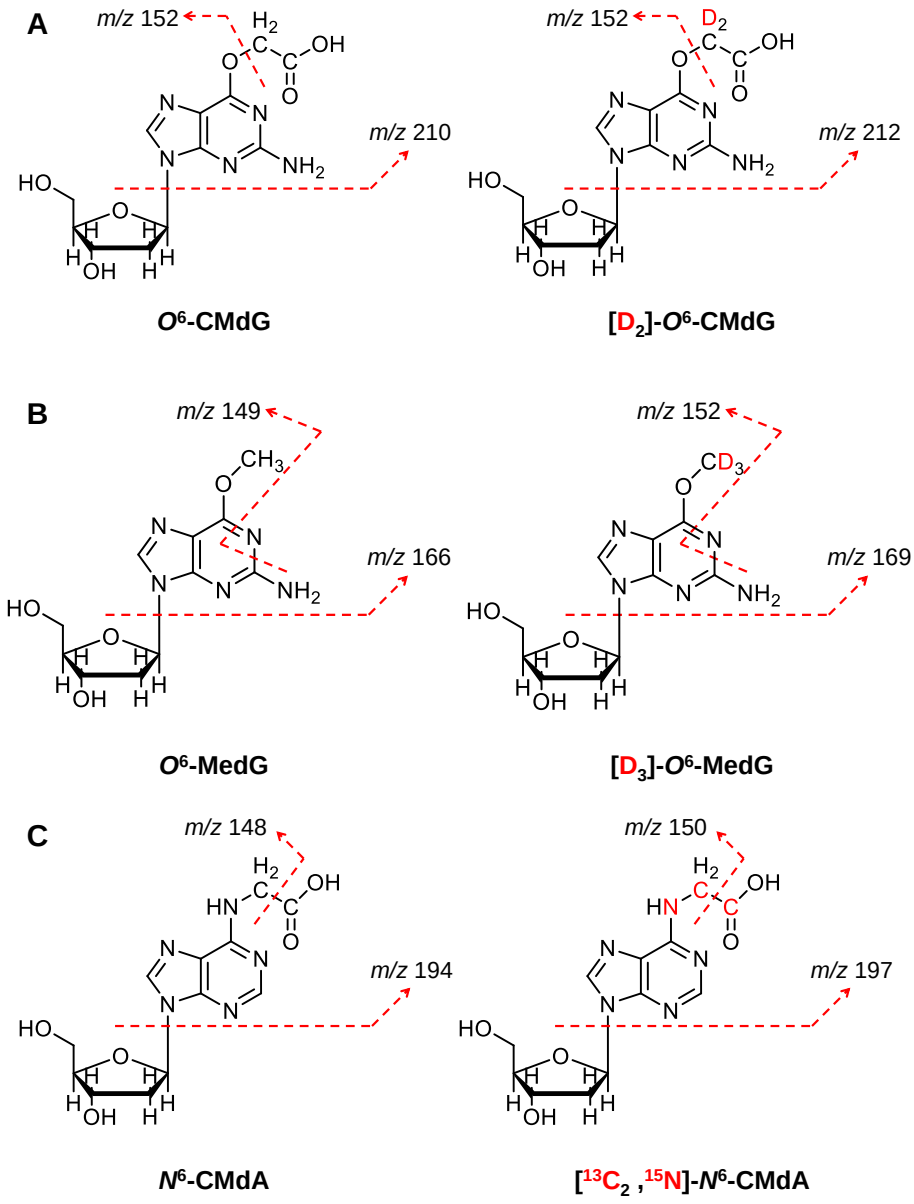


Figure B.3.Proposed major fragmentation pathways for the $[M + H]^+$ ions of unlabeled and labeled O^6-CMdG (A), O^6-MedG (B) and N^6-CMdA (C) observed in MS/MS and MS/MS/MS. The "N", "C" in red represent ^{15}N and ^{13}C, respectively, and the site of deuterium atom incorporation is indicated with a "D".

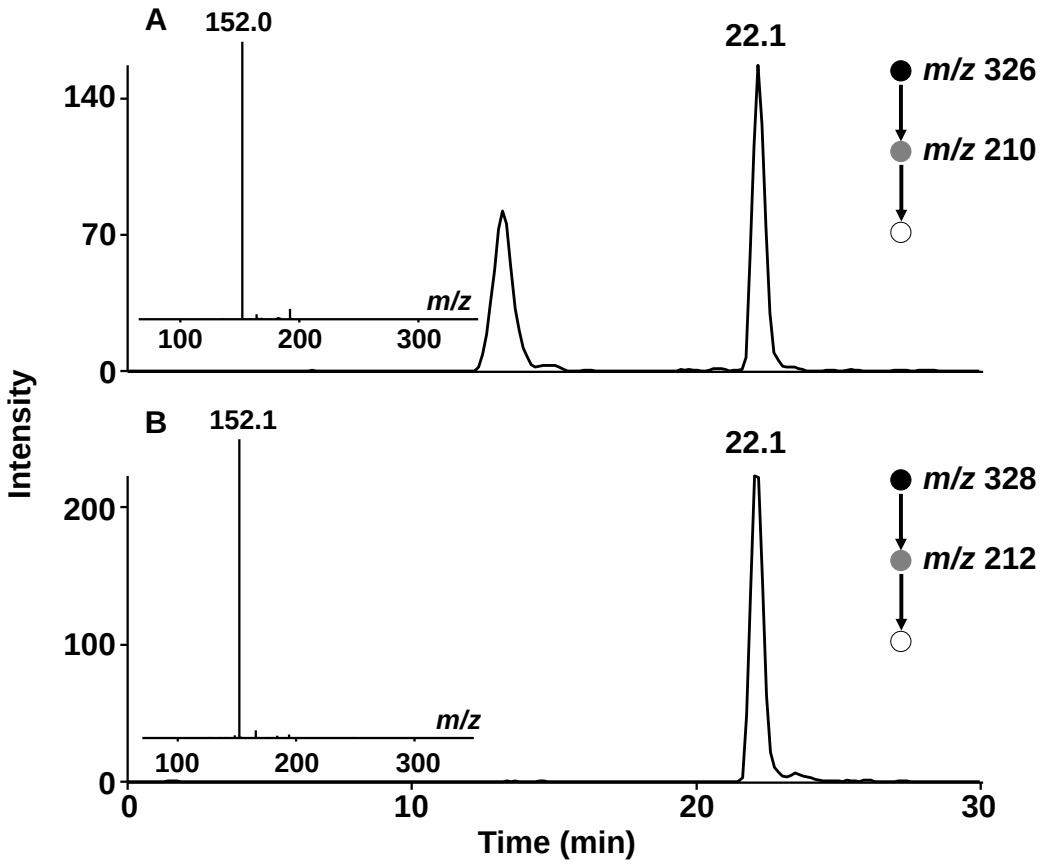


Figure B.4.Representative selected-ion chromatograms (SICs) for monitoring the *m/z* 326→210→152 (A) and 328→212→152 (B) transitions for the $[M+H]^+$ ions of the unlabeled O^6-CMdG and $[D_2]$-O^6-CMdG, respectively, in the nucleoside mixture of genomic DNA extracted from the XPA-deficient human skin fibroblast cells treated with azaserine. Shown in the insets are the MS^3 spectra for the unlabeled and labeled O^6-CMdG.

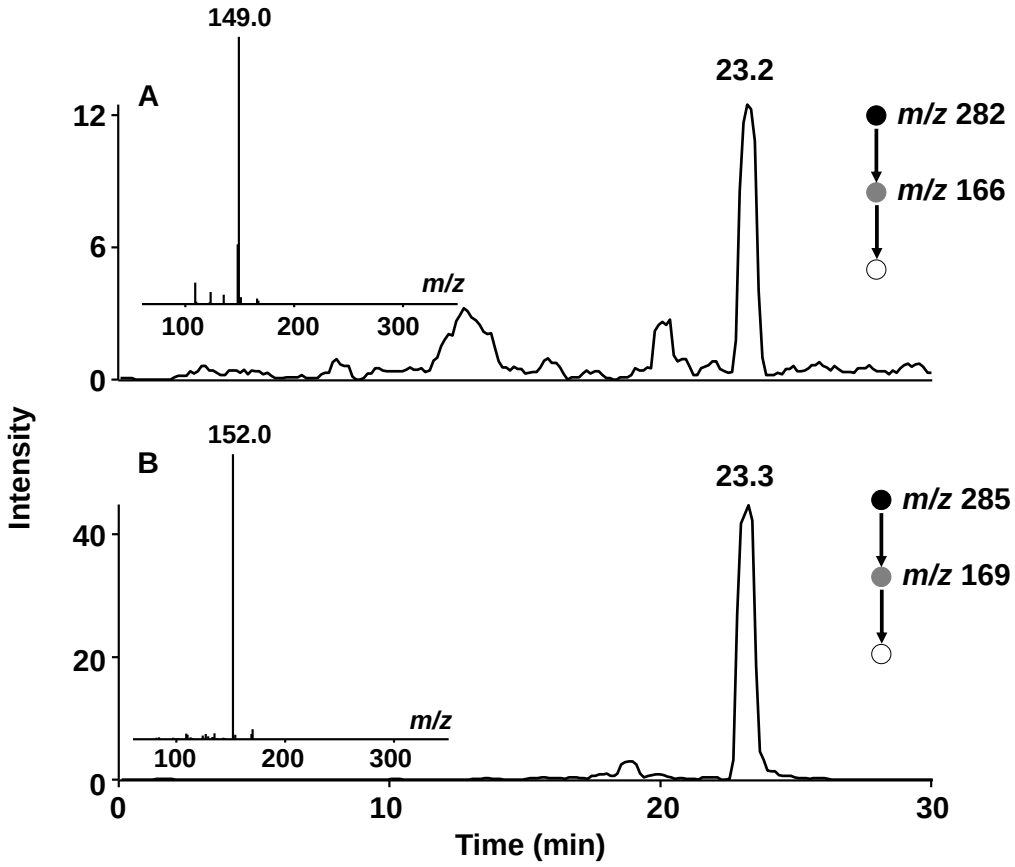


Figure B.5.Representative SICs for monitoring the *m/z* 282→166→149 (A) and *m/z* 285→169→152 (B) transitions for the $[M+H]^+$ ions of unlabeled O^6-MedG and $[D_3]$-O^6-MedG, respectively, in the nucleoside mixture of genomic DNA extracted from the XPA-deficient human skin fibroblast cells treated with azaserine. Shown in the insets are the positive-ion MS^3 spectra for the unlabeled and labeled O^6-MedG.

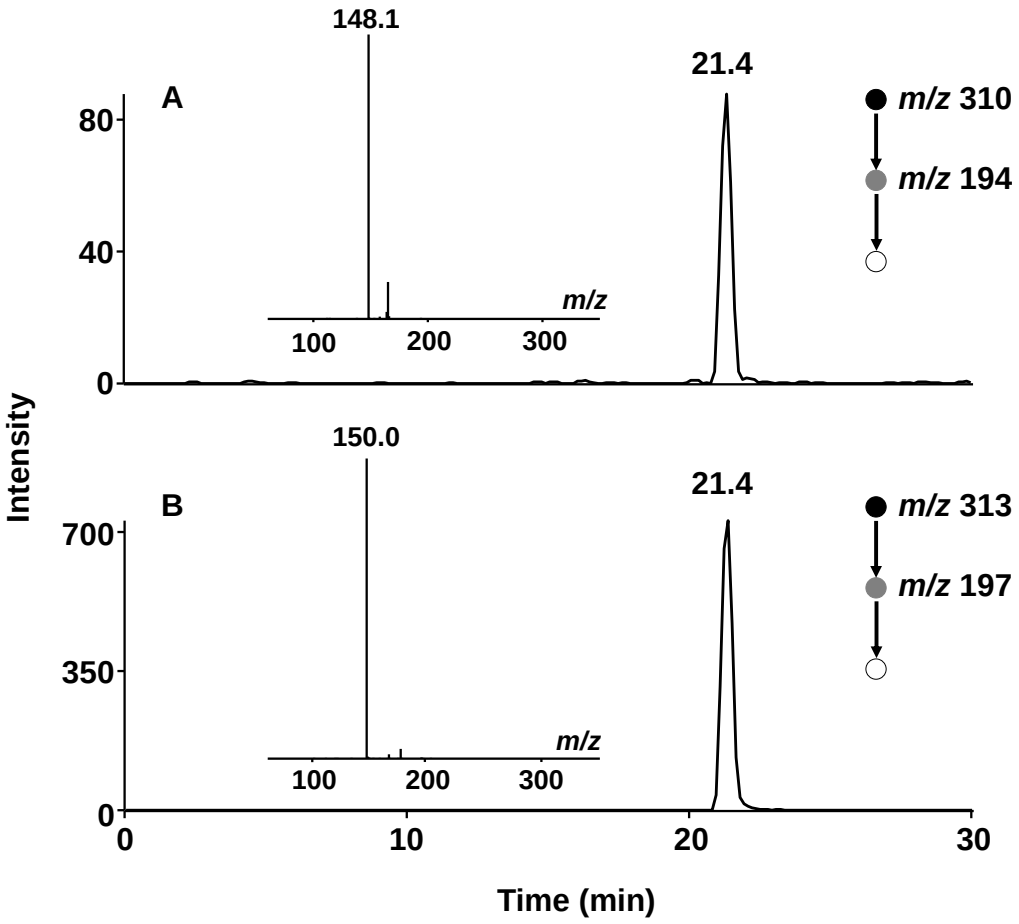


Figure B.6.Representative SICs for monitoring the *m/z* 310→194→148 (A) and *m/z* 313→197→150 transitions (B) for the $[M+H]^+$ ions of the unlabeled N^6-CMdA and $[^{13}C_2,^{15}N]$-N^6-CMdA, respectively, in the nucleoside mixture of genomic DNA extracted from the XPA-deficient human skin fibroblast cells treated with azaserine. Shown in the insets are the positive-ion MS^3 spectra for the unlabeled and labeled N^6-CMdA.

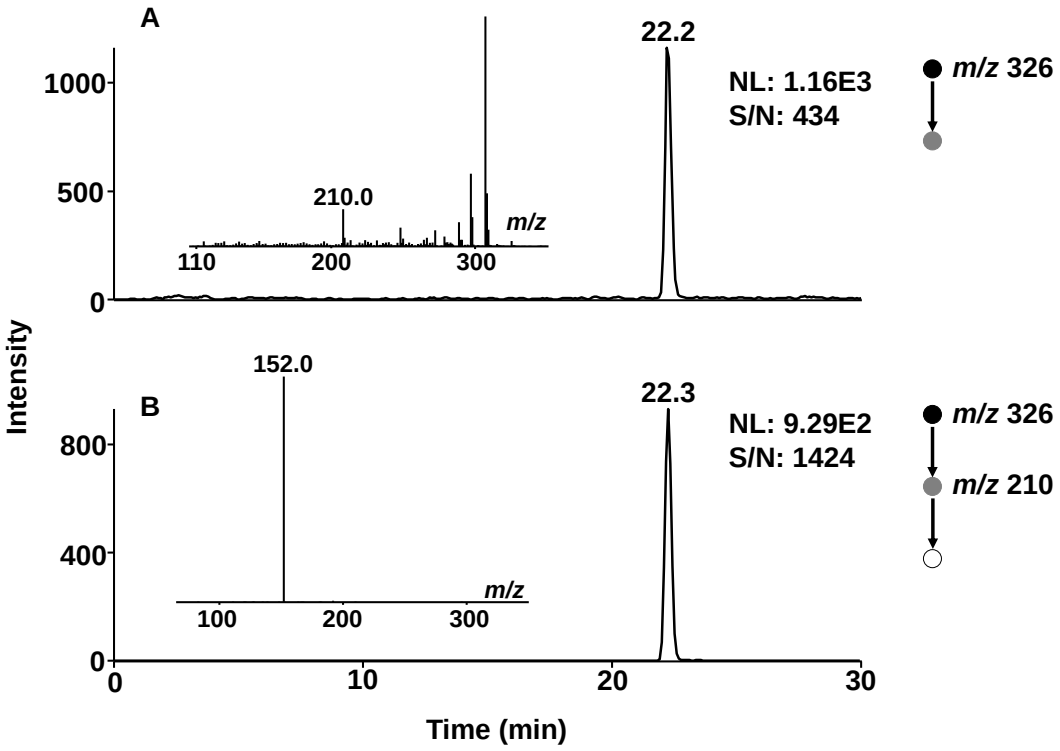


Figure B.7.Representative selected-ion chromatograms (SICs) for monitoring the *m/z* 326→210 (A) and 328→212→152 (B) transitions for the $[M+H]^+$ ions of the unlabeled O^6-CMdG, respectively, in standard solution. Shown in the insets are the MS^2 (top) and MS^3 (bottom) spectra for the unlabeled O^6-CMdG.

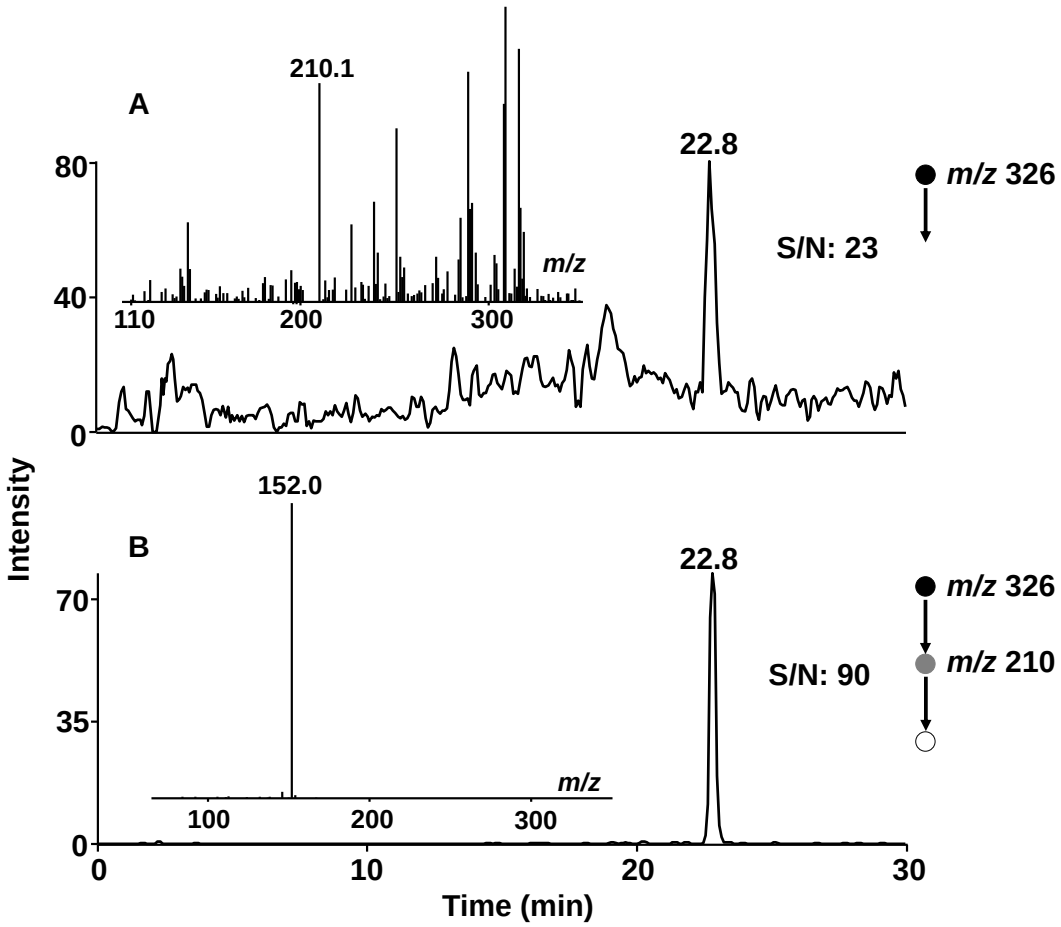


Figure B.8.Representative selected-ion chromatograms (SICs) as qualifier for monitoring the *m/z* 326→210 (A) and 328→212→152 (B) transitions for the $[M+H]^+$ ions of the unlabeled O^6-CMdG, respectively, in the nucleoside mixture of genomic DNA extracted from the HCT-116 human colorectal carcinoma cells treated with azaserine. Shown in the insets are the MS^2 (top) and MS^3 (bottom) spectra for the unlabeled O^6-CMdG.

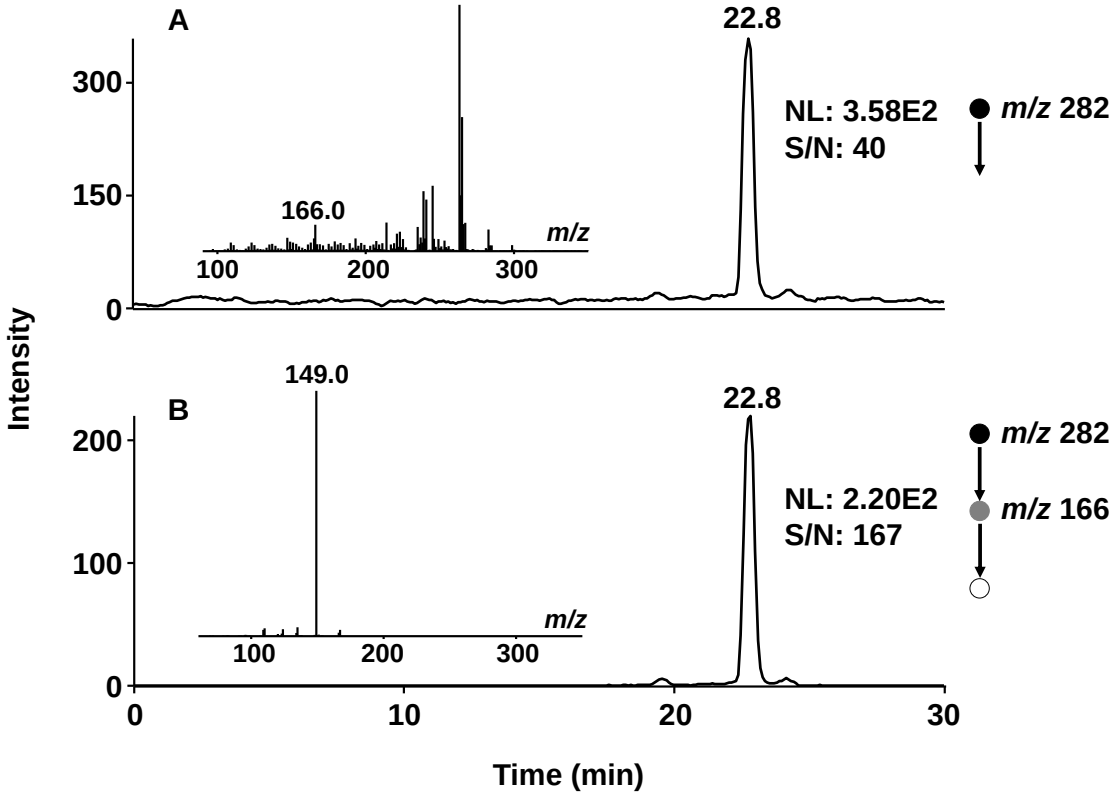


Figure B.9.Representative SICs as qualifier for monitoring the *m/z* 282→166 (A) and *m/z* 285→169→152 (B) transitions for the $[M+H]^+$ ions of unlabeled O^6-MedG, respectively, in standard solution. Shown in the insets are the positive-ion MS^2 (top) and MS^3 (bottom) spectra for the unlabeled O^6-MedG.

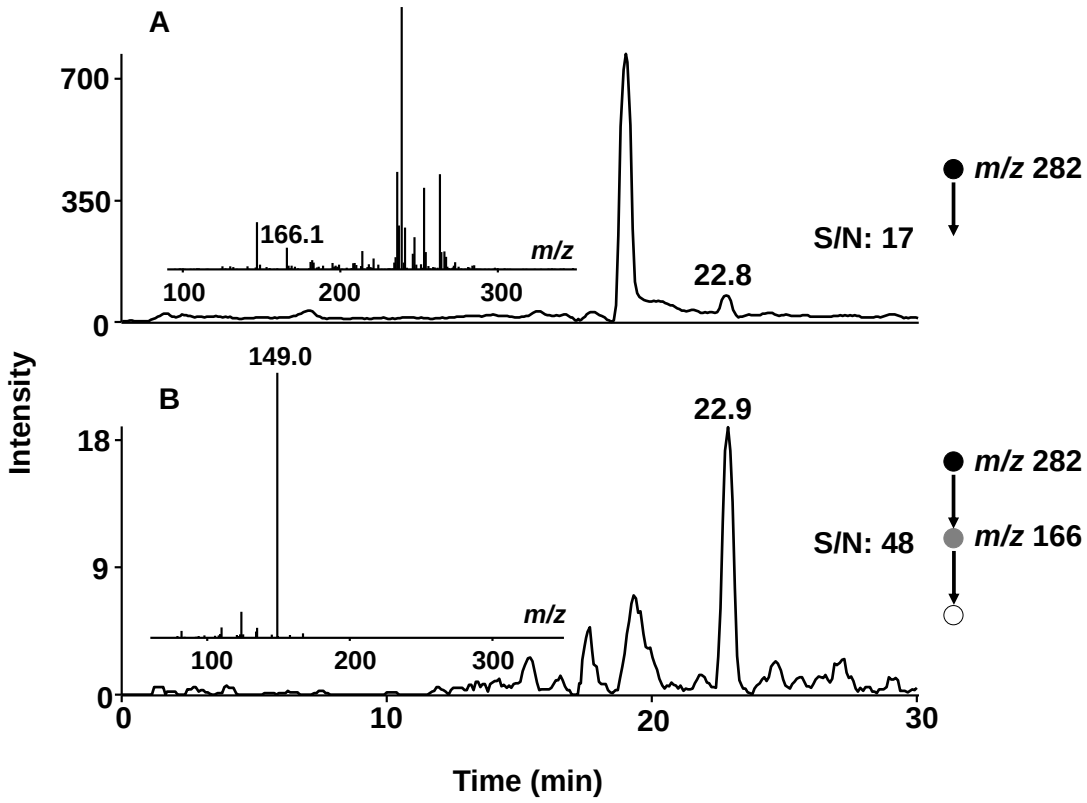


Figure B.10.Representative SICs as qualifier for monitoring the *m/z* 282→166 (A) and *m/z* 285→169→152 (B) transitions for the $[M+H]^+$ ions of unlabeled O^6-MedG, respectively, in the nucleoside mixture of genomic DNA extracted from the HCT-116 human colorectal carcinoma cells treated with azaserine. Shown in the insets are the positive-ion MS^2 (top) and MS^3 (bottom) spectra for the unlabeled O^6-MedG.

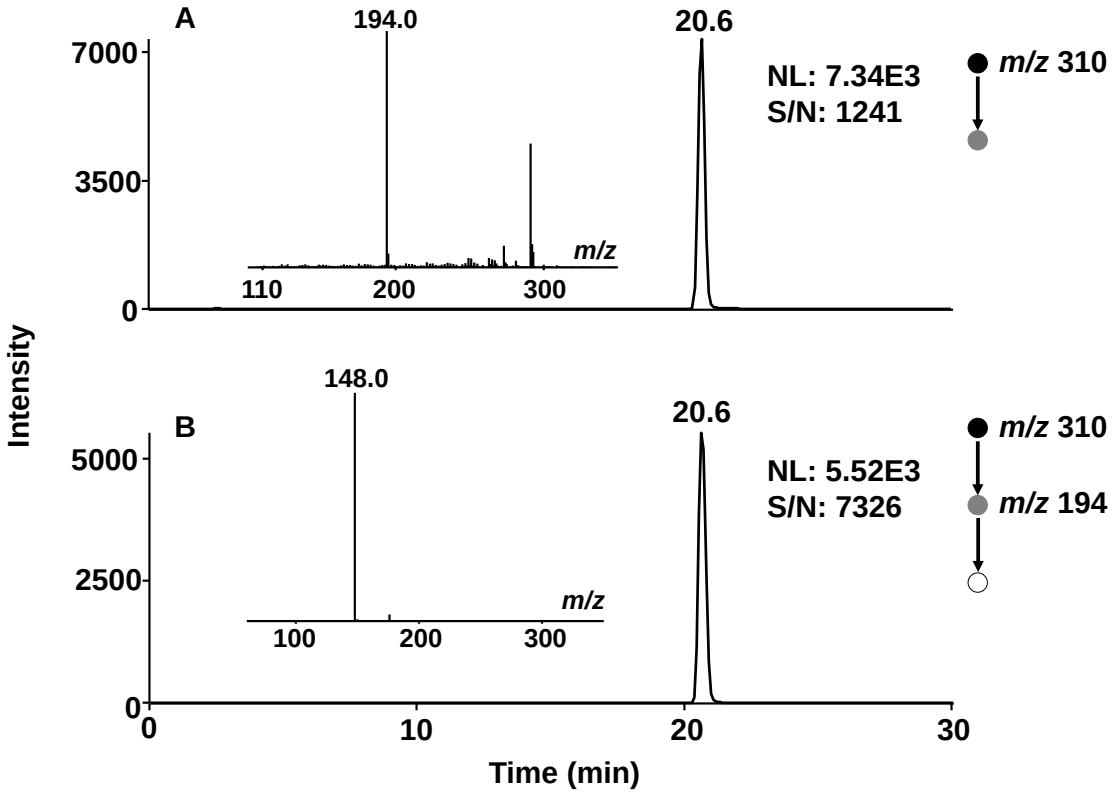


Figure B.11.Representative SICs as qualifier for monitoring the *m/z* 310→194 (A) and *m/z* 313→197→150 transitions (B) for the $[M+H]^+$ ions of the unlabeled N^6-CMdA, respectively, in standard solution. Shown in the insets are the positive-ion MS^2 (top) and MS^3 (bottom) spectra for the unlabeled N^6-CMdA.

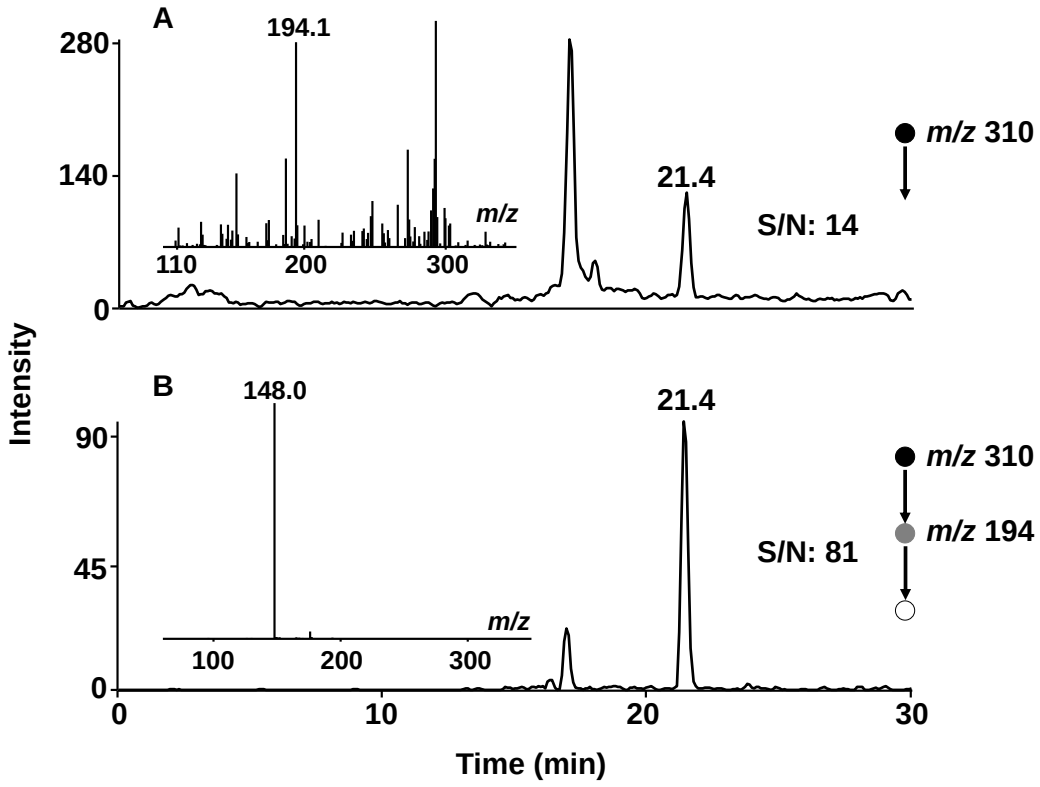


Figure B.12.Representative SICs as qualifier for monitoring the *m/z* 310→194 (A) and *m/z* 313→197→150 transitions (B) for the $[M+H]^+$ ions of the unlabeled N^6-CMdA, respectively, in the nucleoside mixture of genomic DNA extracted from the HCT-116human colorectal carcinoma cells treated with azaserine. Shown in the insets are the positive-ion MS^2 (top) and MS^3 (bottom) spectra for the unlabeled N^6-CMdA.